Characterization of the Neurovascular Pathology in CADASIL: A Model for Subcortical Vascular Dementia

Yumi Yamamoto
MRes. Medical and Molecular Bioscience

Neurovascular Research Group
Institute for Ageing and Health
Newcastle University
Campus for Ageing and Vitality
Newcastle upon Tyne
NE4 5PL

Dissertation submitted for the degree of Doctor of Philosophy in
Newcastle University
March, 2011

"Pooh, promise me you won't forget about me, ever.
Not even when I am a hundred."
Pooh thought for a little.
"How old shall I be then?"
"Ninety-nine."
Pooh nodded. "I promise," he said.

A.A. Milne
The House at Pooh Corner

Abstract

Cerebral autosomal dominant arteriopathy with subcortical infarcts and leukoencephalopathy (CADASIL) is one of the most common forms of hereditary vascular dementia (VaD). Characterised by early-onset strokes and cognitive impairment in the absence of vascular risk factors, CADASIL is an ideal model to understand the pathophysiology of VaD. Pathogenic mutations in the *NOTCH3* gene, which encodes a single-pass transmembrane cell surface receptor expressed predominantly in vascular smooth muscle cells (VSMC), cause severe vascular alterations including VSMC degeneration, hyalinosis, deposition of CADASIL-specific granular osmiophilic material (GOM) and white matter (WM) changes. While these changes have been well-described, their causative mechanism or difference between sporadic VaD is poorly understood. The aim of the project was to quantitatively characterise various aspects of cerebral pathology of CADASIL in order to reveal the pathological basis of CADASIL phenotypes, especially of cognitive dysfunction.

Firstly, we assessed vascular and perivascular changes in CADASIL brain areas and found significant vessel wall thickening and perivascular space enlargement, even compared to sporadic VaD. Secondly, by using immunogold electron microscopy, NOTCH3 extracellular domain (N3ECD) was located within GOM in the wall of cerebral arteries/arterioles/capillaries, establishing at least one component of GOM and its wide-spread existence in the vasculature. This study also suggested the possible existence of intracellular N3ECD accumulation and involvement of inflammatory response in the pathogenesis of CADASIL. Finally, we provide neuronal density data from the hippocampal formation in CADASIL brains to identify the neural substrates of VaD in CADASIL. Overall, the number of neurons in CA1, CA2 and entorhinal cortex was relatively spared in CADASIL while pyramidal neuronal subpopulation, as shown by SMI32 immunoreactivity, was slightly decreased. In addition, SMI32 staining revealed extensive chronic damage to WM tracts, especially those in the frontal-parietal area. These data suggest that vascular dysfunction and inflammation result in frontal disconnection, which could underlie cognitive impairment in CADASIL patients.

Acknowledgement

First and foremost, I would like to thank my supervisor, Prof.Raj N Kalaria, who has supported me throughout my MRes and PhD with his enthusiasm, inspiration and knowledge whilst allowing me independence and the room to work in my own way. During these years he has greatly helped me to learn and improve my research skills, and to acquire a more in-depth knowledge of the vascular dementia field.

My eternal gratitude goes to Arthur Oakley who has not only patiently answered all my questions but also provided encouragement, sound advice, good teaching (especially on British colloquialism), good company, and lots of good ideas. He also helped me with my ultrastructural research using electron microscopy, which constituted one of the vital chapters in this thesis.

In my daily work I have been blessed with friendly and cheerful members of our group. I am grateful to Janet Slade and Ros Hall for sharing their great knowledge and extensive techniques in immunohistochemistry and to Dr. Ahmad Khundakar who helped me to learn the basics of three dimensional stereology and provided advice when I encountered problems. I also wish to extend my gratitude to Mary Johnson, Drs Masafumi Ihara, Matt Burke, Stefano Cabras, Conor Lawless and staffs at the Newcastle Brain Tissue Resource Centre for their support and expertise.

My PhD was partly funded by ORS Awards from Newcastle University.

Finally, I thank my family for supporting me throughout all my studies at Newcastle University. This thesis is dedicated to my grandmother, who died during my PhD.

Yumi Yamamoto

27th March, 2011

Table of Contents

List of Figures and Tables

Abbreviations

Θ: Cutting plane angle

%PVS: Percentage of total PVS area in WM

AD: Alzheimer's disease

ADAM: a disintegrin and metalloprotease

Aβ: Amyloid-β

BA: Brodmann area

BBB: Blood-brain barrier

CAA: Cerebral amyloid angiopathy

CAMCOG: Cambridge cognitive examination

CBF: Cerebral blood flow

CBV: Cerebral blood volume

CCD: Chip charge-coupled device

CE: Coefficient of error

CERAD: Consortium to establish a registry for Alzheimer's disease

CFV: Cresyl fast violet

COGFAST: Cognitive function after stroke

CSF: Cerebrospinal fluid

DLB: Dementia with Lewy bodies

Dpvs: Diameter of perivascular space

ECV: Entorhinal cortex layer V

EGF: Epidermal growth factor

EM: Electron microscopy

GM: Grey matter

GOM: Granular osmiophilic material

H&E: Haematoxylin and eosin

HSP27: Heat shock protein 27

ICD: Intracellular domain

IHC: Immunohistochemistry

ISF: Interstitial fluid

L: Apparent length of axons

Larea：Area of lumen

LFB: Luxol fast blue

mDint: Mean internal diameter of blood vessel

mDext: Mean external diameter of blood vessel

mL: Mean apparent length of axons

MMSE: Mini-Mental State examination

MRI: Magnetic resonance imaging

NECD: Notch extracellular domain

NO: Nitric oxide

OL: overlap width

Ocont: Old controls

OsO_4: Osmium tetroxide

OVaD: Old vascular dementia

PEFA: Protein-elimination failure arteriopathy

PVS: Perivascular space

PVSc: Perivascular space calculated using the formulae in **Figure 3.1**

PVSi: Perivascular space measured using Image Pro Plus ver. 4

ROI: Region of interest

SI: Sclerotic index

SD: Standard deviation

SLF: Superior longitudinal fasciculus

Sn: Sampling number

SVD: Small vessel disease

T: Section thickness

TEM: Transmission electron microscopy

Tg: Transgenic

TIA: Transient ischemic attack

VaD: Vascular dementia

VSMC: Vascular smooth muscle cell

Vwall: Area of blood vessel wall

W: Width of sampling frame

WM: White matter

Ycont: Young controls

YVaD: Young vascular dementia

List of Original Publications

This thesis is based on the following original publications, referred to in the text by Roman numerals, and some unpublished data.

I. **Yumi Yamamoto**, Masafumi Ihara, Carina Tham, Roger W.C. Low, Janet Y. Slade, Tim Moss, Arthur E. Oakley, Tuomo Polvikoski, Raj N. Kalaria. Neuropathological correlates of temporal pole white matter hyperintensities in CADASIL. Stroke. American Heart Association. 40, pp2004-2011, 2009

II. **Yumi Yamamoto**, Lucy Craggs, Marc Baumann, Hannu Kalimo and Raj N Kalaria. Molecular Genetics and Pathology of Hereditary Small Vessel Diseases of the Brain. Neuropathol Appl Neurobiol. 37(1), pp94-11, 2011.

III. **Yumi Yamamoto**, Atsushi Watanabe, Raj N Kalaria. The Molecular pathogenesis of CADASIL. *In Revision*

Chapter 1. Introduction

1.1 Introduction

Cerebrovascular disease is not only one of the major causes of death in many developed countries, but is also a principle cause of dementia and disability. Vascular dementia (VaD), Alzheimer's disease (AD) and dementia with Lewy bodies (DLB) are the most common forms of dementia. In the past, they were considered three different diseases of old age unconnected in terms of pathogenesis, but it is now widely accepted that 'pure' VaD, AD or DLB are rare and they usually coexist to a varying extent. Of all the factors affecting their pathology, vascular abnormalities and their effects on brain are attracting considerable attention from researchers as the involvement of neurovascular dysfunction in AD pathology is becoming more clear (Bell and Zlokovic, 2009). In 1997, Snowdon et al. (1997) reported an interesting observation from the nun study; those who have experienced lacunar infarcts in the basal ganglia, thalamus, or deep white matter have higher risk and severity of AD, suggesting the interaction between VaD and AD. Subsequent studies have also supported this result (Heyman et al., 1998, Esiri et al., 1999), and at the same time, helped to characterize clinical and pathological differences and resemblances of VaD and AD. While the need to understand VaD has been increasing, most VaD cases are sporadic and thus difficult to study due to their heterogeneous pathogenesis: age, hypertension, diabetes, smoking, cardiovascular disease, hypercholesterolemia and other risk factors create varying pathologies, obscuring the pure effect of vascular abnormalities (Román, 2004). Given these circumstances, studies on the pathology of recently widely recognised familial type of VaD, cerebral autosomal dominant arteriopathy with subcortical infarcts and leukoencephalopathy (CADASIL) could have significant implications in understanding the pathogenesis of cerebrovascular disease and dementia.

1.1.1 Vascular dementia and small vessel disease

VaD is defined as cognitive dysfunction as a result of cerebral infarcts, haemorrhages, and white-matter changes due to cerebrovascular diseases (Román et al., 1993). Due to its nature, VaD develops suddenly or gradually, and often (though with exceptions) progresses in a slow and stepwise manner as patients experience repeated ischemic events while AD always develops and progresses gradually (Román, 2003, Fischer et al., 1990). Diagnosis of VaD is affected by the criteria used, and of all the diagnosis criteria based on different definitions of VaD, National Institute of Neurological Disorders and Stroke-*Association Internationale pour la Recherche et l'Enseignement en Neurosciences* (NINDS-AIREN) (Román et al., 1993) is one of the most widely used criteria proposed mainly for research purposes. The criteria include 1) dementia: impaired memory and two or more impaired cognitive domains, 2) cerebrovascular disease demonstrated by neurological examination and neuroimaging, 3) a temporal link between stroke and dementia, 4) other clinical features consistent with probable VaD, and 5) features that make diagnosis of VaD uncertain. It should be noted that diagnosis of VaD is applicable only with the absence of other dementia-causing pathologies (Erkinjuntti, 1994). Their specificity for diagnosis of VaD is markedly high, but the sensitivity is low and thus many VaD patients can be misdiagnosed as other forms of dementia (Wetterling et al., 1996).

VaD can be divided into two main subtypes by using blood vessel size: large-vessel (18%) and small-vessel dementia (74%) (Staekenborg et al., 2008). The large-vessel dementia, which is often acute-onset, occurs after multiple large-vessel or subcortical strokes, or after a single infarct in a strategic arterial location, such as right posterior cerebral artery, anterior cerebral artery, and left gyrus angularis (Román, 2003). Small-vessel dementia, on the other hand, is caused by lacunar infarcts, microinfarcts, and

incomplete infarction in the white matter (WM). The underlying cause of these infarcts is cerebral small-vessel diseases (SVD), which can be subdivided into atherosclerosis type, cerebral amyloid angiopathy (CAA) type, hereditary non-CAA SVD (*e.g.* CADASIL), inflammatory and immunologically-mediated SVD (*e.g.* Wegener's granulomatosis) and venous collagenosis type (Pantoni, 2010). It has been suggested that SVD is deeply involved in the onset of VaD (Esiri et al., 1997).

Cerebral (arterial) SVD is characterised by progressive pathological changes of intracerebral end-arteries and arterioles, such as hyalinosis, arteriosclerosis and fibroid necrosis, which cause occlusion, stenosis and loss of vascular reactivity, consequently promoting the incomplete infarcts and/or acute focal ischemia with complete tissue necrosis (lacunar infarcts) (Kalaria and Erkinjuntti, 2006, Pantoni, 2010). Blood-brain barrier (BBB) disruption, focal inflammation, and apoptosis of oligodendrocytes may also contribute to the development of cerebral pathology. Those brain pathologies usually manifest as gait disorder, articulation disorder, emotional disturbances and cognitive dysfunction (Schmidtke and Hüll, 2005). The cognitive dysfunction in SVD is often milder compared to that in AD, showing impaired frontal and subcortical functions (*e.g.* memory retrieval and attention/executive functions) with rather spared hippocampal functions (*e.g.* episodic and recognition memory) (Kertesz and Clydesdale, 1994, Traykov et al., 2002).

1.1.2 Familial small vessel diseases

Hereditary cerebral SVD with an early onset of dementia was first described in a Swedish family in 1977 (Sourander and Walinder, 1977). The autosomal dominant disease, which is here referred to as "Swedish VaD," caused multiple small infarcts affecting central WM, grey matter (GM) and pons. In response to the report, Stevens et

Disorder	Onset age	Mutated gene	Characteristic clinical features
CADASIL	36.7	*NOTCH3*	Migraine, stroke/TIA, dementia, mood disorder, WMH in temporal poles, frontal lobes, external capsules, periventricular WM
Swedish VaD	34.6	?	Stroke, dementia, mood disorder , motor dysfunction, WMH in basal ganglia and thalamus
CARASIL	20-30	*HTRA1*	Gait disturbance, scalp alopecia, lumbago, stroke, dementia and WMH in brain stem, middle cerebellar peduncle, external capsule
PADMAL	36.7	?	Gait disturbance, dysarthria, mood disorder, dementia, WMH in brain stem and basal ganglia, pontine infarcts
Portuguese-French SVD	40-50	*?*	Motor hemiplesia, executive dysfunction, WMH in temporal lobes, internal capsules, periventricular WM
HIHRATL	36.1	*COL4A1*	Infantile hemiparesis, migraine, intracranial aneurysms, leukoaraiosis, subcortical microbleeds, lacunar infarcts,
RVCL	30-40	*TREX1*	Retinopathy, nephropathy, stroke, migraine, dysarthria, apraxia, stroke, dementia

Table 1.1. Hereditary small vessel disease (SVD). CADASIL: cerebral autosomal dominant arteriopathy with subcortical infarcts and leukoencephalopathy, VaD: vascular dementia, CARASIL: cerebral autosomal recessive arteriopathy with subcortical infarcts and leukoencephalopathy, PADMAL: pontine autosomal dominant microangiopathy and leukoencephalopathy, HIHRATL: hereditary infantile hemiparesis, retinal arteriolar tortuosity and leukoencephalopathy, RVCL: retinal vasculopathy and cerebral leukodystrophy, WMH: white matter hyperintensities as seen on T_2-weighted MRI.

al. (1977) described a similar early-onset autosomal dominant SVD with recurrent cerebral ischemic episodes affecting basal ganglia, thalamus, corpus callosum and cerebral WM. The existence of hereditary VaD has been increasingly recognised since then. A French group also reported a family of early-onset stroke syndrome characterised by migraine attacks, leukoencephalopathy, subcortical infarcts and vascular smooth muscle cell (VSMC) degeneration (Baudrimont et al., 1993), which were later described as major clinical phenotypes of CADASIL (Chabriat et al., 1995). CADASIL was linked to mutations in the *NOTCH3* gene (MIM# 600276) and distinguished from the Swedish VaD, which lacked the CADASIL-characteristic magnetic resonance imaging (MRI) WM hyperintensities and *NOTCH3* mutations

(Joutel et al., 1996, Low et al., 2007). Several other CADASIL-like familial SVD have also been identified, including CARASIL (cerebral autosomal recessive arteriopathy with subcortical infarcts and leukoencephalopathy, or Maeda syndrome) (Fukutake, 1999), PADMAL (pontine autosomal dominant microangiopathy and leukoencephalopathy) (Ding et al., 2010), Portuguese-French type familial SVD (Verreault et al., 2006), HIHRATL (Hereditary infantile hemiparesis, retinal arteriolar tortuosity, and leukoencephalopathy) (Vahedi et al., 2003), and RVCL (retinal vasculopathy and cerebral leukodystrophy) (Richards et al., 2007) (**Table 1.1**). Whilst they are not linked to *NOTCH3* mutations, there may be similar underlying pathogenic mechanisms to those associated with CADASIL.

1.2 NOTCH3

1.2.1 Structures of NOTCH receptors and ligands

The *NOTCH* gene family, which encodes relatively large single-pass transmembrane cell surface receptors, includes four homologues in mammals (*NOTCH1-4)*. The four NOTCH homologues share the same basic structure comprising the extracellular domain (NECD, or amino (N)-terminal) consists of epidermal growth factor (EGF)-like repeats followed by 3 cysteine rich lin-12/Notch repeats and one trans-membrane domain, and an intracellular domain (ICD) which includes RAM (RBP-jκ-associated molecule) domain, cdc-10/ankyrin repeats and PEST (proline, glutamic acid, serine and threonine) sequence at the carboxyl (C)-terminal (**Figure 1.1**) (Bellavia et al., 2008). Of all the NOTCH homologues, NOTCH3 (UniProtKB/Swiss-Prot #Q9UM47), ~300kDa receptor comprised of 2321 amino acids, has a distinctively different structure compared to the others. NOTCH3 lacks the equivalent of EGF-repeat 21 and parts of EGF-2 and 3, resulting in only 34 EGF-repeats compared to 36 in NOTCH1 and 2 (Lardelli et al., 1994). NOTCH3 ICD also shows significant differences, with higher amino acid

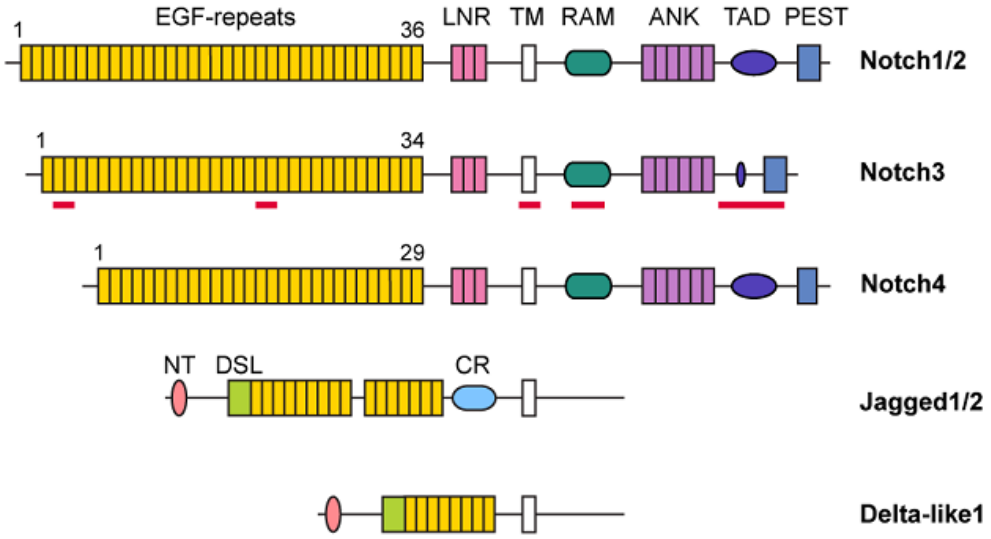

Figure 1.1. Structures of NOTCH homologues and Notch ligands. Red bars indicate regions significantly different from Notch1/2. LNR: lin/Notch repeats, TM: trans-membrane domain, RAM: RBP-jκ-associated molecule domain, ANK: cdc-10/ankyrin repeats, TAD: transactivation domain, PEST: proline, glutamic acid, serine and threonine sequence, NT: N-terminal domain, DSL: Delta-Serrate-Lag2 domain and CR: cysteine-rich region.

identity and shorter TAD (transactivation domain), which could underlie the weak transactivation ability of NOTCH3 ICD (Bellavia et al., 2008). Moreover, a recent study claimed that EGF7-10 and 21-22 in NOTCH3 are involved in ligand binding as opposed to the commonly accepted EFG- repeat 10 and 11 (Peters et al., 2004, Lin et al., 2010), though its validity should be carefully evaluated Those structural differences may contribute to the functional differences between NOTCH homologues (Bellavia et al., 2008).

NOTCH receptor proteins regulate cell fates or control the ability of non-terminally differentiated cells, during development, to respond to proliferation and maturation signals via local cell interactions (Artavanis-Tsakonas et al., 1999). The four NOTCH receptors may interact with the DSL (Delta-Serrate-Lag2) family of ligands, Serrate-like (Jagged1 and 2) and Delta-like (Delta-like1, 3 and 4), or non-DSL ligands (*e.g.* F3/Contactin, DNER, MAGP-1/-2) to signal various downstream targets (Fortini, 2009).

The DSL domain, N-terminal domain and the first two of the multiple tandem EGF-repeats in the extracellular domain are required for NOTCH receptor-ligand binding (Parks et al., 2006). Jagged1 and 2 contain twice as many EGF-repeats as Delta-like ligands and also specific cysteine-rich regions (CR) (D'Souza et al., 2008). The intracellular region of DSL ligands varies, but often contains C-terminal PDZ (PSD-95/Dlg/ZO-1) ligand motif and multiple lysine residues (D'Souza et al., 2008). In VSMC, NOTCH3, Jagged1, NOTCH1 and Jagged2 are expressed (Hofmann and Iruela-Arispe, 2007), the former two are down-regulated via the ERK pathway after vascular injury (Campos et al., 2002).

1.2.2 Sequential regulations in Notch signalling pathway

The activity of the NOTCH receptor is regulated by modification at EGF-repeats and also by a series of proteolytic processes (S1-4) mediated by three different proteases: furin-like convertase, a disintegrin and metalloprotease (ADAM 10) (Bozkulak and Weinmaster, 2009), and presenilin-dependent γ-secretase (**Figure 1.2**). NOTCH EGF-repeats are first modified by O-fucosyltransferase-1 (O-FucT-1) in endoplasmic reticulum (ER). It glycosylates serine or threonine residues at consensus sequences of EGF repeats after binding, recognizing the sequences of the conserved cysteine residues that form disulphide bonds (Luo and Haltiwanger, 2005). Following the O-glycosylation, some of the O-fucose residues are further glycosylated by an O-fucose-β1,3-N-acetylglucosaminyltransferase called Fringe in the trans-Golgi network (Blair, 2000, Rampal et al., 2005). The NOTCH heterodimer produced by the first S1 cleavage in the Golgi apparatus is presented on the plasma membrane to interact with Jagged/Delta at EGF-repeats 10-13 (Peters et al., 2004, Hambleton et al., 2004). The interaction triggers transendocytosis of ubiquitinated NECD-ligand complex by the ligand- presenting cell through clathrin/AP2/Epsin1 dependent or independent pathways

(Sorkin and Von Zastrow, 2009, Fortini, 2009). The physical force of trans-endocytosis exposes the transmembrane domain (S2 site), enabling cleavage by ADAM 10, which dissociates NECD (Chitnis, 2006, Le Borgne et al., 2005, Nichols et al., 2007). The subsequent S3 and S4 cleavages by intramembrane aspartyl protease γ-secretase on the plasma membrane or endosomal compartment releases ICD, which translocates to the nucleus and binds a transcription factor called CSL (CBF-1/RBP-Jκ, Su(H) and Lag-1) (Fortini, 2009, Fortini and Bilder, 2009). The two cleavages by γ-secretase also produce a short fragment called NOTCH β-peptide (Nβ), suggesting a close resemblance between amyloid precursor protein cleavages by α/β and γ-secretase in AD (Okochi et al., 2006). The following dissociation of corepressors and recruitment of Maml (mastermind-like) promotes the expression of its target genes, for example, Hairy/enhancer of split (HES) and HES-related transcription factor (HRT). HES and HRT families are transcriptional factors that regulate the expression of various down-stream target genes, of which examples were discussed in 1.2.3 (Artavanis-Tsakonas et al., 1999, Beatus et al., 1999, Iso et al., 2001, Jarriault et al., 1995, Utatsu et al., 1997).

Although both Jagged and Delta promote the release of the ICD, it has been reported that the consequent cellular response differs between Jagged- and Delta-induced Notch signalling (de La Coste and Freitas, 2006, Jaleco et al., 2001, Neves et al., 2006). For example, Jagged1-induced Notch3 signalling promotes the differentiation of VSMCs via RBP-Jκ, while Delta4-induced signalling does not (Doi et al., 2006). The mechanism of the ligand-selective effects is yet to be determined, but a key factor modulating the preference of NOTCH to either of the ligands was identified: glycosylation of EGF-repeats. Fringe, which has three homologues (Lunatic, Manic, and Radical), modifies various EGF repeats and the differences in the glycosylation pattern affects the Notch signalling activation by ligands, either positively or negatively,

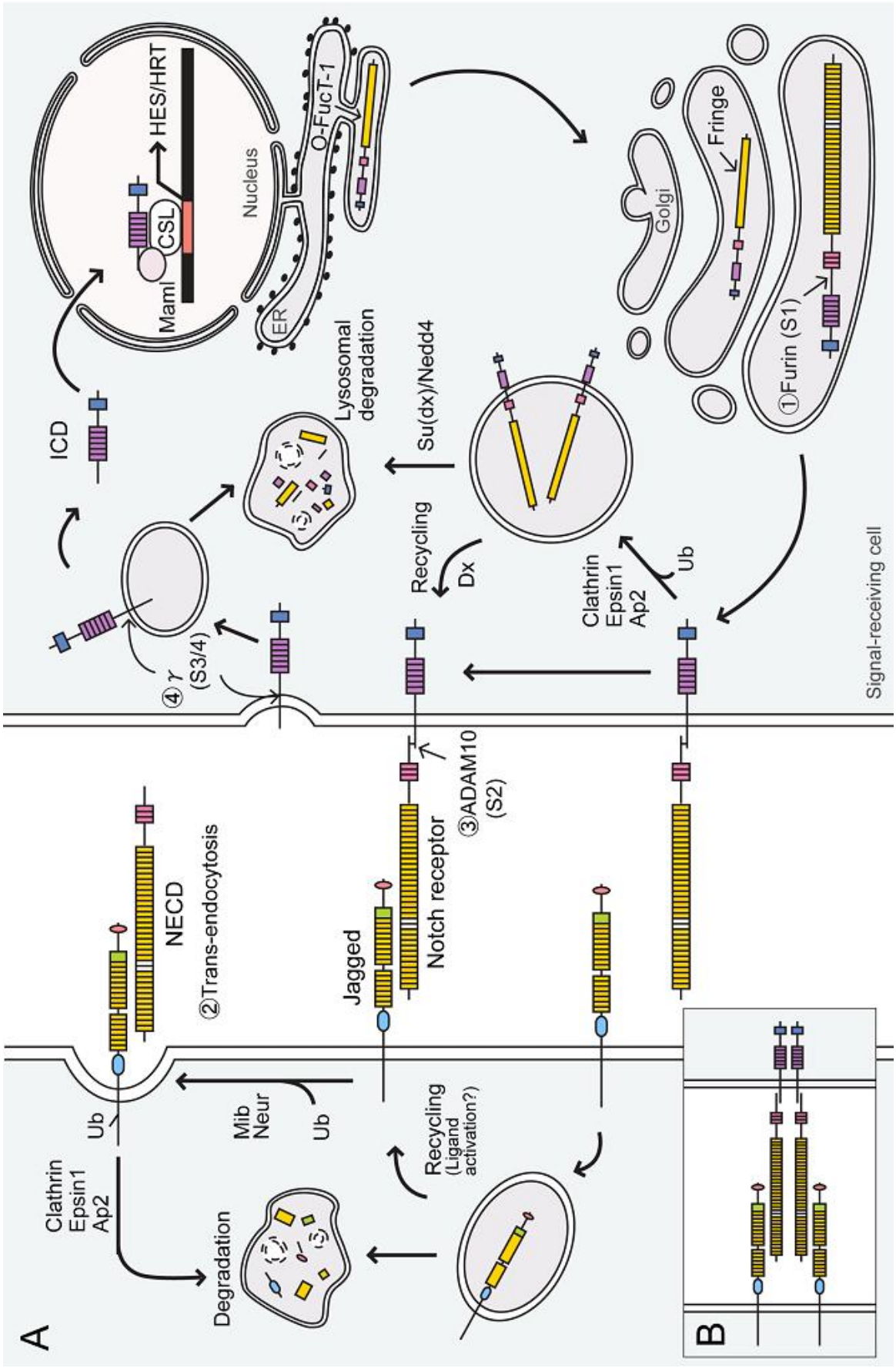
A
B
Signal-receiving cell
①Furin (S1)
Golgi
Fringe
O-FucT-1
ER
Nucleus
HES/HRT
CSL
Maml
ICD
④ γ (S3/4)
Lysosomal degradation
Su(dx)/Nedd4
Recycling
Dx
Clathrin
Epsin1
Ap2
Ub
③ADAM10 (S2)
Notch receptor
Jagged
②Trans-endocytosis
NECD
Mib
Neur
Recycling (Ligand activation?)
Degradation

Figure 1.2. Notch signalling pathway. (A) illustrates the series of proteolytic cleavage and modification events in the Notch signalling pathway. NOTCH receptor is glycosylated by O-fucosetransferase1 (O-FucT-1) and Fringe in the endoplasmic reticulum (ER) and the trans-Golgi network, respectively, after translation. (1) NOTCH is first cleaved at S1 site by a furin-like convertase to form a functional heterodimeric receptor. Binding of NOTCH receptor to ligands (Jagged and Delta-like) induces trans-endocytosis of the extracellular domain (NECD) by the ligand-presenting cell in Mib1/Neur1 dependent way (2). (3)The NECD dissociation enables a second cleavage at S2 site by ADAM-10, followed by S3/4 cleavage by γ-secretase on the plasma membrane or in the endosome (4). The resulting intracellular domain (ICD) translocates to the nucleus and binds to a DNA binding protein, CSL (for CBF1/RBP-Jκ, Suppressor of Hairless and Lag-1). The following recruitment of the coactivator, Maml (mastermind-like), promotes transcriptional activity of its target genes, such as the hairy/enhancer of split (Hes) and HES-related transcription factor (HRT). The surface expression of NOTCH is modulated by suppressor of deltex (Su(dx))/Nedd4-mediated degradation and deltex (Dx)-mediated recycling. (B) depicts how NOTCH dimer is thought to interact with the ligand from the signalling cell.

depending on the combination of NOTCH receptor and Fringe. Lunatic and Manic Fringe are suggested to enhance Delta1-induced Notch1 signalling whilst inhibiting Jagged1-induced Notch1 signalling. However, Radical Fringe activates both in the same way as Lunatic Fringe does in Notch2 signalling induced by Delta1 and Jagged1 (Hicks et al., 2000, Yang et al., 2005). Interestingly, Lunatic Fringe glycosylation does not suppress NOTCH1-Jagged binding, yet the interaction does not induce following S2 cleavage (Yang et al., 2005). As adequate physical force of trans-endocytosis is essential for S2 cleavage (Chitnis, 2006, Parks et al., 2000), this could be explained by the fact that fringe modifies the potency of the receptor-ligand binding but does not affect the binding itself (Yang et al., 2005). Few studies so far have investigated the differential effects of Fringe on Notch3 signalling and its downstream targets, which would greatly help the understanding of CADASIL molecular pathogenesis.

1.2.3 Physiological functions of Notch3 signalling in vasculature

Notch signalling is involved in various physiological processes including neurogenesis, retinal development, somitogenesis, adipogenesis, limb development, myogenesis and hematopoiesis (Shawber and Kitajewski, 2004). *NOTCH3* gene is expressed

ubiquitously both in vascular and nonvascular components of brain until the early postnatal developmental stage, but is restricted to arterial VSMCs in adults (Irvin et al., 2001, Lacombe et al., 2005), suggesting the VSMC specific function of Notch3 signalling.

1.2.3.1 Arterial development and formation

Although the specific expression of *NOTCH3* implies its critical role in VSMC, *NOTCH3* knockout mice are viable and fertile without serious abnormalities in embryonic vascular development while knockout of *NOTCH1*, which is expressed in vascular endothelial cells, results in embryonic lethality due to the defects in angiogenic vascular remodelling (Krebs et al., 2000, Krebs et al., 2003). Arteries in *NOTCH3*-/- mice were normal at birth but developed abnormal clustering of α-actin- and smooth muscle-myosin heavy chain (SM-MHC)-positive cells and failed to form a normal VSMC layer in the tunica media of arteries during the postnatal stage. The significant decrease in the expression of smoothelin, a specific arterial VSMC marker, was also observed in the mutant arteries, suggesting impaired terminal differentiation of VSMCs (Domenga et al., 2004). An *in vitro* study using aortic smooth muscle cells supported the NOTCH3 function in VSMC differentiation by showing that NOTCH3 ICD promotes the expression of SM22α, SM-MHC, h-caldesmon and smoothelin (Doi et al., 2006) (**Figure 1.3**).

Several other *in vitro* studies demonstrated that both Notch1 and Notch3 signalling similarly affects VSMC proliferation and migration via CBF-1/RBP-Jk-dependent pathway (Wang et al., 2007, Campos et al., 2002, Sweeney et al., 2004). The VSMC growth was promoted upon Notch3 signalling activation by the suppression of cell-cycle inhibitors p27KIP1 and p21WAF1/CIP1 (Campos et al., 2002, Wang et al., 2003), or by the increased expression of platelet-derived growth factor receptor (PDGFR) –β

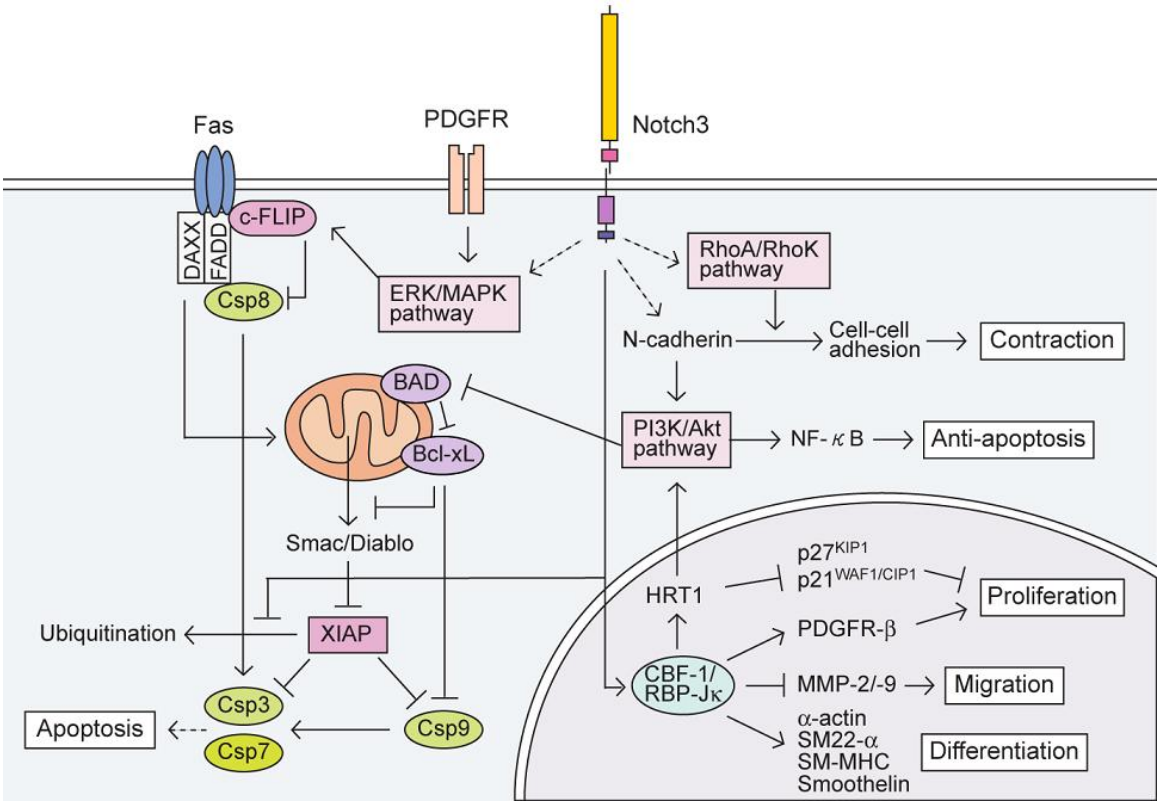

Figure 1.3. Putative molecular mechanisms of VSMC functions and Notch3 signalling. Notch3 signalling plays a critical role in VSMC functions. Notch3 signalling regulates expression of HES-related transcription factor (HRT)-1, platelet derived growth factor receptor (PDGFR)–β, matrix-metalloproteinase (MMP) -2/-9 and VSMC markers (α-actin, SM22α , SM-MHC etc.), which are involved in proliferation, migration and differentiation of VSMCs. HRT-1 activate phosphatidylinositol 3-kinase (PI3K)/Akt pathway which acts as an anti-apoptotic mechanism. Notch3 signalling can activate RhoA/Rho kinase pathway, which organises actin and cell adhesion molecules necessary for myogenic tone. The crosstalk with ERK/MAPK pathway up-regulates the expression of caspase (Csp) 8 inhibitor, c-FLIP. Noth3 ICD may inhibit the degradation of X-linked inhibitor of apoptosis (XIAP), which inhibit Csp3, 7 and 9. Dot arrows indicate unknown molecular mechanisms.

(Jin et al., 2008). The activation of Notch3 signalling was also suggested to increase the expression of N-cadherin on the cell surface, which contributes to alter cell growth/ migration behaviour with preference to the colony formation over spreading (Wang et al., 2007, Lyon et al., 2010). Moreover, the expression of matrix-metalloproteinase (MMP) -2 and -9, which are crucial for VSMC migration, was shown to be down-regulated by Notch3 signalling though its molecular basis is still unclear (Delbosc et al., 2008). Contrary to the above reports, however, only *NOTCH1*+/- and not *NOTCH3*-/- mice exhibited reduced VSMC proliferation and migration (Domenga et al., 2004, Li et

al., 2009). As shown by Kitamoto et al. (2005), the lack of Notch3 signalling did not affect the expression of NOTCH1, which also interact with Jagged1 to promote proliferation and repress migration, thus Notch1 signalling may act as a redundancy mechanism in *NOTCH3* deficient mice.

Viewed collectively, the data indicates that the main role of Notch3 signalling in the vasculature is the regulation of postnatal arterial differentiation and maturation of VSMCs rather than of migration and proliferation during the embryonic stage, which can be partially compensated for by NOTCH1 (Domenga et al., 2004, Kitamoto et al., 2005, Li et al., 2009, Sweeney et al., 2004).

1.2.3.2 Apoptosis

Though not vital, Notch3 signalling has an important role in deciding VSMC fate; the activation of NOTCH3 inhibits apoptosis while loss of NOTCH3 does not result in the opposite (Wang et al., 2007, Sweeney et al., 2004, Domenga et al., 2004). Several NOTCH-apoptotic mechanisms have been proposed so far. The main pathway is the inhibition of Fas-mediated apoptosis, which is a major apoptotic pathway in VSMCs. Notch3 signalling was suggested to increase the expression of c-FLIP (Fas-associated death domain like interleukin-1β-converting enzyme-like inhibitory protein), which competitively inhibits caspase-8, via cross-activation of ERK/MAPK pathway rather than RBP-Jκ-HRT1 (Wang et al., 2002). NOTCH1 ICD was shown to increase the expression of X-linked inhibitor of apoptosis (XIAP), which inhibits the activation of caspase-3, -7 and -9, by direct binding to prevent its ubiquitination (Liu et al., 2007). It is highly plausible that NOTCH3 ICD has a similar function and promotes cell survival via XIAP together with c-FLIP activation. Another proposed mechanism involves HRT1, a Notch signalling downstream target. HRT1 activates phosphatidylinositol 3-kinase (PI-3K)/Akt pathway, which is known to promote cell survival via NF-κB, Bcl-

2-associated death promoter (BAD), glycogen synthase kinase 3 (GSK3) and others (Downward, 2004, Wang et al., 2007, Wang et al., 2003).

1.2.3.3 Vascular tone

Studies on *NOTCH3* deficient mice revealed decreased pressure-induced myogenic tone and increased flow-induced dilation in cerebral resistance arteries (Domenga et al., 2004, Belin De Chantemèle et al., 2008). The underlying mechanism may involve the activation of RhoA/Rho kinase pathway by Notch3 signalling (Büssemaker et al., 2007, Belin De Chantemèle et al., 2008). RhoA/Rho kinase is suggested to modulate the organization of actin filaments, integrins and cadherins, of which integrity is pivotal for unperturbed myogenic tone, as well as the phosphorylation of myosin light chain (Belin De Chantemèle et al., 2008, Dubroca et al., 2005b). CADASIL patients are known to exhibit impaired vascular autoregulation (Gobron et al., 2007, Peters et al., 2005a, Hussain et al., 2004), further emphasising the importance of Notch3 signalling in vascular mechanotransduction.

1.3 CADASIL

Since the report of Swedish hereditary multi-infarct dementia (Sourander and Walinder, 1977), the presence of hereditary stroke disorders have been increasingly recognised. CADASIL is probably the most common and well-studied disease of all, which was linked to the pathogenic mutations in the *NOTCH3* gene (Joutel et al., 1996). It is characterized by arteriosclerosis of small vessels with degeneration of VSMC, and multiple small infarcts in WM and deep (subcortical) GM of the brain. More than 600 CADASIL families have been estimated to exist worldwide, with over 100 reported families in UK, France and Germany (Adib-Samii et al., 2010, Opherk et al., 2004, Peters et al., 2005b). The reports of CADASIL families are rather concentrated in the

developed countries, but it is more likely to be the simple reflection of accessibility to accurate diagnostic tools than actual disease predilection. The world wide prevalence of CADASIL is unknown, but it was calculated to be 1.98 patients with a definite diagnosis per 100,000 and 4.14 per 100,000 if the predicted mutation carriers were included in the west Scotland population (Razvi et al., 2005). There is no gender difference in the prevalence though the long-term prognosis for disability and death is worse for men than women by 6 years (Opherk et al., 2004). Hypertension and smoking are risk factors for strokes, which is a main cause of dementia and disability in CADASIL (Adib-Samii et al., 2010).

1.3.1 Clinical and pathological features of CADASIL

1.3.1.1 Diagnosis

CADASIL often manifests as migraine attacks around individuals second to third decade, followed by TIAs/strokes and depression 10 years after onset (Chabriat et al., 1995) (**Figure 1.4**). Over 80% of patients suffer recurrent strokes and dementia by the time of death, which is 54.8 ±10.6 years (Felician et al., 2003, Desmond et al., 1999). Thus, CADASIL is suspected when WM hyperintensity on MRI, especially in temporal poles or external capsules, coincides with a history of migraine (often with aura) or transient ischemic attack (TIA) despite the relative young age (<60 years) (Chabriat et al., 1995, Pantoni et al., 2010). Family history of stroke and dementia is also considered as a strong indication of CADASIL. As those clinical or neuroimaging features are frequent in CADASIL but not specific, the genetic screening for *NOTCH3* mutation is essential to confirm CADASIL and distinguish from CADASIL-like disorders. General mutational hot spots (exon 3, 4 and 5) or frequent mutational spots in a specific genetic background (e.g. exon11 in Italian population) are often targeted for the screening (Peters et al., 2005b). It should be noted that full genetic screening is necessary to

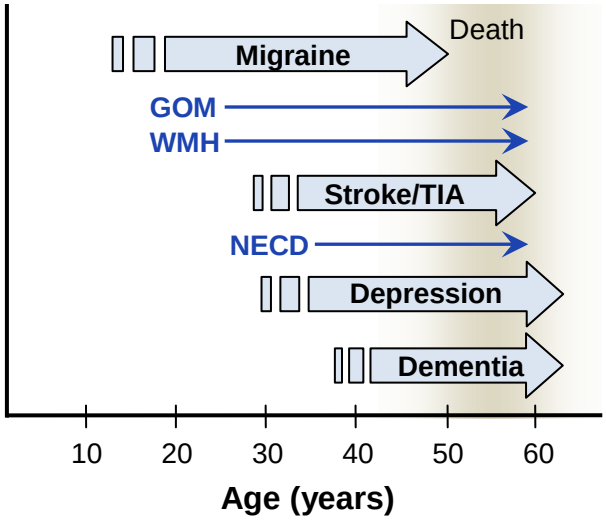

Figure 1.4. Time course of CADASIL symptoms and pathologies. The initial symptoms manifest as migraine or transient ischemic attack (TIA) around 20-30 years of age, when white matter hyperintensity (WMH) is detected by MRI.

completely eliminate the diagnosis of CADASIL as >100 potential *NOTCH3* mutational spots spread over 23 exons. Alternative to the genetic diagnosis, skin biopsy is performed to confirm CADASIL-specific granular osmiophilic material (GOM), which show 100% congruence with *NOTCH3* mutations (Tikka et al., 2009). Immunostaining of skin biopsy samples for N3ECD also provide a good indication of CADASIL with 96% sensitivity and 100% specificity though caution should be taken to avoid false-negative results (Lesnik Oberstein et al., 2003, Joutel et al., 2001)

1.3.1.2 Neuroimaging

Neuroimaging features in CADASIL are rather unique as it demonstrates a relatively specific spatial distribution of lesions. Characteristic lesions in CADASIL brain are small subcortical infarcts and diffuse white matter abnormality with enlarged perivascular spaces (PVSs) (Singhal et al., 2005, Coulthard et al., 2000) (**Figure 1.5**). MRI abnormalities have been demonstrated to correlate with strokes, disability and cognitive dysfunction from extensive neuroimaging studies (Dichgans et al., 1999, Singhal et al., 2005). In particular, lacunar infarcts were associated with cognitive

decline, but not WM hyperintensities on T_2-weighted MRI (Viswanathan et al., 2007, Liem et al., 2007).

Abnormal WM changes often start from the frontal lobes even before the manifestation of symptoms (Chabriat et al., 1995, Dichgans et al., 1998, Stromillo et al., 2009), helping the early diagnosis in the presence of family history. The WM pathologies gradually spread to the periventricular WM, frontal, temporal and parietal lobes, external capsules, corpus callosum, basal ganglia and brain stem, frequent and severe in this order in symptomatic CADASIL patients as the disease progresses with ageing. The involvement of the anterior temporal poles is common and a strong indication of CADASIL though no study so far has sufficiently explained the unique susceptibility of anterior temporal poles (Singhal et al., 2005). Those lesions are mostly subcortical, and cortical, as cerebellar lesions are rarely observed in CADASIL (Chabriat et al., 1998). However, SPECT (single photon emission computed tomography) studies reported hypoperfusion in temporal and frontal cortices, basal ganglia, cingulate cortex in addition to the subcortical areas, and it was not always consistent with the area of hyperintensities (Mellies et al., 1998, Scheid et al., 2006). This is actually due to a

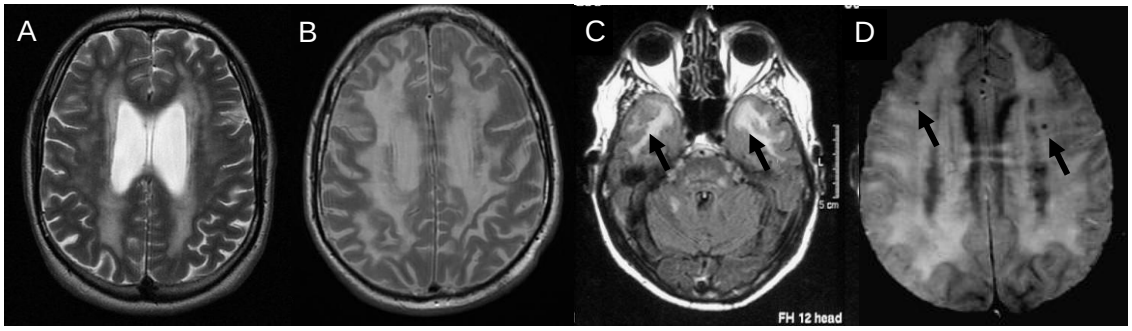

Figure 1.5. Neuroimaging in CADASIL. Axial MR images of genetically confirmed CADSIL patients. A-B, T2 weighted MR image showing variable degrees of periventricular and deep WM hyperintensities in patients of the same age at 50 years. One patient (A) had severe psychiatric symptoms and the other (B) exhibited aggressive behaviour. C, FLAIR MR sequence demonstrating high signals (diagnostic for CADASIL) in WM of the temporal poles in a 61-year-old CADASIL patient. D, shows localization of microbleeds (arrows) in a CADASIL patient (kind courtesy of M Dichgans, Munich).

limitation of conventional MRI, which is good at detecting the presence of macro- but not microscopic lesions. Indeed, MTI (magnetization transfer imaging) and DTI (diffusion tensor imaging) scans revealed ultrastructural damage, such as axonal and myelin loss, in normal appearing WM in CADASIL (Iannucci et al., 2001, Chabriat et al., 1999), suggesting that the WM disturbance and destruction are more extensive than it appears on T_2-weighted MRI. The damage is also evident in the form of reduced glucose metabolism in cortical and subcortical regions (Tatsch et al., 2003).

1.3.1.3 Cognitive profiles

The cognitive profiles of CADASIL are very similar to sporadic SVD. Several large cohort studies have characterised the neuropsychological deficits in CADASIL. At the early stage of the disease before incidents of TIA or strokes, the neuropsychological symptoms are relatively restricted to the impairment of frontal executive functions, which monitor, select and control cognitive processes; diminished working memory, attention and error monitoring are observed in CADASIL (Amberla et al., 2004, Peters et al., 2005c). The executive dysfunction is usually assessed by the verbal fluency (semantic) test as recalling categorical words requires constant planning of retrieval strategies, attention and monitoring of the processes, and shifting of the effective strategies (Abrahams et al., 2000). Verbal fluency impairment is a characteristic of SVD, however, it is more severe in CADASIL, implying the additional contribution of CADASIL's unique pathology, namely WM lesions in the temporal poles (Charlton et al., 2006). Left prefrontal, temporoparietal, and bilateral anterior temporal regions are suggested to be the main components of semantic cognition (Pobric et al., 2007), and thus WM abnormalities in those regions as described previously would underlie the diminished verbal fluency in CADASIL.

As the disease progresses, the broader spectrum of neuropsychiatric functions are affected. At the post-stroke stage, cognitive processing speed, visuospatial ability, reasoning, set shifting and ideational praxis are often impaired while orientation, recognition and receptive language skills remain intact (Peters et al., 2005c, Buffon et al., 2006, Amberla et al., 2004). After 60 years of age, most CADASIL patients start to manifest cognitive deficit with impaired verbal function and motor speed (Buffon et al., 2006, Amberla et al., 2004), but the pattern of memory impairment differs from that in AD, with relatively spared episodic memory (Amberla et al., 2004). Verbal memory tests, which examine encoding, storage and retrieval processes of episodic memory, reveal worse immediate and delayed free recall in CADASIL. However, the recall usually improves when cues are given even in demented patients, indicating that memory impairment in the majority of CADASIL patients is not due to the defect in encoding and storage but in the retrieval process, though the minority show poor delayed recall even with cueing, which is indicative of hippocampal-type amnesia as in AD (Epelbaum et al., 2010, Buffon et al., 2006, Peters et al., 2005c).

Collectively, CADASIL is characterised by executive dysfunction, slow memory processing speed and memory retrieval deficit with relatively intact episodic memory, which are feature of subcortical ischemic vascular dementia.

1.3.1.4 Migraine with aura

Migraine is one of the most frequently observed initial symptoms in CADASIL, often manifesting from 10-30 years of age. Approximately 70% of migrainous patients experience typical aura prior to the attack, which is the combination of visual (*e.g.* Scintillating scotomas, photopsia and blurred vision), sensory (mainly face and arm), aphasic or motor aura (predominantly arm) (Vahedi et al., 2004). One of the proposed mechanism of migraine involves vascular factors: the migraine attack is triggered by

vasodilation and hyperperfusion following aura caused by vasoconstriction (Pollock et al., 2008, Dalkara et al., 2010). Indeed, Yetkin et al. (2007) reported decreased flow-mediated and increased NO-mediated vasodilation in CADASIL patients with migraine. The impact of migraine on cognitive functions is controversial. Some argue that migraine affects executive functions (Schmitz et al., 2008, Mulder et al., 1999) while others claim no effect (Baars et al., 2010). In either case, there may be a common mechanism between migraine disorders and migraine in CADASIL as migraine itself is a risk factor for strokes (MacClellan et al., 2007).

1.3.1.5 Other common symptoms

The other common symptoms include mood disturbances, seizure, ataxia, dysarthria and visual defects. Ataxia is the most frequent, with 90% of patients showing gait disturbance, limb akinesia with rigidity and psychomotor slowing, but without resting tremor or abnormal movements as in Parkinson's disease (Dichgans et al., 1998). As a result, 63% of individuals aged over 65 are classified as Rankin Disability Scale 4 or above, requiring assistance with walking and other activities. Male gender is a risk factor for early immobilisation: mean ages for requiring walking assistance and bedriddenness are 59 and 62 in men and 62 and 67 in women, respectively (Opherk et al., 2004). Mood disorders including dysthymia, apathy, depression, anxiety and jealousy delusion occur in 20-30% of patients often with underlying dementia (Dichgans et al., 1998, Chabriat et al., 1995, Reyes et al., 2009). They manifest in the course of disease progression and rarely present at the onset (Valenti et al., 2008).

While most of the symptoms are exclusively related to the central nervous system, a few cases with visual abnormality have been reported. CADASIL arteriopathy affects the vasculature of the eyes and causes arterial narrowing and sheathing, leading to optic nerve rarefaction and retinal dysfunction, though the visual function is not always

damaged (Rufa et al., 2005, Roine et al., 2006, Parisi et al., 2007, Parisi et al., 2003). Several studies also reported sensorineural hearing loss, but its significance is unknown (Phillips et al., 2005, Scheid et al., 2006).

1.3.1.6 Vascular changes

Similar to the *NOTCH3* deficient mice, cerebral and peripheral arteries in CADASIL develop normally during the embryonic period with no sign of vascular pathologies, which gradually accumulate postnatally and are prominent by the age of 20 (Brulin et al., 2002, Oberstein et al., 2008, Ruchoux et al., 2003). The most striking change is observed in VSMCs, which are destroyed and lost completely or partially from vessel walls, especially in small arteries (<500 μm in diameter) in contrast to the *NOTCH3* deficient mice, which showed no alteration in VSMC death (Domenga et al., 2004, Okeda et al., 2002). Remaining VSMCs are irregular-shaped or swollen, with partially disturbed plasma membrane and dense granular osmiophilic material (GOM) at a close proximity to the cell surface (Schröder et al., 2005, Kalimo et al., 2002). GOM is uniquely found in the vessel wall of CADASIL and is suggested to contain some lipids or lipoproteins and N3ECD (Kalaria et al., 2004, Ishiko et al., 2006). N3ECD accumulation is also found on the plasma membrane of VSMCs, but the toxicity of those CADASIL characteristic deposits are unknown (Joutel et al., 2000).

Ultrastructural changes are also found in vascular endothelial cells. The skin biopsy findings include dense and irregular-shaped cytoplasm of vascular endothelial cells with large vacuoles and notably increased microfilament bundles at their abluminal side (Ruchoux and Maurage, 1998). Adjacent basal lamina is also disrupted, either focally duplicated or detached from endothelial cells (Ruchoux and Maurage, 1998, Schröder et al., 2005). As the disease progresses, cells are disorganized and the disjunction between

VSMCs and endothelial cells becomes pronounced, further exacerbating the vascular destruction (Brulin et al., 2002). Apparently, the ultrastructural changes of endothelial cells damage the arterial autoregulatory function: CADASIL shows impaired endothelial vasodilation in the resistance arteries (Stenborg et al., 2007). Marked thickening of vessel wall due to the intimal and adventitial hyalinosis and fibrosis may also prevent normal flow-mediated vasodilation (Okeda et al., 2002, Miao et al., 2004).

The above pathological changes seem to alter the integrity of the vessel wall, making them susceptible to infarcts. Indeed, intracerebral microbleeds are often found around degenerated small vessels (Dichgans et al., 2002). Whereas intracerebral haemorrhages are rare, multiple small infarcts are commonly found in WM, deep GM and brain stem (Kalimo et al., 2002). Damage to brain tissue can be more extensive than normal due to the impaired vasoconstriction after stroke as demonstrated by the Notch3 mutant mice study (Arboleda-Velasquez et al., 2008).

1.3.2 Mechanisms of CADASIL pathogenesis

1.3.2.1 *NOTCH3* mutations and polymorphisms

Over 150 pathogenic mutations have been identified in *NOTCH3* so far (**Table 1.2**). A mutational hot spot lies between the second and sixth of the 33 exons where almost 90% of the mutations cluster (**Figure 1.6A**). From the protein structural point of view, the mutation clusters are roughly divided into three regions: N-terminal region (or mutational hot spot, EGF1-6), ligand binding region (EGF8-14) and Abruptex region (EGF24-27) (**B**). The majority of mutations are missense (or point) involving either loss or gain of a cysteine residue. Other types of mutations include seven coding region deletions, one insertion, two splice site, one frameshift mutation and one duplication (Federico et al., 2005, Mazzei et al., 2004, Mazzei et al., 2008, Opherk et al., 2004, Peters et al., 2005b, Tikka et al., 2009), all of which result in an uneven number of

cysteines in the mutated EGF repeats instead of the normal even number of six. It has been suggested the 3D structural change due to abnormal disulphide bridging plays a role in the molecular pathology of CADASIL. Six studies, however, have reported point mutations and deletions, which involve no cysteine residue (marked with * in **Table 1.2**) (Adachi et al., 2006, Kim et al., 2006, Mazzei et al., 2004, Mizuno et al., 2008, Santa et al., 2003, Ferreira et al., 2007). Ungaro et al. (2009) also identified eight possible pathological mutations without cysteine involvement (R107W, Q151E, A198T, R207H, E309K, R592S, V644D and H1235L). The cysteine-sparing mutations may imply the significance of the positions on structural formation, enzymatic modification or protein interactions. It should be noted that six of those mutations result in loss of arginine, which is known to be involved in the maintenance of protein conformation and the enhancement of protein stability in other proteins (Borders Jr. et al., 1994, Mrabet et al., 1992, Woods, 2004).

A number of *NOTCH3* polymorphisms have also been identified in CADASIL. The most frequently found polymorphisms include c.684G>A (rs1043994) in exon 4 and c.381C>T (rs3815188) in exon 3 followed by c.2616T>C (rs1043996) in exon 16 (Ungaro et al., 2009).

exon	EGF	aa change
2	1	C43R
		C43G
		C43F
		C49G
		C49F
		C49T
		C49Y
		R54C
		S60C
		C65S
		C65T
		C65Y
3		C67S
		C67Y
		W71C
		R75P*
		C76R
		C76W
	2	Q77_C82del
		D80_S84del
		C87R
		C87Y
		A88_G91del*
		R90C
		C93F
		C93Y
		C93_Q94insC
		C106W
		C108R
		C108W
		C108Y
		R110C
4		G114_P120del
		C117R
		C117F
		S118C
	3	C123F
		C123Y
		C128PfsX32
		C128G
		C128F
		C128Y
		G131C
		A133C
		R133C
		C134W
		C134Y
		R141C
		F142C
		C144F

exon	EGF	aa change
4	3	C144S
		C144Y
		S145C
		C146R
		C146F
		C146Y
		G149C
		Y150C
		R153_C155del
		R153C
		C155S
		C155Y
	4	C162R
		C162S
		C162W
		R169C
		G171C
		C174R
		C174F
		C174S
		C174T
		C174Y
		S180C
		F181C
		R182C
		C183R
		C183F
		C183S
		R184C
		C185R
		C185G
		C185S
		Y189C
		P192_V200del
		C194R
		C194F
		C194S
		C194Y
	5	C201R
		C201Y
		C206R
		C206Y
		R207C
		C212S
		R213K*
		Y220C
		C222G
		C222Y
		C224Y
5		C233R

exon	EGF	aa change
5	5	C233S
		C233W
		C233Y
	6	V237M*
		D239_D253del
		C240S
		C245R
		C245S
		C251R
		C251G
		C251S
		C251Y
		Y258C
		C260G
		C260Y
6		C271F
	7	G296C
		S299C
	8	A319C
		R322C
		R332C
		S335C
		Y337C
		C338R
7	9	C366W
		C379S
		G382C
		C388Y
	10	C395R
8		C419R
		G420C
		R421C
		R427C
		C428R
		C428S
		C428Y
	11	E434_L436dup
		C435R
		C440R
		C440G
		C440S
		C446F
		C446S
		R449C
		C455R
		C457S
9		Y465C
	12	C484F
		C484Y
		C495Y

exon	EGF	aa change
10	12	C504R
	13	C511R
		C511Y
		G528C
		C531S
		R532C
11		C542Y
	14	R544C
		C549R
		C549Y
		R558C
		C568Y
		Y574C
		T577A*
		R578C
	15	R587C
		C591R
		R592C
		R607C
12	16	R640C
13	17	G667C
14	18	R728C
15	20	C775S
intron		P805_N856del
18	24	G953C
		R953C
	25	C977S
		S978R*
		F984C
		R985C
		C988Y
		C997G
19	26	C1004Y
		R1006C
		C1015R
		A1020P*
		Y1021C
		W1028C
		R1031C
20	27	G1058C
		G1063C
		Y1069C
		R1076C
	28	C1099Y
21	29	C1131W
22	31	R1231C
23	32	C1261R
		C1261Y

Table 1.2. *NOTCH3* mutations in CADASIL reported since 1996. Most mutations are clustered in exon 3 and 4. Five mutations which do not involve cysteine residue are indicated with *. del: deletion, ins: insertion, fs: frameshift, dup: duplication.

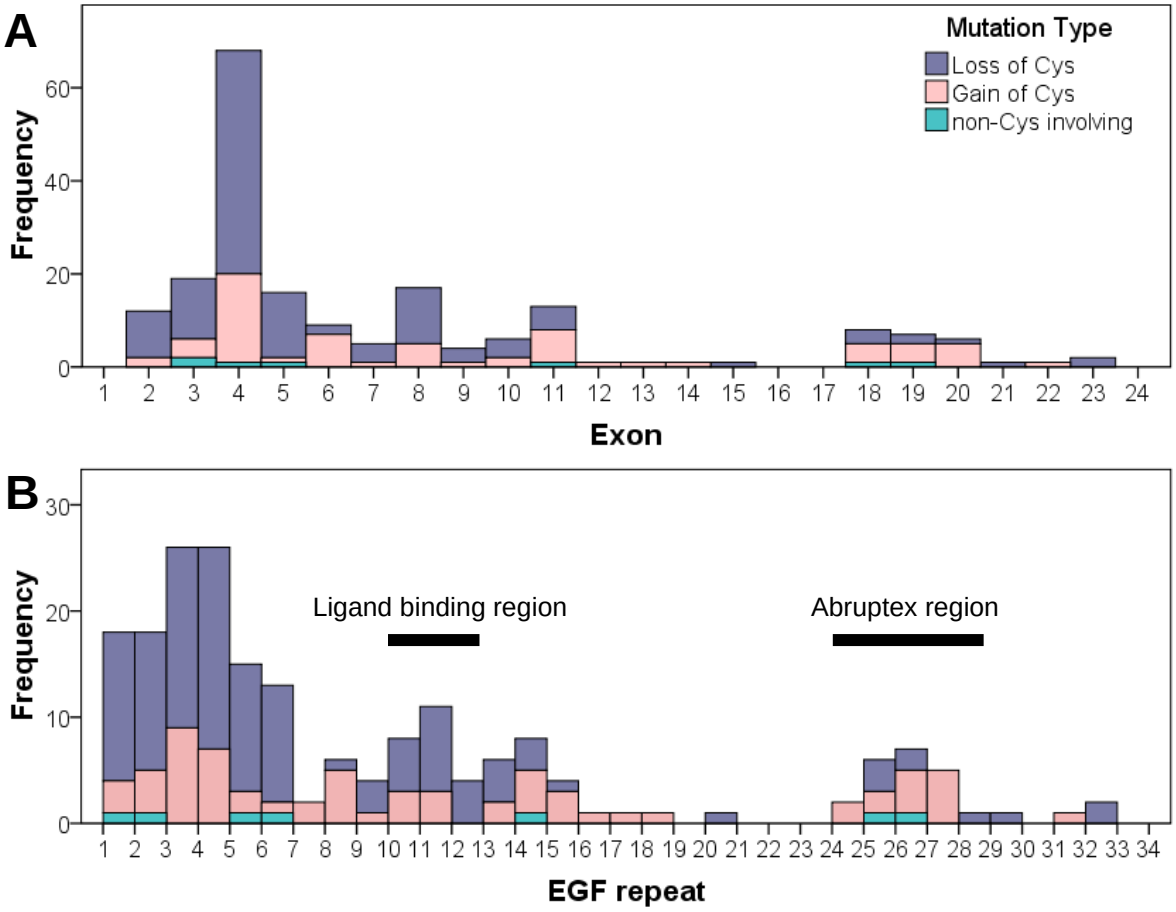

Figure 1.6. Distribution and frequency of *NOTCH3* mutations. Bars show number of loss/gain of cysteine and non-cysteine involving mutations per exons (A) and EGF-repeats (B). Details of mutations are listed in **Table 1.2**.

1.3.2.2 Animal models

Animal models, either knock-in or Tg, are useful tools to investigate the molecular and clinical pathology using conditions which are closer to those found in humans. Several mouse models have been developed to explore the effects of CADASIL mutations, and have succeeded in reproducing CADASIL pathologies to some extent.

Knock-in mice with R142C mutation in mouse *NOTCH3* (R141C in human) showed no vascular, WM or cognitive abnormalities, suggesting only human *NOTCH3* mutation (R141C) is pathogenic (Lundkvist et al., 2005). On the other hand, Tg mice with restricted expression of full-length human *NOTCH3* (R90C) mutant to VSMCs successfully exhibited CADASIL specific features such as GOM, N3ECD accumulation

and disruption of VSMC anchorage; consistent with these morphological changes, the mice exhibited significant deficits in cerebrovascular response and reactivity (Ruchoux et al., 2003, Lacombe et al., 2005). Tg mice with C428S mutation also developed N3ECD accumulation and GOM (Monet-Leprêtre et al., 2009). The problem with those Tg mice is that while they exhibit characteristic vascular pathologies, they failed to develop brain parenchyma lesions. The limitation probably stems from insufficient disease duration for the development of pathology, which is dependent on age, due to the significantly shorter life span of mice. Recently, Joutel et al. (2010) solved the problem by overexpressing mutant NOTCH3 (R169C) in a pattern similar to endogenous NOTCH3. The Tg mice succeeded to exhibit most of the CADASIL pathologies such as GOM, N3ECD accumulation, and progressive WM damage. They also showed reduced capillary density, impaired cerebrovascular autoregulation and subsequent decreased cerebral blood flow even without apparent structural abnormality of arteries, suggesting the vascular functional deficiency underlies the disease initiation.

1.3.2.3 Molecular pathogenesis

The key question is how the *NOTCH3* mutations lead to vascular degeneration and dysfunction, eventually resulting in arteriopathy and leukoencephalopathy in CADASIL patients. Many studies have tried to define the molecular pathogenesis of CADASIL without definitive success; loss and gain of functions have been considered and tested, resulting in varying and sometimes contradicting results. Although those studies shed light on a part of the molecular pathogenesis, the initial trigger of CADASIL vascular pathology is still shrouded in mystery.

There are various stages in the Notch3 signalling pathway which could be affected by the mutations. The most likely sites are at the proteolytic cleavages of NOTCH3 and the NOTCH3 receptor-ligand binding (**Figure 1.2**). Three reports demonstrated that

NOTCH3 receptors with mutations within and near the ligand binding domain (*e.g.* C428S, C455R and C542Y) exhibited diminished signalling activity due to varying mechanisms. C428S mutation either impaired ligand binding or obtained dominant-negative property, while C542Y mutation retarded presentation to the cell surface (Joutel et al., 2004, Monet-Leprêtre et al., 2009). C455R mutation was also shown to disrupt NOTCH3-ligand binding (Peters et al., 2004). On the other hand, mutations located in the mutational hot spot (*e.g.* R133C, R141C, C183R and C185R) seem to affect S1 cleavage possibly due to the impaired glycosylation by Fringe (Haritunians et al., 2005, Karlström et al., 2002, Peters et al., 2004, Arboleda-Velasquez et al., 2005). However, while impaired S1 cleavage may result in the reduced surface expression of mutant NOTCH3 (R141C), Jagged1-induced signalling activity remained intact (or even increased with C185R) in all of the cases (Haritunians et al., 2005, Peters et al., 2004, Karlström et al., 2002). Moreover, contradictory to the above reports, at least three other *in vitro* studies on CADASIL (R90C, R133C, C185R) or CADASIL-like mutations have shown that *NOTCH3* mutations in exons 3 and 4 do not impair full-length receptor maturation, intracellular trafficking or the signalling mechanism and retain the ability to activate RBP-Jκ (Joutel et al., 2004, Haritunians et al., 2002, Low et al., 2006). A transgenic mouse study further confirmed that mutant NOTCH3 (R90C) was fully functional and RBP-Jκ activity remained normal despite the presence of arterial defects and NECD/GOM accumulation (Monet et al., 2007). In contrast to the mutations in the ligand binding domain and the mutational hot spot, little is known about the impacts of mutations near the Abruptex region. At least one *in vitro* study reported that R1006C mutation did not impair receptor processing or RBP-Jκ-dependent Notch3 signalling activity (Joutel et al., 2004). Albeit from a NOTCH1 study, however, the Abruptex region, which is highly glycosylated by Manic Fringe, was demonstrated to compete with Delta for the Notch ligand binding domain (Shao et al., 2003, Pei and Baker, 2008).

The mutations in this region seem to alter the Fringe modification, resulting in enhanced Notch1 signalling (de Celis and Bray, 2000, de Celis et al., 1991). Thus, *NOTCH3* mutations in EGF24-27 may result in increased Notch3 signalling but we await the confirmation from *in vitro* and *in vivo* studies.

The above data indicate that there are no consistent outcomes of *NOTCH3* mutations in regards to Notch3 signalling activity. It suggests that *NOTCH3* mutations subtly and differentially affect receptor trafficking, processing and/or signalling activity depending on the position of the mutation. Or, the mutation affects the function specific to VSMC, possibly under a specific condition, as NOTCH3 function can be cell-type and context specific while many of those *in vitro* studies used non-VSMC cell lines (Beatus et al., 1999, Iso et al., 2003). Another thing to be noted is that the phenotypes of CADASIL or *NOTCH3* transgenic (Tg) mice only partially overlap with those of *NOTCH3* deficient mice: both showed impaired arterial myogenic response (though again, the type of alteration differs between studies), but VSMC degeneration, N3ECD accumulation and GOM were only reported in *NOTCH3* Tg mice (Domenga et al., 2004, Dubroca et al., 2005a, Hussain et al., 2004, Peters et al., 2005a, Joutel et al., 2010, Belin De Chantemèle et al., 2008). Hence, loss of NOTCH3 function cannot sufficiently explain the whole range of CADASIL pathologies.

An alternative hypothesis is (toxic) gain of function, a common mechanism in many neurodegenerative diseases. This hypothesis is supported by the fact that most mutations are located in the regions of poorly conserved sequence (Donahue and Kosik, 2004, Federico et al., 2005), and that in most cases, Notch signalling activity remains intact. Deposits or aggregations of misfolded proteins due to a novel folding pathway are often the cause of toxicity (Bucciantini et al., 2002, Kirkitadze et al., 2002), and as described

earlier, characteristic accumulations of N3ECD and GOM are found in the CADASIL vasculature, indicating that the clearance of the NECD may be damaged by the mutations (Joutel et al., 2000, Dziewulska and Rafalowska, 2008). The increased cytoplasmic expression of ubiquitin, which modulates NOTCH3 endocytosis and lysosome degradation (Jia et al., 2009, Sorkin and Von Zastrow, 2009) in VSMC and vascular lamina media also support the idea. In fact, several studies demonstrated the accumulation of Notch3 mutants (R133C and C185R) in ER, upregulation of unfolded protein response related proteins and increased susceptibility to stress, proposing ER stress responses as a cause of VSMC degeneration (Ihalainen et al., 2007, Takahashi et al., 2010). The ER stress hypothesis is also supported by the studies demonstrating the increased multimerization and intracellular aggregation of Notch3 mutants (R133C, R141C and C183R) (Opherk et al., 2009, Karlström et al., 2002). However, those results derived from *in vitro* studies over-expressing mutant NOTCH3 and no report has been made of intracellular NOTCH3 accumulation in human biopsy samples. Moreover, arteries in Tg mice (R90C) start to exhibit pathological changes even before the accumulation of N3ECD and GOM (Ruchoux et al., 2003). The authors stated that the first apparent pathological changes were the disjunction of VSMCs and increased number of dense intracellular plaques. Another study on Tg mice also reported that overexpression of both Notch3 mutant (R169C) and wild type did result in cytoplasmic inclusions in mice as seen in *in vitro* studies but only mutant Tg mice developed vascular defects and WM lesions (Joutel et al., 2010). Therefore, cerebrovascular dysfunction and rarefaction were proposed as the causes of WM damages. Although there still is a possibility that abnormal accumulations exacerbate the existing vascular pathology – especially considering that overexpression of NOTCH3 accelerated the onset of WM lesion formation – other alterations which result in the disturbance of VSMC adhesion followed by impaired myogenic response, seem to be the initial trigger.

Structural integrity maintained by cell-cell adhesion molecules, such as cadherin and connexin, is important for the regulation of myogenic tone, which was suggested to be modulated through the RhoA/Rho kinase pathway (Lagaud et al., 2002, Earley et al., 2004, Belin De Chantemèle et al., 2008). In addition, Lyon et al. (2010) recently demonstrated that inhibition of N-cadherin in VSMC resulted in decreased migration (contributing to reduced intimal thickening, which is not observed in CADASIL) and increased apoptosis further supporting the possible involvement of cadherin in CADASIL pathology. As mentioned in 1.2.3.1, N-cadherin expression is regulated by Notch3 signalling though its exact mechanism is still unclear (Wang et al., 2007). As all the *in vitro* and *in vivo* studies mentioned previously examined only CBF-1/RBP-Jκ-dependent Notch3 signalling activity and found no change in some cases, the cadherin expression and myogenic tone may be regulated by RBP-Jκ-independent pathway.

Considering all the data presented above, the alteration of cell-cell adhesion molecules due to unknown mechanisms may play an important role in the initiation of the vascular pathology leading to impaired vascular tone, while the other pathologies, such as N3ECD accumulation and GOM deposits, could stem from other mechanisms (*e.g.* impaired endocytosis or degradation) and may be contributing to the development of vascular and neuronal pathologies in CADASIL. Interestingly, Joutel and colleagues (2008) reported an SVD case with *NOTCH3* mutation characterized by CADASIL-like features including TIA/stokes, diffuse WM hyperintensity and enlarged PVS, but lacked hallmarks of CADASIL, *e.g.* involvement of temporal pole on MRI, GOM and NECD accumulation. The mutation L1515P was in the juxtamembranous region critical for NOTCH3 heterodimerization, and resulted in activated Notch3 signalling despite the defect in S1 cleavage due to the unstable NECD-ICD heterodimer. The pathologies and phenotypes of this mutation imply that CADASIL pathologies cannot be simply

explained by loss or gain of NOTCH3 functions, and unidentified NOTCH3-mediated pathway or crosstalk may be involved in the pathogenesis. Future studies should include investigation into the molecular basis of cell-cell adhesion molecule induction by NOTCH3, crosstalk between NOTCH3 and other pathways, and also RBP-Jκ-independent pathway.

1.3.2.4 Phenotypic variability and modifiers

Another confounding feature of CADASIL is its diverse phenotypic variability between individuals: patients with the same mutation, even from the same family, often manifest different clinical symptoms and different ages of onset, while patients with different mutations or zygosity can exhibit similar symptoms (Uyguner et al., 2006, Singhal et al., 2004, Dichgans et al., 1998, Tuominen et al., 2001). Several studies have reported associations between certain genotypes and phenotypes. Mutations in the ligand binding domain (*e.g.* C428S, C440G and C455R), which result in the reduced Notch3 signalling activity, were linked to milder cognitive impairment and disability despite the higher volume of WM hyperintensity on MRI (Arboleda-Velasquez et al., 2002, Monet-Leprêtre et al., 2009, Singhal et al., 2004). C455R was also associated with the early onset of stroke (Arboleda-Velasquez et al., 2002). Two mutations from the mutational hot spot (exon 4) resulted in similar phenotypic features: C117F was associated with a lower age at death and the C174Y mutation with a lower age at onset for stroke and death (Opherk et al., 2004). On the other hand, patients with R153C, also in the mutational hot spot, exhibited increased number of microbleeds and those with S180C showed anticipation of onset age (Lesnik Oberstein et al., 2001, Nakamura et al., 2005). However, even with those mutations, the phenotypic differences are subtle, and with most of the mutations, there is no clear genotype-phenotype association (Adib-Samii et

al., 2010, Singhal et al., 2004, Opherk et al., 2004), suggesting the involvement of modifying factors, either genetic or environmental, in CADASIL.

A population-based study has suggested the strong genetic influence on severity of WM hyperintensity though the modifying gene(s) has yet to be identified (Opherk et al., 2006). The connection between *NOTCH3* polymorphisms and onset or strokes has been suspected but no association have been found (Mizuno et al., 2002). The only association between CADASIL phenotype and genetic variance found so far was between the *NOTCH3* polymorphism rs1043994 (G684A), which is frequently found in CADASIL patients, and migraine (especially without aura) (Ungaro et al., 2009, Schwaag et al., 2005). The authors speculated that the polymorphism may be in linkage disequilibrium with another *NOTCH3* variant as it does not lead to the amino acid substitution. Also, the influence of apolipoprotein-E genotype, which was implicated in various brain injuries, and cardiovascular risk factors were tested without any positive results, except for the elevated homocysteine level and migraine (Singhal et al., 2004, Van Den Boom et al., 2006). Another candidate for genetic modifier was mitochondrial mutation for two reasons. Firstly, mitochondrial dysfunction has been reported in CADASIL (Dotti et al., 2004, De La Peña et al., 2001). Secondly, a mitochondrial mutation (5650G > A), which was also reported in a CADASIL patient, was previously related to myopathy (McFarland et al., 2008, Annunen-Rasila et al., 2007). However, no association was identified in a small-scale study (Abu-Amero et al., 2008).

Environmental factors require special attention especially when the study subjects are from the same family. As Mykkänen et al. (2009) pointed out in the report of an identical twin, environmental and life style factors seem to significantly affect the severity and the progression of disease. The twin with the smoking habit from a very

young age experienced the first stroke 14-years earlier than the other, and suffered more lacunar infarcts and exhibited more severe functional disability compared to the other, who had no smoking history and participated in intense physical activity. Another study also confirmed the association between early onset of stroke and smoking (Singhal et al., 2004). Although no other environmental factors have been associated to the CADASIL phenotypes so far, other factors already related to neurodegenerative diseases, such as air pollution, diet, and exercise, should also be considered (Migliore and Coppedè, 2009).

1.3.3 Therapeutic approaches

Treatment of CADASIL is currently restricted due to the poor understanding of the disease pathogenesis. Cholinesterase inhibitors have been proven to be effective in improving cognitive decline and disability in AD, especially in those with cerebrovascular factors (Erkinjuntti et al., 2002, Kumar et al., 2000). Cholinesterase inhibitors including donepezil were also tested on VaD and have been shown to improve cognitive function (but not global, functional or behavioural outcome), and work better for patients with cortical and multiple territorial lesions (compared to those predominantly with subcortical lesions) or without hippocampal atrophy (Kavirajan and Schneider, 2007, Román et al., 2010). A randomised clinical trial of donepezil on CADASIL patients showed a similar result, demonstrating no positive effect on global cognitive function or physical functions but enhanced executive functions and processing speed (Dichgans et al., 2008). The lack of significant clinical improvement with cholinesterase inhibitors has lead to the search for new treatment strategy, *i.e.* improvement of cerebral perfusion, which correlates with disability and cognitive impairment (Bruening et al., 2001). Ca2+ channel blocker lomerizine successfully increased cerebral blood flow (CBF) and improved the cognitive decline in CADASIL

during 2-year treatment period, demonstrating the efficacy of this approach (Mizuno et al., 2009). Acetazolamide, a carbonic anhydrase inhibitor which works as cerebral vasodilator, has also been tested on CADASIL patients and was shown to increase CBF though whether it can improve cognitive impairment is yet to be tested (Huang et al., 2010, Chabriat et al., 2000). Another approach, albeit from *in vitro* study, was recently proposed by an American group, which showed that long-term treatment with valproate, an anticonvulsant/mood stabiliser, can inhibit VSMC apoptosis by activating Notch3/c-FLIP cascade (Yuan et al., 2009). Though its potential is unknown, it may help to delay the disease progression.

These treatments, however, are only symptomatic and thus it is important to establish the basic knowledge of CADASIL pathology to find a complete therapy.

1.4 Vascular functions and cerebrovascular disorders

The brain is heavily dependent on constant blood supply and its interruption, even momentary, can cause serious damage that manifests as neurological symptoms. Regardless of the molecular pathogenesis in CADASIL, it is the disruption of the physiological cerebrovascular functions that is the most likely direct cause of brain damage. The following sections describe the structure and function of the cerebrovasculature from the physiological viewpoint, and also document pathological changes in SVD.

1.4.1 Blood-brain barrier

At the luminal surface, blood vessels in the brain are lined with single-layer cerebral endothelial cells tightly adhered to the basement membrane and joined end to end by tight junctions. The cerebral endothelium is further surrounded by an elastic lamina, VSMCs and loose connective tissues in arterioles and arteries (**Figure 1.7**). The tight

endothelial layer called the BBB functions as a physical barrier, which restricts the molecular traffic to and from the brain. There are only three routes through the BBB, carrier-mediated transport, receptor-mediated transcytosis, and active efflux transport, which transports nutrition to the brain (*e.g.* oxygen and glucose), remove neurotoxins or metabolic byproducts from the brain, and modulate ion balance of which disruption is critical for neurons (Eisert and Schlachetzki, 2008). Additionally, the intracellular and extracellular enzymes help to inactivate potentially neurotoxic lipophilic substrates, preventing them from penetrating BBB via a diffusive route (Abbott et al., 2006). The proper functioning and integrity of BBB requires the interactions between cerebral endothelial cells and astrocytes, pericytes, and the extracellular matrix as well as neuronal activities (Persidsky et al., 2006). The significance of the so-called neurovascular unit in brain homeostasis has been extensively studied. Astrocytes, of

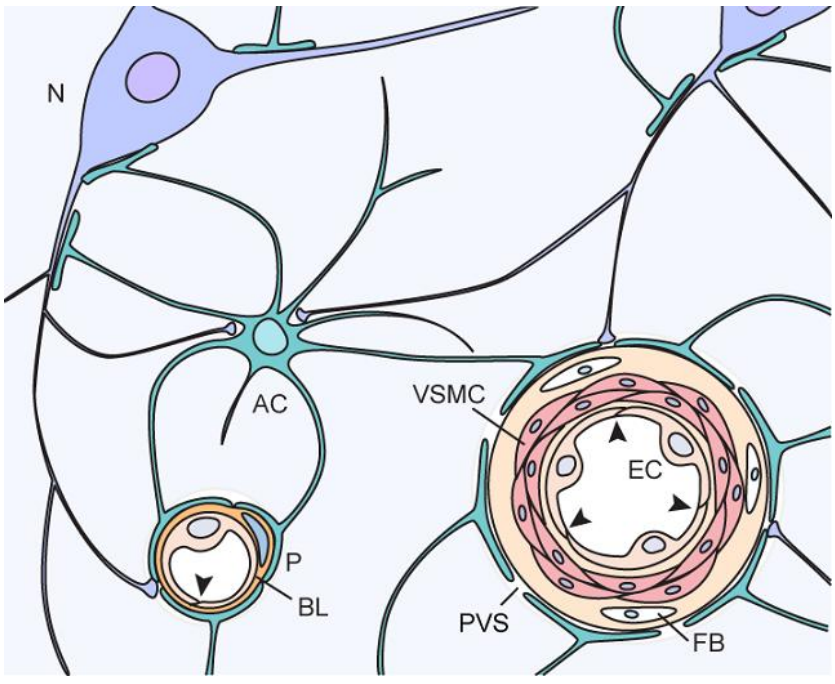

Figure 1.7. Neurovascular unit. Endothelial cells (EC) are connected with tight junctions (arrowheads) to form the Blood-Brain Barrier (BBB). In the larger vessels, the EC layer is further surrounded by vascular smooth muscle cells (VSMC), fibroblasts (FB) and connective tissues. The structure and functions of BBB and arterial myogenic tone are controlled by the interactions between vessels and pericytes (P), astrocytes (AC) and neurons (N). BL: basal lamina, PVS: perivascular space

which end feet almost completely surround the capillary surface, play an important part in the formation and maintenance of the BBB. They not only promote the expression of tight junctions and strengthen the physical barrier, but also modulate the expression of membrane transporters and enzymes to maintain transport and metabolic barrier function (Abbott et al., 2006). The functions of other neurovascular components are rather ill-defined compared to astrocytes. The lack of pericytes results in capillary deformation, suggesting their role in BBB formation (Sandoval and Witt, 2008). Several different subtypes of neurons have been reported to interact with endothelial cells and/or astrocytes, and their decreased activities were found in pathological states with BBB dysfunction, but no direct evidence of their function over the BBB has been found so far (Hawkins and Davis, 2005).

BBB dysfunction is often observed in SVD patients with leukoaraiosis (Topakian et al., 2010). Although BBB dysfunction can be a part of the disease progression as in multiple sclerosis, it is suggested to be secondary pathology to ischemia and hypoxia in SVD (Hawkins and Davis, 2005). Initial changes observed after ischemia are swelling of endothelial cells, astrocytes and neurons, and degradation of the vascular extracellularmatrix (Sandoval and Witt, 2008). Secretion of cytokines (*e.g.* interleukin-1β and TNF-α) and chemokines (*e.g.* monocyte chemoattractant protein-1) by the endothelium, and the following infiltration of leukocytes also occur at the early stage of post-ischemic changes and are suggested to contribute to inflammation, oedema and neuronal injury (del Zoppo, 2009). In addition, ischemia causes the disruption of tight junctions, basal lamina and glia limitants, and the increased activity of pinocytosis and vesicular transport in endothelial cells, all of which contribute to the increased permeability of the BBB (Eisert and Schlachetzki, 2008). Of all the components of the neurovascular unit, neurons and astrocytes are particularly vulnerable to ischemia-

induced inflammation and oxidative stress compared to microglia/pericytes and endothelial cells (Eisert and Schlachetzki, 2008).

1.4.2 Cerebrovascular tone

Cerebral arteries are generally divided into the leptomeningeal and perforating arteries and extend into various brain regions to supply oxygen and nutrition (Tatu et al., 2008). Here again, the neurovascular unit plays a pivotal role in ensuring stable cerebral perfusion. CBF is modulated by the neuronal activity directly or indirectly via astrocytes and endothelial cells. Vasoactive substances from neurons (*e.g.* acetylcholine, norepinephrine and 5-HT), astrocytes (*e.g.* 20-HETE and prostaglandin E2) or endothelial cells (*e.g.* NO, prostacyclin and endothelin) induces changes in intracellular ion concentration (K+, H+ and Ca2+) and light chain myosin phosphorylation in VSMC to promote vasodilatation or vasoconstriction (Iadecola, 2004, Hamel, 2006). The local vasodilation is transmitted to upstream vessels, through the conduction of the vessel response or change in flow (shear stress) that induces endothelium-dependent vasodilation, for the efficient control of blood flow and pressure within the cerebrovasculature (Iadecola, 2004).

Impaired cerebrovascular tone has been suggested to contribute to the development of chronic ischemia and the following leukoaraiosis in SVDs (Markus, 2007). Some of the recently characterised examples of the hereditary SVDs are CADASIL, CARASIL and HIHRATL (**Table 1.1**). Not only the *NOTCH3* gene mutations in CADASIL but also those in HtrA serine protease 1 (*HTRA1*) gene and procollagen type IV α1 (*COL4A1*) gene are demonstrated to cause cerebrovascular dysfunction (Dubroca et al., 2005a, Stenborg et al., 2007, Oide et al., 2008, van Agtmael et al., 2010). CARASIL is an autosomal recessive SVD with leukoencephalopathy and severe arteriopathy

characterised by VSMC degeneration, vessel wall thickening, medial hyaline degeneration and splitting of the internal elastic lamina (Oide et al., 2008, Arima et al., 2003). The mutations in *HTRA1*, a repressor of TGF-β signalling, result in increased TGF-β activity in the small cerebral arteries (Hara et al., 2009) while constitutive activation of TGF-β was reported to result in the inhibition of endothelin1–induced p38 MAPK/27kDa heat shock protein pathway, leading to the vasoconstriction defect (Tong and Hamel, 2007). On the other hand, *COL4A1* mutations in HIHRATL, which cause detachment of endothelium, affect NO-mediated vasodilation. Although the mechanism is yet to be determined, deposition of mutant collagen type IV was suggested to induce ER stress response, leading to reduced NO synthesis (van Agtmael et al., 2010). The presence of hereditary SVDs with mutations in genes related to vascular autoregulation emphasises the importance of unperturbed cerebral perfusion.

1.4.3 Perivascular lymphatic drainage system

Two cerebral drainage pathways, namely cranial/spinal arachnoid villi and the lymphatic drainage, are responsible for the drainage of cerebral interstitial fluid (ISF) and cerebrospinal fluid (CSF) into the blood circulation and the lymphatic system, respectively (Weller et al., 2009). While the former pathway is the main route of CSF drainage in human, the latter is important for the perivascular drainage of ISF. ISF flows along the basement membrane of capillaries and also between VSMCs in arterial walls, eventually draining to deep cervical lymph nodes at the base of the skull (Clapham et al., 2010, Weller et al., 2009) (**Figure 1.8**). The perivascular drainage helps the removal of solutes from the brain; the best example would be Aβ, which accumulates in cerebrovascular walls of the elderly and AD to cause CAA due to the disrupted clearance of amyloid-β through the perivascular pathway (Weller et al., 2008). Weller's group (2006) proposed cerebrovascular tone as the driving force that generates reverse

flow against blood flow along the perivascular pathway. Thus, the disruption of cerebrovascular tone, either by ageing or disease pathology, results in the prolonged time for ISF/solutes to be in close contact with vessel walls, promoting the deposition of proteins prone to accumulate, such as Aβ within the basement membranes. The deposition causes "protein-elimination failure arteriopathy (PEFA)" that may increase susceptibility to haemorrhage and ischemia, and further disrupts the drainage of ISF and solutes (Weller et al., 2010). Given the overall evidence for cerebrovascular dysfunction in SVD, it is plausible that PEFA is involved in their pathogenesis.

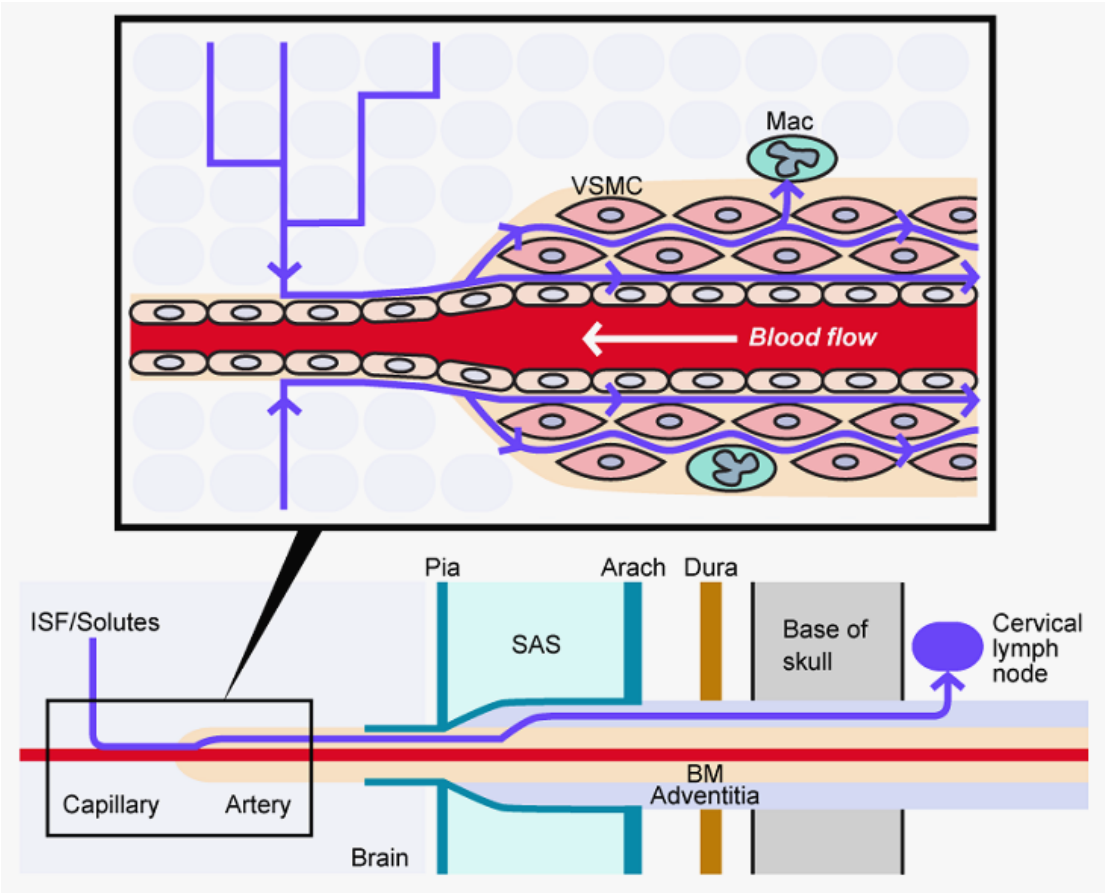

Figure 1.8. Perivascular lymphatic drainage pathway. Interstitial fluid (ISF) and solutes from brain parenchyma move along the basement membrane of capillaries and arteries, and then adventitia around leptomeningeal arteries to drain out into cervical lymph nodes at the base of the skull. Arterial pulsation is the driving force of the perivascular drainage pathway, which flows opposite to the blood flow. Solutes can be ingested by vascular smooth muscle cells (VSMCs) and perivascular macrophages (Mac). Pia: pia mater, Arach: arachnoid, SAS: subarachnoid space, BM: basement membrane

1.5 Aims and thesis outline

In view of the foregoing background, the aims of the study were to characterise the cerebral pathology of CADASIL in order to reveal the pathogenic basis of the disorder phenotypes, especially related to cognitive dysfunction. The main issues addressed in this thesis are:

1) The extent of vascular and perivascular changes and the difference between sporadic SVD, with reference to the characteristic anterior temporal pole MRI hyperintensity in CADASIL.

2) Relationship of GOM and N3ECD and possible involvement of a perivascular drainage system in CADASIL pathogenesis.

3) Involvement of hippocampal pathology and/or WM disconnection to CADASIL cognitive impairment.

The following chapter describes general materials and methods used in this study, chapters three to six contain results, and the final chapter contains an overall discussion. Chapter three and four were devoted to the characterisation of the vascular and perivascular pathology in CADASIL. Vessel wall thickening and PVS enlargement were quantitatively assessed and compared with controls and sporadic SVD cases. Localisation of GOM and the N3ECD accumulation in CADASIL in relation to arterioles and capillaries were also evaluated using bright-field immunohistochemical and electron microscopic immunohistochemical methods. The subsequent chapters address neuronal pathology in CADASIL. The density of neurons in hippocampal formation, which has been reported to be decreased in several forms of dementia, was quantified using a 3-dimentional stereology method. The result provided an insight into

the neuronal basis for the cognitive features in CADASIL, for the first time. The density of damaged axons, as indicated by SMI32 immunostaining, was also measured to evaluate the distribution and extent of WM damage in CADASIL. In conclusion, a comparison of pathological changes associated with cognitive deficit in CADASIL and other dementias were discussed.

Chapter 2. Materials and Methods

2.1 Introduction

This chapter describes the diagnostic criteria for CADASIL, SVD and Cognitive function after stroke (COGFAST) cases, and definition of controls. It also outlines the brain sampling methods and histological protocols used to stain brain sections followed by the details of image and statistical analysis.

2.2 Study subjects

2.2.1 Cognitive tests

Cognitive functions of COGFAST and CADASIL patients were evaluated by clinical psychologists using following cognitive tests.

2.2.1.1 Mini-mental state examination

Mini-Mental State examination (MMSE) is a short questionnaire test for screening cognitive impairment (Folstein et al., 1975). It is the most commonly used cognitive test for its sensitivity and specificity though they can be affected by age, sex, cultural background and educational level (Gagnon et al., 1990, Crum et al., 1993). The MMSE is comprised of five sections: orientation, registration, attention and calculation, recall, and language and praxis. Most frequently used cut off score is 23 and a score of 23 or less suggest the presence of cognitive impairment. For classification purpose, scores of 27-30 is considered normal, 21-26 as mild cognitive impairment, 10-20 as moderate and <10 as severe cognitive impairment (van Gorp et al., 1999, Mungas, 1991).

2.2.1.2 CAMCOG

CAMCOG (Cambridge Cognitive Examination), which is a cognitive test section of CAMDEX (Cambridge Mental Disorders of the Elderly Examination), was designed to

assess various cognitive functions for the diagnosis and grading of dementia (Roth et al., 1986). It comprises of 67 items covering broader range of cognitive functions (orientation, language, memory, praxis, attention, abstract thinking, perception and calculation) and is modified by age and educational level, thus more effective in differentiating non-demented and demented (including mild dementia) individuals than MMSE (de Koning et al., 1998, Lindeboom et al., 1993). The commonly-used cut point of CAMCOG is 79/80 where 92% sensitivity and 96% specificity can be achieved (Roth et al., 1986).

2.2.2 Diagnosis and definition of groups

2.2.2.1 Cerebral small vessel disease and CADASIL

Cerebral SVD is a general term for diseases with pathological alternations of small arteries, arterioles venules and capillaries of the brain, which result in small, and often silent, subcortical infarcts, WM lesions, haemorrhages and microbleeds. The cause of the pathological changes varies between cases, well-known examples including Binswanger's disease and CADASIL (Kalaria and Erkinjuntti, 2006). SVD cases in this study include those of mixed sex with pathological changes in small vessels and multiple small/micro infarcts or lacunar infarcts. Age range was 67 - 96 years.

CADASIL is a familial form of cerebral SVD caused by defects in VSMC. The CADASIL cases in this study were either a member of the known CADASIL families or individuals initially suspected of CADASIL based on MRI, clinical features and family history, and confirmed of the diagnosis by the genetic screening for the *NOTCH3* mutation. Alternatively, skin biopsy was performed to confirm CADASIL-specific GOM. For details, see **Table 2.1**.

Subjects	Age(yr)	Sex	Mutation	Disease Duration (yr)	Notable clinical features and risk factors
CAD1	44	F	Arg153Cys	8	Cardiac arrhythmias
CAD2	52	M	Arg141Cys	10	No vascular risk
CAD3	53	F	Arg133Cys	6	No vascular risk
CAD4	55	M	Arg558Cys	11	Brief history of gout
CAD5	58	M	-	n/a	n/a
CAD6	59	M	Arg169Cys	12	No vascular risk
CAD7	61	M	Arg169Cys	10	Obesity (55yr -)
CAD8	63	M	Arg141Cys	10	Enlarged thyroid
CAD9	65	M	Arg141Cys	13	Parenchymatous goitre
CAD10	66	F	-	n/a	n/a
CAD11	68	F	Arg133Cys	18	Smoking history
CAD12	68	M	Arg153Cys	28	Smoking, prostate tumour

Table 2.1. Details of CADASIL cases.

2.2.2.2 COGFAST cases

COGFAST study is a prospective cohort study following up cognitive functions of post-stroke patients. The aims of the study are to elucidate the mechanism of delayed cognitive impairment after stroke and to determine factors influencing the fate of post-stroke survivors. To eliminate acute post-stroke cognitive impairment and noise, patients who were older than 75 years old and without cognitive impairment at three months after stroke were recruited for the study. MRI and cognitive tests were conducted at the entry to the study and subsequently, changes in cognitive functions were evaluated once a year after stroke using MMSE and CAMCOG. Follow-up MRI scans were also taken for patients enrolled into structural of functional study. Autopsy was performed 24-92 hours after death and the brain was fixed in 10 % buffered formalin for 1- 8 months. Braak stage and CERAD (consortium to establish a registry for Alzheimer's disease) score were determined by a neuropathologist. From 54 COGFAST cases autopsied so far, demented cases were selected for analysis based on the criteria that they have no or little AD pathology (Braak stage ≤ 3) and with MMSE score of less than 21. The age range of the resulting cases was 82 – 98 years.

2.2.2.3 Control criteria

Controls were selected on the basis of the absence of any significant vascular or neurological pathology. As the mean age of CADASIL and SVD or COGFAST cases were significantly different, two control groups (young and old controls) each age-matched to each disease group were prepared. Cause of death varied between cases but cancer (gastric, bowel and lung) was inevitably frequent in young controls.

2.2.3 Brain tissues

Formalin fixed, paraffin embedded blocks of human brain tissue were obtained from the Newcastle Brain Tissue Resource Centre, Institute for Ageing and Health, Newcastle University. Some of the control cases were acquired from the Medical Research Council Sudden Death Brain & Tissue Bank, the University of Edinburgh. 2 CADASIL cases were acquired by courtesy of Dr. Kretzschmar, Ludwig Maximilians University, Munchen, Germany. The use of the tissue for our research project was additionally approved by the Brain Bank Committee. The primary Neuropathological diagnosis and observations were transcribed from postmortem reports. Brains with fixation length of less than 10 months were selected for the studies where possible to reduce the variability in immunohistochemical (IHC) staining intensity due to the fixation length. CADASIL brains were obtained from Newcastle (n = 4), Oxford (1), London (1), Bristol (3), America (1) and Germany (2) (**Table 2.1**). As the Bristol cases (CAD2, 8 and 9) were fixed for notably long time, they were excluded when fixation length significantly affects the intensity of IHC. Brain areas investigated in this study are frontal lobe, temporal lobe (hippocampus and entorhinal cortex) and temporal pole.

2.2.3.1 Frontal lobe

Frontal lobe, which consists of motor, premotor and prefrontal regions, is associated with executive functions, attention, long-term memory, speech, emotions and reasoning

(Chayer and Freedman, 2001). Impairment in frontal lobe functions is implicated in various disorders such as SVD, schizophrenia and attention deficit disorder (Nakamura et al., 2008, Krain and Castellanos, 2006, Chen et al., 2009). As hyperintense MRI signal is observed in the frontal lobes of asymptomatic and symptomatic CADASIL patients (Coulthard et al., 2000), frontal lobe tissues at the coronal level of 4-5 in Newcastle Brain Map were selected for the analysis (**Figure 2.1**). The area contains Brodmann areas (BA) of 8 and 9, dorsolateral prefrontal cortex, which are involved in management of uncertainty, attention and working memory.

2.2.3.2 Hippocampal areas and entorhinal cortex

Hippocampus and adjacent entorhinal cortex are important areas for autobiographical, declarative and episodic memory. Information from other areas of the brain is sent to dentate gyrus and CA1 through layer II and III of entorhinal cortex, respectively. The information travels through CA3, CA1, subiculum and finally back to layer V of entorhinal cortex, which relay the signal to neocortex via parahippocampal and perirhinal cortex (Amaral and Lavenex, 2006). Temporal lobe block was chosen from coronal level of 16-18, where entorhinal cortex (BA28 and 34) is present. Hippocampal areas and entorhinal cortex were defined as described by the others (Amaral and Insausti, 1990, Insausti et al., 1998). CA2 forms a tight band of large pyramidal cells, which broaden at the border between CA1 containing a substantially heterogeneous group of neurons. Layer V of entorhinal cortex, consisting of large pyramidal neurons, is located above medium-sized pyramidal layer III (caudal or rostral) or cell-sparse layer IV (intermediate).

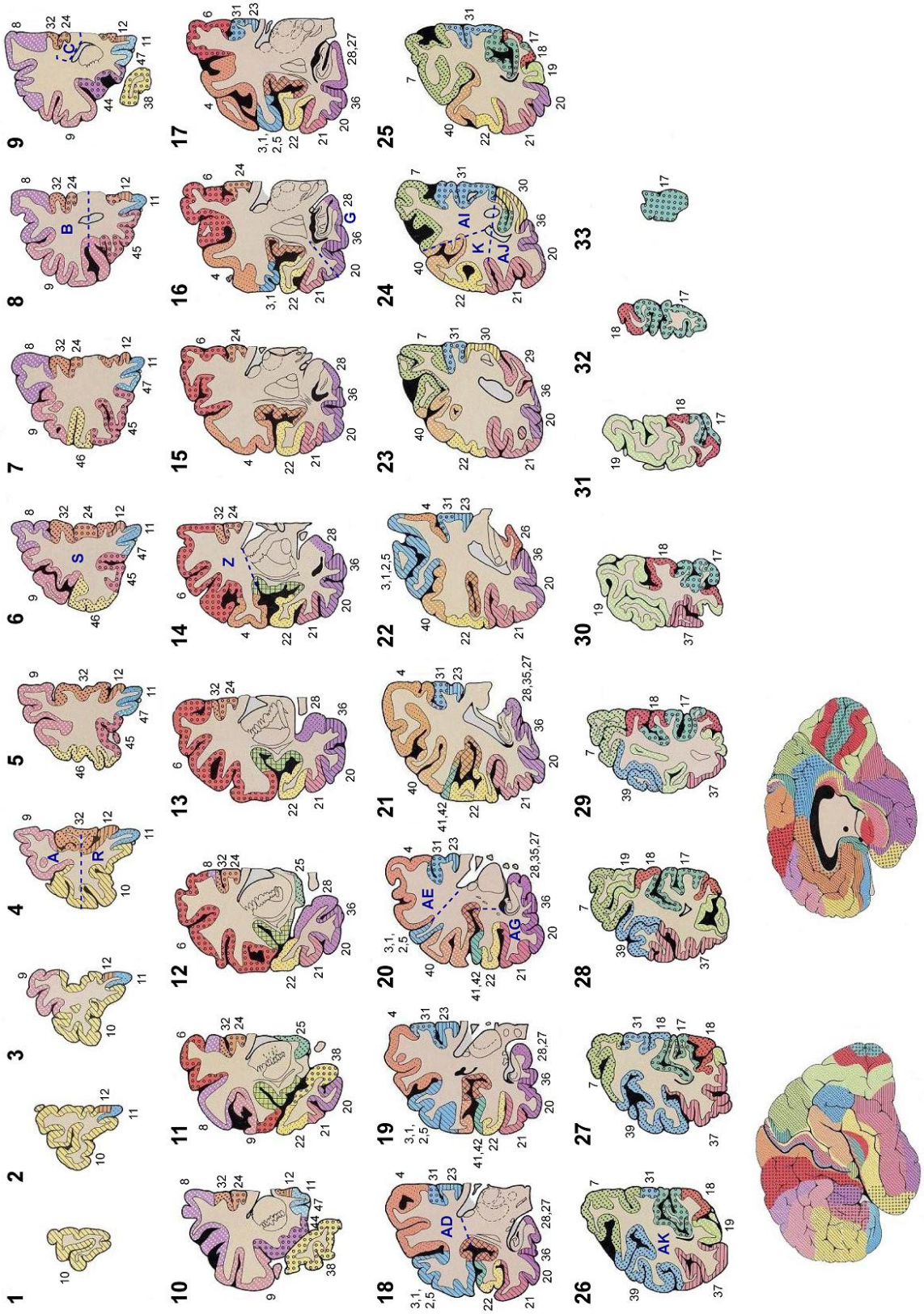

Figure 2.1. Newcastle Brain Map. Brain tissues were obtained from the described coronal levels. Numbers indicate Brodmann areas. Block code was marked with alphabets (navy letters).

2.2.3.3 Temporal pole

Temporal pole is an area where MRI hyperintense signal is frequently found in memory and personal semantic memory (Olson et al., 2007). Temporal pole blocks from the coronal level of 10-12, including BA20, 21, 22, 28, 36 and 38, were used for the study.

2.2.3.4 Routine pathological evaluations

As a routine diagnostic procedure, brain samples were examined by neuropathologists for the pathological changes consistent with AD, DLB and vascular dementia. Routine staining methods include silver staining, modified Bielschowsky, Gallyas and Palmgren's stain, luxol fast blue (LFB), and haematoxylin and eosin (H&E). Vascular lesions were noted as cortical/subcortical multiple infarcts, lacuna infarcts, microinfarcts and small vessel disease. AD pathology was evaluated using Braak staging and CERAD rating. Cortical Braak staging is commonly used pathoanatomical classification of AD stages. The pathological states are categorized into six distinct stages based on the topographical distribution pattern of neurofibrillary tangles and neuropil threads in the brain (Braak and Braak, 1991). Those tangles are primarily restricted to the transentorhinal region at stage I-II and spread to entorhinal region, moderately affecting CA1 at stage III and then severely at stage IV. At stage V, all regions in hippocampus and neocortex are affected and the pathology is aggravated at stage VI. Stages I and II are asymptomatic with more than 50% of individuals over 50 years old reaching these stages (Duyckaerts and Hauw, 1997). From stage III, neurofibrillary tangles and neuropil threads begin to cause neuronal death, causing cognitive impairment, and patients are diagnosed of dementia by stage V.

CERAD is also a neuropathological criterion for the diagnosis of AD. The plaque score is graded based on the number of neuritic plaques per x100 light microscopic field (none, sparse, moderate and frequent) and age at death: score A indicates uncertain

evidence of AD, B is suggestive of AD and C is an indication (Mirra et al., 1991). The plaque score is further integrated with clinical history of dementia to determine the certainty of AD diagnosis.

2.3 Histology

Paraffin embedded blocks were cut into 10 - 30 µm sections using a microtome (Shandon Finesse E+, Thermo Electron Corporation) and sections were mounted onto 4 % APES coated slides. Slides were dried in 37 ˚C incubator for 2 days and the wax was melted at 60 ˚C for 30 minutes prior to the dewaxing in xylene. The concentration of the primary antibody was determined for each by titering using positive control sections.

2.3.1 H&E

H&E staining was used to visualize brain tissue for PVS and sclerotic index (SI) analysis. After dewaxing and re-hydration, 10-µm sections were immersed in haematoxylin solution for 30 seconds and rinsed in water. The sections were differentiated in 1% acid alcohol, washed in water and then in ammonia water to blue. Rinsed sections were counterstained in eosin for 3-4 minutes, dehydrated in increasing alcohol, and cleared in xylene before mounted in DPX.

2.3.2 LFB

LFB is a suitable staining for the visualisation of myelinated axons in WM. 10-µm sections were incubated in LFB solution for two hours at 60 °C and left at room temperature for 10 minutes before rinsed in 70% alcohol and then in water. The differentiation was conducted by immersing sections in 1% lithium carbonate for approximately 10 seconds followed by 70% alcohol until GM and WM are clearly distinguishable. The sections were counterstained with 0.1% cresyl fast violet (CFV) in

1% acetic acid for up to 5 minutes at room temperature and differentiated in 95% alcohol before mounted in DPX.

2.3.3 CFV

Nissl substance is granular basophilic bodies consisting of RNA and polyribosomes in the cell body and dendrites (Nievel and Cumings, 1967, Scott and Willett, 1966). CFV was used to visualize neurons and glial cells (cell nuclei) for the evaluation of neuronal and glial density changes in CADASIL and COGFAST. 30 µm sections were incubated in 0.1 % CFV in 1% acetic acid at 60 ˚C for 15 minutes. After rinsed in water, they were differentiated in 95% alcohol until only neuronal body and nuclei were stained purple and mounted in DPX.

2.3.4 Standard procedure of single label immunohistochemistry

Paraffin-embedded brain tissue blocks were cut into 10 - 30 µm sections. After incubated at 60 ˚C for 30 minutes, sections were transferred into xylene to dewax, followed by rehydration in decreasing concentrations of alcohol. The antigen retrieval was performed by microwaving sections in 0.01M citrate buffer (pH 6.0) for 10 minutes. The sections were quenched by 3% H2O2 for 15 minutes and blocked with normal horse serum (for anti-mouse antibody) or normal goat serum (for anti-rabbit antibody) for 30 minutes. Primary antibody diluted to a specific concentration with buffer was applied to the sections, which were then incubated at the room temperature for the specified length of time (1.5 – 2.5 hours). Biotinilated secondary anti-mouse/anti-rabbit antibody was applied to the sections with the blocking serum for 30 minutes, followed by incubation in tertiary antisera SABC for 30 minutes. Sections were treated with 3,3'-Diaminobenzadine for 5 minutes to visualize the positive antibody reaction as a brown

stain. After each step except blocking, sections were rinsed in buffer (PBS/TBS) for 5 minutes x 3 times.

2.2 Image analysis

2.3.1 Image capture

Zeiss Axioplan2 microscope coupled to a JVC 3 chip charge-coupled device (CCD) camera or an Infinity2 CCD camera was used to capture digital images of brain sections unless otherwise specified. While capturing images of cortex or stained axons in WM, the goniometer stage was adjusted to attain desired angle to the pial surface or the axonal tract, respectively. Magnification was chosen to reveal details of changes but give enough statistical power upon image analysis.

2.3.2 Digital image analysis

Images were analysed using Image Pro-Plus 4.0 (Media Cybernetics®). Area of the total immunoreactivity in the image or its percentage (PerArea) was measured by quantifying pixels attributed to the immunoreactivity (*i.e.* dark brown staining). The values in pixel were converted to μm2 by calibration. The image analysis, which is difficult to perform by Image Pro-Plus 4.0, was done using novel computer software created using Microsoft Visual Basic 2008/2010 Express Edition. The details of the software are described in each chapter.

2.3 Statistical analysis

Statistical analysis was performed using SPSS version 17. Kruskal-Wallis test was performed to assess the differences between groups, followed by Mann–Whitney U test to obtain p-values for each pair. When normal distribution was expected, One-Way ANOVA with Tukey's post hoc test was used instead. Spearman (rho) correlation was

used to test the relationships between ages, length of fixation, postmortem delay and quantified variables.

Chapter 3. Vascular and Related Perivascular Pathology in CADASIL

3.1 Introduction

CADASIL is characterized by multiple small infarcts in periventricular WM, subcortical GM and the pons. Hyperintensity upon T_2-weighted and FLAIR sequences on MRI is frequently observed in WM, especially the temporal poles, thus is highly useful for the diagnosis of CADASIL (Kalaria et al., 2004, Dichgans et al., 1998). The characteristic arteriopathy, among which the most prominent are degeneration of VSMCs and thickening of blood vessel wall (Ruchoux et al., 1995, Miao et al., 2005), underlies the reduction of CBF (Tuominen et al., 2004, Lacombe et al., 2005). Thickening of tunica media of arteries/arterioles is caused by the increased matrix protein deposits, *e.g.* collagen and laminin (Lammie et al., 1997). Such a change occurs during the process of ageing (Uspenskaia et al., 2004), though slowly, and is accelerated in disease states such as chronic hypertension and SVD. Components and structure of endothelial cell also changes in CADASIL (Ruchoux and Maurage, 1998). Endothelial dysfunction, also reported in SVD, has been implicated in brain tissue deterioration via decreased CBF, impaired vascular autoregulation and increased BBB permeability (Topakian et al., 2010).

The mechanism of how these vascular abnormalities lead to cognitive decline in CADASIL remains controversial. Much of the work in the area of dementia has reported the relationship between reduced CBF/Cerebral blood volume (CBV) and cognitive function in various types of dementia including CADASIL (Bruening et al., 2001, Chabriat et al., 2000, Spilt et al., 2005, Osawa et al., 2004). In those studies, significant decrease in CBF/CBV was observed in patients with dementia compared to

those with no or mild cognitive impairment, suggesting severity of angiopathy is related to cognitive decline. Also, several studies have suggested the link between the enlarged PVSs, also referred to as Virchow-Robin spaces, and cerebral SVD with dementia including CADASIL (Cumurciuc et al., 2006, Doubal et al., 2010, Uggetti et al., 2001, Patankar et al., 2005). PVSs are cerebrospinal fluid-filled spaces around small perforating arteries and found more abundantly in WM. They are normally small and asymptomatic and are known to dilate further with age (Heier et al., 1989). The significantly enlarged PVSs are detectable as hyperintense areas in T_2-weighted MR images similar to the infarcts. As an MRI study on the healthy elderly linked enlarged PVSs and worse cognitive function (non-verbal reasoning and visuospatial cognitive ability) (MacLullich et al., 2004), the enlarged PVSs in CADASIL may have significant impact on the pathology. The limitations of those MRI studies are that PVSs are only visible on MRI when the diameter exceeds 0.66mm while many of the vessels affected in SVD and their enlarged PVS are much smaller (Wang, 2009), and that those MR images are too low in resolution to quantify the size and thus only number of enlarged PVSs was scored. Hence, the aims of the study were (1) to quantify the arterial wall thickening and PVS enlargement using histologically stained human tissues from frontal lobe and temporal pole, where MRI hyperintensity is frequent, (2) to define CADASIL specific pathological features, and (3) to evaluate the relationship between vascular pathology and PVS enlargement. The results were presented in the publication I.

3.2 Materials and Methods

3.2.1 Subjects

Demographic details of the subjects from which the brain samples were obtained at autopsy are given in **Table 3.1**.

Frontal lobe

Disease Group	n	Age (years)	
		Mean	SD
Young controls	6	60	7.3
Old controls	7	79	6.3
CADASIL	6	57	8.1
Small vessel disease	9	78	8.2

Temporal pole

Disease Group	n	Age (years)	
		Mean	SD
Young controls	5	60	7.5
Old controls	5	83	6.0
CADASIL	9	58	7.5
Small vessel disease	8	83	10.0

Table 3.1. Sample number, mean age and standard deviation (SD) of the subjects. Two control groups were age-matched to each disease group.

Brain samples from frontal lobe and temporal pole were used in this study. Each case was selected based on the criteria detailed in chapter 2.1. Half of the SVD cases were demented at the time of death. Coronal sections at the level of BA9 were used for the analysis of the frontal lobe and BA20 to 22 for the temporal pole. Where available to match for similar age and gender, CADASIL cases were compared to young controls (Ycont) and SVD cases to old controls (Ocont).

3.2.2 Histopathology

Formalin fixed, paraffin embedded brain tissues from frontal lobe and temporal pole were serially cut into 10-µm-thick sections. Sections were stained in batches with H&E to minimize intra-assay variation. The slides were assigned random numbers and all analysis was performed blind to the diagnosis.

3.2.3 Image capture and analysis

Sections were viewed with a Leitz Wetzlar Dialux 20 bright field microscope at 6.3x magnification and images were captured using a JVC 3CCD camera attached to an image capture board. As the area of frontal lobe sections is usually limited, all the arterial/arteriolar vessels (>50 µm) in WM were selected for the measurement of PVS and SI in frontal lobe. For temporal pole, at least 30 randomly-selected arterial/arteriolar vessels per case were sampled.

Sclerotic index (SI), area of vessel wall (Vwall), lumen (Larea) and PVS were calculated from the mean internal diameters (mDint), mean external diameters (mDext) and mean diameter of PVS (mDpvs) using the formulae shown in **Figure 3.1**. SI was first mentioned by Lammie et al. (1997) and now widely used to evaluate the thickening

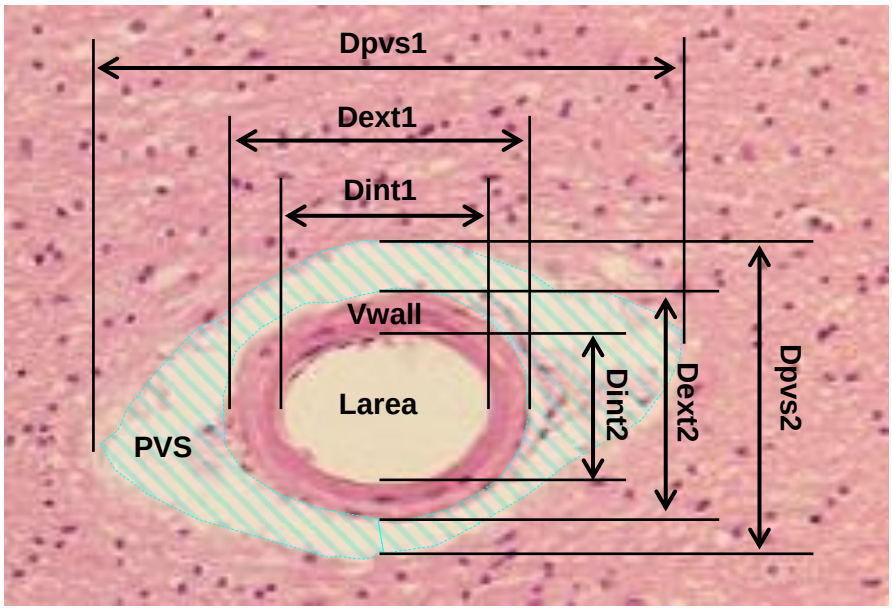

$SI = 1 – (Dint/Dext)$

$Larea = [(Dint1 + Dint2)/4]^2 \pi$

$Vwall = [(Dext1 + Dext2)/4]^2 \pi – Larea$

$PVSc = [(Dpvs1 + Dpvs2)/4]^2 \pi - [(Dext1 + Dext2)/4]^2 \pi$

Figure 3.1. Definition of the SI and PVS measurement variables. Formulae indicate how the variables were derived.

of the blood vessel wall. SI of normal vessels is around 0.2-0.3, which increases to 0.3-0.5 or even over 0.5 in severe SVD. The formulae for area estimation were derived from that for circular area, regarding the structure of blood vessels as a deformed circle. However, as the blood vessels and PVS have various shapes in reality, area of vessel (Vwall + Larea) and PVS in frontal lobe were quantified both by calculating from their mean diameters (PVSc) and by measuring in pixel using Image Pro-Plus Version 4.0 (Media Cybernetics®, PVSi) at the beginning of the experiment. After the accuracy of the area estimation by calculation was confirmed, Vwall, Larea and Dpvs in temporal pole were quantified using the formulae only. Ratios of Larea and Vwall against PVS were calculated to assess the effect of vessel thickening on PVS. For temporal pole where MRI hyperintensity is most prominent, total PVS was estimated by measuring all the PVS larger than 100 μm in diameter in WM, and was divided by whole temporal pole WM area measured with Image Pro-Plus 4.0 to obtain the percentage of total PVS area in WM (%PVS).

3.2.4 Image analysis software development

To reduce the error caused while measuring lengths, computer software (VasCalc) was developed for the analysis, which greatly simplified SI and PVS evaluation. The user was prompted to draw user-specified number of lines, which was 2 in this study, to measure mDint, mDext and mDpvs. The centre of the first line was marked by a cross and the second line was drawn to cross the first line perpendicularly through the point. VasCalc calculated SI, Larea, Vwall and PVS using the formulae in **Figure 3.1**. See appendix I for full Visual Basic code.

3.2.5 Statistical analysis

Kruskal-Wallis test was performed to determine the difference between groups. For the variables that showed significant difference, Mann-Whitney U test was used to obtain p values for each group pair. Correlation was tested using Pearson's correlation test.

3.3 Results

Gross examination of the sections revealed enlarged PVSs in frontal lobe and temporal pole of CADASIL cases (**Figure 3.2**). The PVSs were often located at the boundary between WM and GM. There was no obvious sign of infarcts in the temporal pole sections though many of CADASIL sections had significantly paler H&E staining - as pale as GM - in the WM, possibly due to the WM lesions. Some of CADASIL cases exhibited micro-infarct like lesions in frontal lobe, but the extent of decolorization of WM was less compared to that in temporal pole.

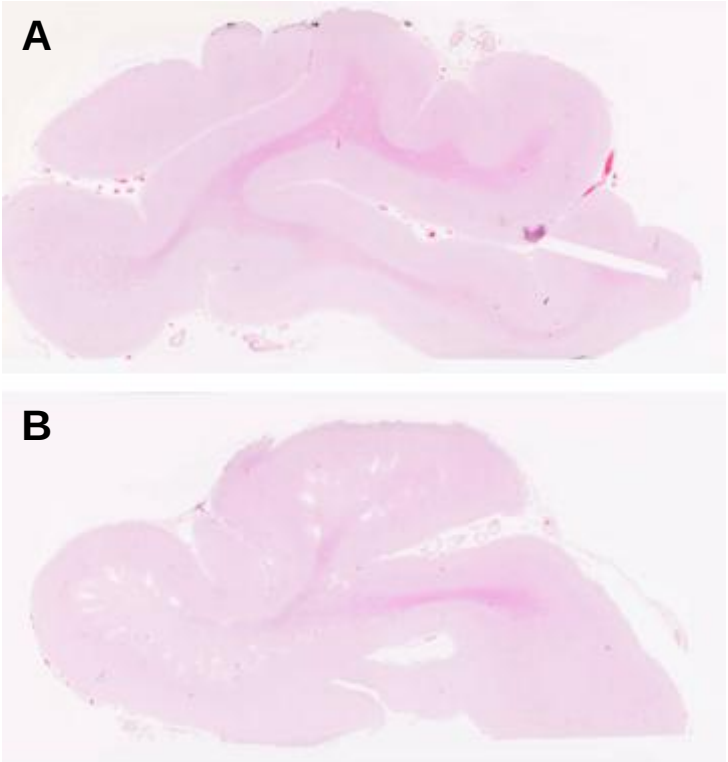

Figure 3.2. Gross views of temporal pole sections from Ycont (A) and CADASIL (B). Note the distinctive PVSs in CADASIL.

3.3.1 Increased vessel wall thickness

In general, the arteries/arterioles were slightly larger in frontal lobe than in temporal pole. There was no significant difference in frontal lobe mDint between groups, and mDext was significantly higher only in CADASIL ($p = 0.001$) (**Figure 3.3**). On the contrary, there was no significant difference in mDext but mDint in temporal pole. CADASIL mDint was significantly smaller compared to Ycont and SVD (both $p < 0.0001$). The mDext was slightly larger in CADASIL but failed to reach statistical significance.

SI, which indicates the ratio of vessel wall thickness against Dext, was calculated so that changes between different sized vessels can be compared (**Figure 3.4**). SI for controls was within the normal range defined by Lammie et al. (1997). SI of Ocont was increased compared to that of Ycont only in frontal lobe ($p = 0.04$). However, SI positively correlated with age both in frontal lobe ($r = 0.215$, $p = 0.008$) and temporal

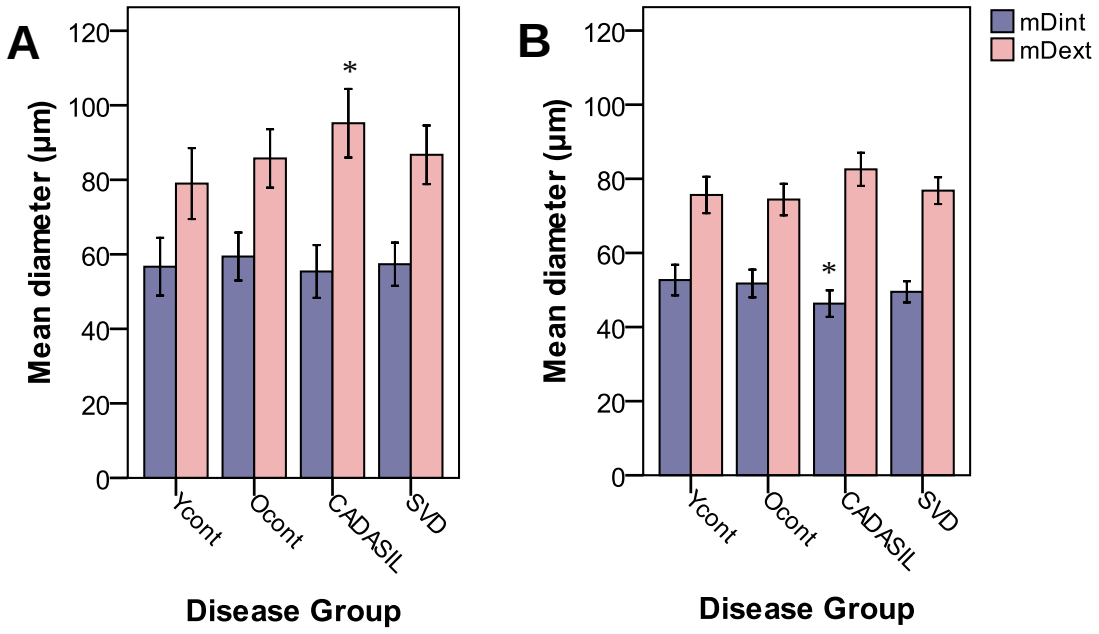

Figure 3.3. mDint and mDext in WM of frontal lobe (A) and temporal pole (B). There was no difference in mDint between groups in frontal lobe while m. Vessels in temporal pole were slightly smaller than those in frontal lobe. Significant differences compared to age-matched controls are marked with *. Error bars ± 2SE.

pole (r = 0.232, p = 0.001) when analyzed combined control groups, implying that there is a subtle effect of ageing on vessel wall thickening both in frontal and temporal lobes. CADASIL had markedly higher SI compared to all other groups (p < 0.0001) both in regions. The SI value of CADASIL was marginally higher in temporal pole than frontal lobe while those of the other groups were kept constant. Unexpectedly, SVD, of which mDint and mDext were not statistically different from Ocont, also showed significance against Ocont (p = 0.014 and < 0.0001 in frontal lobe and temporal pole, respectively) though the increase was moderate in comparison to that of CADASIL (p < 0.0001).

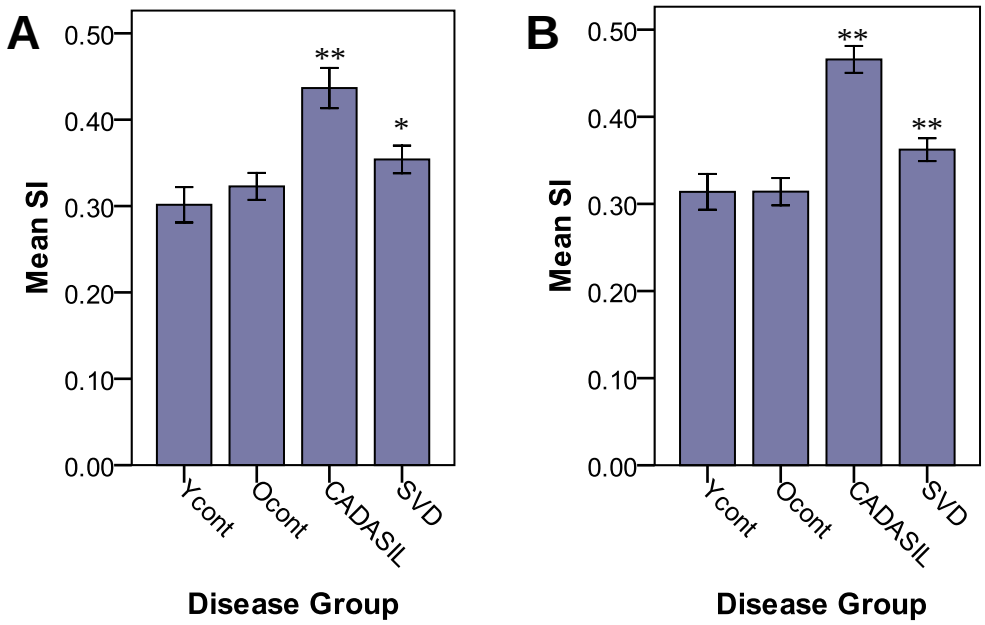

Figure 3.4. SI in frontal lobe (A) and temporal pole (B). CADASIL showed significant increase in SI compared to other groups. Small vessel disease (SVD) also showed increased SI compared to old controls (Ocont). * P < 0.05 and ** P < 0.0001 vs. age-matched controls. Error bars ± 2SE.

3.3.2 Enlarged perivascular spaces in CADASIL

Values of vessel area (Vwall + Larea) and PVS, which were obtained using both VasCalc and Image Pro-Plus, were compared to evaluate the precision of the formula. Vessel area was accurately estimated using VasCalc. Although PVSc was accurate and

there was no significant difference when compared to PVSi, the PVSc were frequently slightly higher than PVSi (**Figure 3.5 A**). The error became larger especially when the shape of PVS was notably elongated in one direction, resulting in the larger difference between two diameters measured to calculate mean. The error was reduced in proportion to the number of lines drawn to calculate the mean diameter. As the accuracy of the formulae was confirmed, PVS in temporal pole was analyzed only with VasCalc (**B**). CADASIL showed significantly larger PVS than the others both in frontal lobe and temporal pole ($p = 0.015$ and < 0.0001 compared to Ycont, respectively). Unexpectedly, PVS in SVD remained at the control level. PVSc was larger in temporal pole compared to frontal lobe, which is consistent with MRI findings of characteristic WM hyperintensity in the temporal poles.

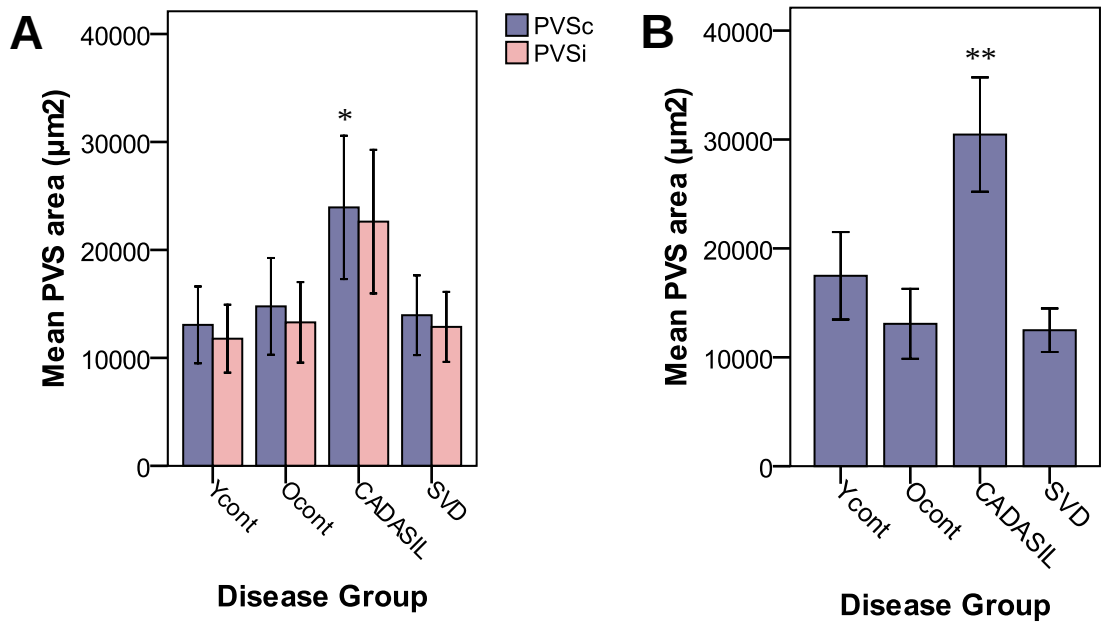

Figure 3.5. PVS area in frontal lobe (A) and temporal pole (B). PVS in frontal lobe was measured both by calculation (PVSc) and Image Pro-Plus (PVSi) (±SE). There was no significant difference in PVS area value between two methods. P values are of PVSc. CADASIL showed significantly increased PVS area, more so in temporal pole. * $P < 0.05$ and ** $P < 0.0001$ vs. age-matched controls. Error bars ± 2SE.

As the area of PVS is strongly dependent on the size of the blood vessel and does not always represent the extent of pathological changes, the ratio of Larea to PVSc was calculated. The magnitude of PVS enlargement in CADASIL became even more prominent with the Larea:PVS ratio especially in temporal pole (**Figure 3.6**). Again, the extent of PVS enlargement was greater in temporal pole irrespective of disease group. Importantly, the ratio of Larea to PVSc significantly correlated with SI not only in CADASIL but also in other disease groups (correlation in combined groups r = 0.312, p = 0.0001), indicating the close relationship between vessel wall thickening and PVS enlargement. There was a trend of positive correlation between PVSi and age (r = 0.213, p = 0. 062) in frontal lobe, but otherwise no effect of ageing on PVS was found.

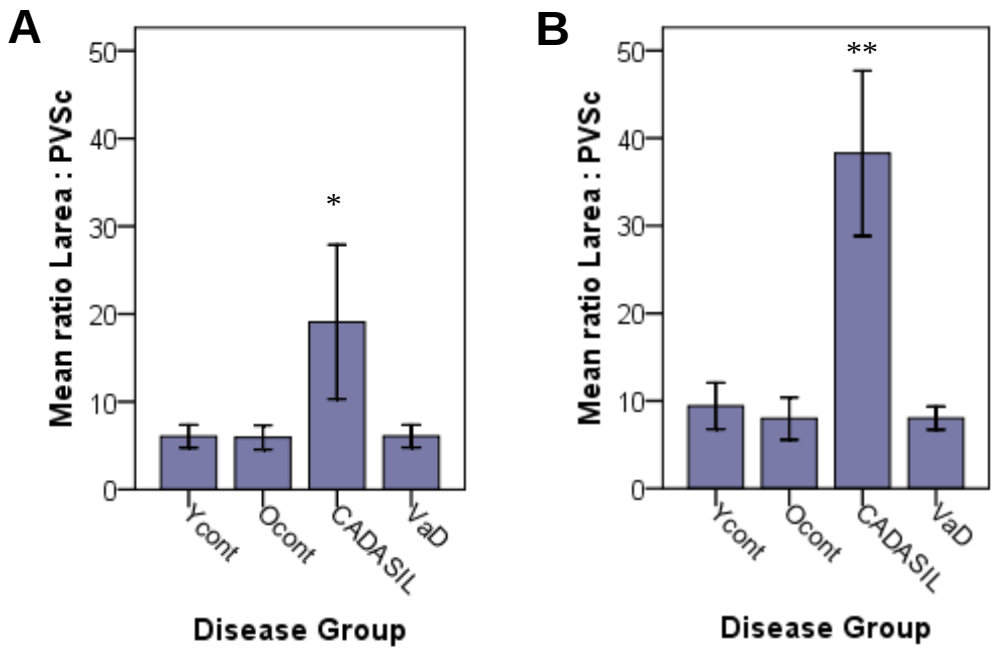

Figure 3.6. Ratio of luminal area (Larea) to PVSc in frontal lobe (A) and temporal pole (B). CADASIL showed significantly larger PVS even considering the size of the vessels. * P < 0.05 and ** P < 0.0001 vs. age-matched controls. Error bars ± 2SE.

3.3.3 Higher percentage of PVS in temporal pole white matter

Area percentage and number of PVS with mDpvs > 100 μm were quantified to relate PVS enlargement to whole temporal pole WM. %PVS was highest in CADASIL (p =

0.009 vs. Ycont) as expected (**Figure 3.7**). Interestingly, Ocont showed highest number of PVS per WM followed by CADASIL (p = 0.10 and 0.064 compared to Ycont, respectively) while age-matched SVD was as low as Ycont. However, the result does not necessarily indicate the increased vascularity in the temporal pole of Ocont as it is possible that the difference between Ycont and Ocont is merely due to Ocont having more blood vessels with PVS larger than 100 μm in diameter. The number of PVS was clearly significantly increased in Ocont than Ycont, but Mann-Whitney test revealed no difference, probably type II error due to the small sample number.

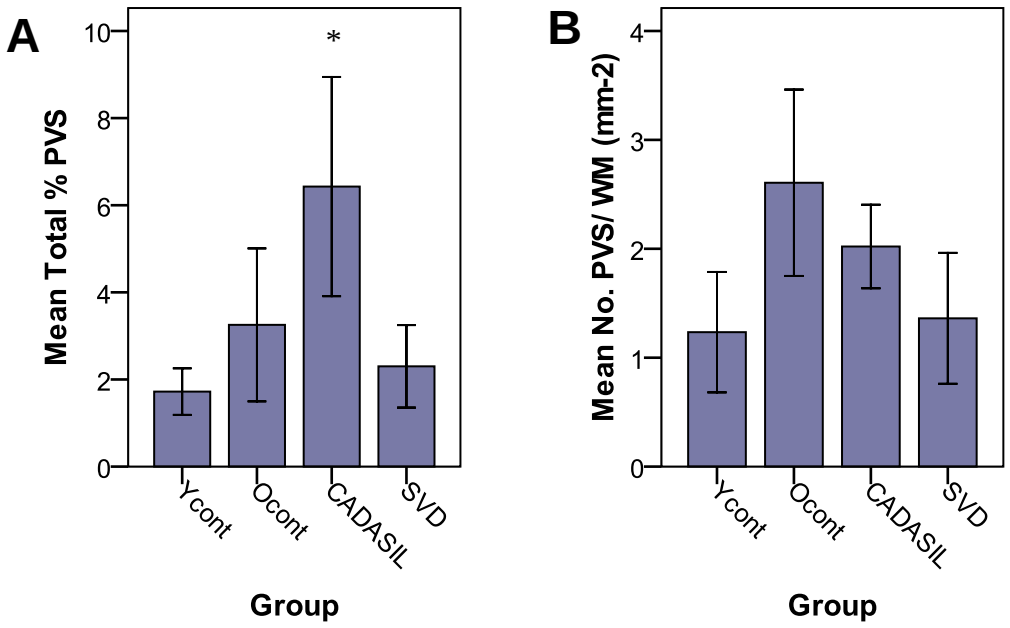

Figure 3.7. PVS in relation to WM area in temporal pole. Percentage and number of PVS (No.PVS/WM) were shown in A and B, respectively. * P < 0.05 vs. age-matched controls. Error bars ± 2SE.

3.4 Discussion

The present study quantitatively examined the hyalinization of arteries/arterioles and PVS enlargement for the first time in CADASIL and SVD using histologically stained human brain tissues. We confirmed the thickening of vessel wall in SVD and even more extensive changes in CADASIL, suggesting that in CADASIL the overall tissue

changes are more severe than that in sporadic cases. PVS size was also significantly increased in CADASIL compared to all the other groups while that in Ocont and SVD group was unchanged. The result contradicted with the previous studies, which linked enlarged PVSs with ageing and cerebrovascular disease (Heier et al., 1989, Doubal et al., 2010, Patankar et al., 2005). Those studies, however, quantified number of enlarged PVS visible on MR images, which were likely to be around much larger blood vessels (*e.g.* perforating arteries with diameter of 50 – 400 μm) than those in this study (50 – 100 μm). As the vessels affected in SVD are mainly small arteries and arterioles, our method provided advantage in detecting subtle changes overlooked in MRI studies. In this regard, the lack of PVS enlargement in SVD in contrast to CADASIL is an interesting implication that their pathophysiology may be different.

The causes of PVS dilation have been argued but remain inconclusive. One of the possible causes is the BBB breakdown. Enlarged PVSs are often observed in patients with hypertension, Binswanger's disease, cerebral SVD etc. (Doubal et al., 2010, Benhaïem-Sigaux et al., 1987). As a MRI study on multiple sclerosis demonstrated, PVSs volume was increased in the proximity of BBB breakdown (Wuerfel et al., 2008). Considering that chronic cerebral hypoperfusion can cause BBB disruption and subsequent changes in vascular morphologies similar to CADASIL (Ueno et al., 2002), it is plausible that dysfunction of BBB, possibly leakage of toxic substances, contributes to PVS enlargement in CADASIL, in which frontal and temporal hypoperfusion have been reported (Mellies et al., 1998). Another possibility is the disrupted perivascular drainage of ISF. Several studies have shown that tracers injected into brain are cleared through the lymphatic drainage route within the capillary/arterial wall to lymph nodes (Weller et al., 2009). The theoretical model of the drainage system suggested that the driving force of the lymphatic drainage flow is vascular pulsation

(Weller et al., 2009), which is disrupted in CADASIL due to the impaired vascular reactivity (Lacombe et al., 2005, Hussain et al., 2004, Dubroca et al., 2005a). The reduced vascular tone, possibly caused by Notch3 signalling dysfunction, would be promoted by the accumulation of extracellular matrix proteins observed in CADASIL vasculature, which thicken and stiffen the arterial wall. The diminished arterial pulsation could lead to the reduced efficiency of lymphatic drainage, consequently accumulating protein deposits and further blocking the drainage pathway as in AD (Weller et al., 2008). Indeed, we noted correlation between vessel wall thickening and PVS enlargement. The hypothesis is also supported by a case report of macroadenoma with dilated PVS in the temporal stem (Cerase et al., 2009). Interestingly, the enlarged PVS on MR image disappeared after surgical resection of macroadenoma. The authors speculated that the PVS dilation was due to the mechanical obstruction of lymphatic drainage system by macroadenoma. In addition to the blockage of drainage system, the abnormal protein accumulation may cause damage to WM, resulting in PVS enlargement though the mechanism of such pathological changes is still unclear. Some suggested the involvement of inflammatory reactions (Wuerfel et al., 2008), which was also supported by our previous study showing increased CD45 immunoreactivity in CADASIL brain (unpublished data).

We noted the increased number of PVS per WM in Ocont and CADASIL but not in SVD (**Figure 3.7B**). The increase may simply be reflecting a larger fraction of arteries/arterioles with mDpvs > 100 μm within total population, especially in case of CADASIL. However, considering the number of PVS in SVD, which was age-matched to Ocont and is more likely to cause PVS dilation, was as low as Ycont, it can also be interpreted as an indication of angiogenesis at least in Ocont. Another interesting finding is that changes in SI and PVS size were always more severe in temporal pole

than in frontal pole (*e.g.* **Figure 3.4** and **Figure 3.6**). MRI hyperintensities are frequently found both in frontal lobe and temporal poles in CADASIL (Coulthard et al., 2000). Our results attest the profound MRI hyperintensity in temporal poles rather than in frontal lobe. However, according to Ihara et al. (2010), WM changes by hemodynamic disturbance in frontal lobe precedes those in temporal pole in vascular dementia. The contradicting higher susceptibility of temporal pole to CADASIL pathology despite the ubiquitous expression of mutant *NOTCH3* may be due to a 'CADASIL specific mechanism,' which needs to be carefully considered in the future. Further research, especially regarding the mechanisms of PVS dilatation, should benefit solving the puzzle of the CADASIL pathology.

Chapter 4. NOTCH3 Accumulation in the Brain Vasculature of CADASIL Subjects

4.1 Introduction

Arteriopathy is a key component of CADASIL pathogenesis, underlying subcortical infarcts and leukoencephalopathy. Whereas the previously examined vascular wall thickening is a characteristic but not a specific change in CADASIL, the N3ECD accumulation and GOM deposits are uniquely found in the vasculature of CADASIL patients (Tikka et al., 2009, Joutel et al., 2001). Joutel et al. (2000) first described the accumulation of N3ECD but not the ICD in the cerebrovasculature including arteries, veins and capillaries, and showed that it was located on the VSMC plasma membranes in apposition to the GOM. Under transmission electron microscopy (TEM), GOM is seen as a particulate, 1-2 μm-sized periodic acid-Schiff positive granular deposit. These are detected as electron-dense masses sited at intervals around VSMCs. Recently, it has also been reported to be found in the capillary basement membrane, frequently associated with pericytes but to a lesser extent when compared to deposits in arterioles of skin and muscle biopsy specimens (Lewandowska et al., 2010). The significance of the localization of GOM in the vasculature in terms of the pathogenesis of CADASIL is still debated. Similarly, the composition of GOM and the mechanisms how it is formed remain largely unknown. Only one report by a Japanese group (Ishiko et al., 2006) demonstrated the existence of N3ECD, but not the ICD, within the GOM found in microvessels in skin biopsy samples and hence questioned the previous widely accepted idea that N3ECD accumulates on the plasma membrane (Joutel et al., 2000). Considering the above data, it is plausible to consider that N3ECD-containing GOM is secreted by VSMC, possibly to remove potentially cytotoxic, aggregation-prone mutant N3ECD. The question to be asked is at what stage this occurs in the processing of

NOTCH3 along the signalling pathway. As described in the introduction, the interaction between NOTCH3 receptor and ligand induces its endocytosis and subsequent proteolytic cleavage, which dissociates NECD from ICD (**Figure 1.2**). Both of the above studies demonstrated the absence of the ICD in GOM (Ishiko et al., 2006, Joutel et al., 2000), suggesting that the N3ECD-GOM secretion or accumulation occurs after the stage of ligand-induced transendocytosis, in which case NOTCH3 ligands, such as Jagged1 and Jagged2, should also be found in GOM.

The aim of the study was to verify the previous reports by assessing the localisation and distribution of the N3ECD accumulation in the cerebrovasculature of genotyped and clinically characterised CADASIL patients. Further, we seek to test the existence of other Notch-associated proteins in GOM in order to provide an insight into its formation mechanism.

4.2 Materials and Methods

4.2.1 IHC for light microscopic examinations

For the screening of NOTCH3 accumulation specificity, the following cases were used: 9 CADASIL (refer to **Table 2.1**, mean age = 58), 8 Ycont (mean age = 58), 7 middle-range age controls (mean age = 75), 6 Ocont (mean age = 97) 7 young VaD (mean age = 66) and 7 old VaD (mean age = 92). 10-μm sections from temporal lobe blocks were stained with anti-N3ECD antibody (A1-1, 1:25000 for 2.5 hours; courtesy of Dr. Watanabe), anti-ubiquitin antibody (1:50 for 2 hours; Dako, Denmark), anti-Jagged1 antibody (1:1000 for 2 hours; abcam, US), anti-CD45 (1:200 overnight at 4 °C, Dako, Denmark) and anti-CD68 (1:200 for 1 hour, Dako, Denmark) which were later labelled with random numbers for blinded analysis. Images of representative areas in GM and WM were taken at x10 magnification. The A1-1 immunoreactivity in blood vessels was

evaluated using semi-quantitative scores: none (–), mild/slight (+), moderate (++) and frequent/abundant (+++). The analysis of A1-1, ubiquitin and Jagged1 was performed by Yamamoto Y, and the CD45 and CD68 immunoreactivity in WM was quantified using Image-Pro Plus 4 by Tham C.

4.2.2 Transmission electron microscopy

4.2.2.1 Subjects

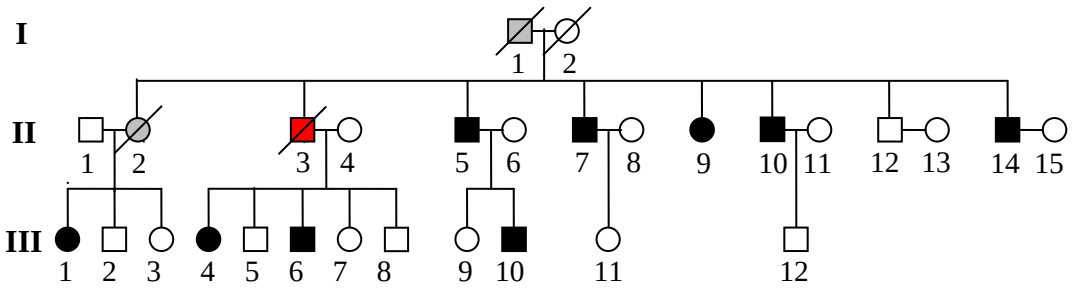

Figure 4.1. Pedigree of the examined CADASIL patient (II-3). Filled symbols indicate affected individuals and stroked line indicates deceased family member.

A male patient (CAD12 in **Table 2.1** and II-3 in **Figure 4.1**) with a strong family history of CADASIL (R153C) first experienced stroke at the age of 39. He had a smoking history and was taking aspirin daily. He suffered from frequent TIAs and multiple cerebrovascular accidents, which often manifest as sudden onset of weakness, vertigo and double vision. MRI revealed lesions in subcortical regions, brainstem and basal ganglia and signs of cerebral and corpus callosum atrophy. In later life, his physical functions were severely impaired with abulic, pseudobulbar, pyramidal, cerebellar and extrapyramidal signs, requiring him to use a wheelchair and be fed by percutaneous endoscopic gastrostomy. He showed symptoms of mild anxiety and depression. His cognitive functions were also seriously diminished and exhibited typical stepwise progression of subcortical type dementia. The patient experienced a massive stroke 9 days prior to death and died at the age of 68. The cause of death was suspected

to be pneumonia, but the autopsy also revealed an extensive prostate tumour causing pyelonephritis. The brain was removed and dissected within 12 hours postmortem. The brain had a more gelatinous consistency than was normal.

As a control, brain tissue from an 89 year-old female was also sampled. The patient had a history of hypertension and an episode of possible TIA, but was cognitively intact. She died of ischemic bowel disease and multiple organ failure following surgery.

4.2.2.2 Tissue sampling and embedding

Brain tissue was sampled from GM and WM in frontal and temporal lobes, and also from meninges. After 16-hours fixation in 2% paraformaldehyde and 0.05% glutaraldehyde in 0.1M phosphate buffer (PB, pH7.4), the samples were rinsed in two changes of PB for 15 minutes each. Half of each batch of samples was treated with 1% osmium tetroxide (OsO4) in 0.1M PB for 1 hour followed by rinses in PB for 4x15 minutes. All the samples were then dehydrated in increasing concentrations of alcohol from 50% to absolute at 15 minutes intervals. The samples were cleared in two 10 minutes changes of propylene oxide and then incubated in a 50/50% propylene oxide / epoxy resin mixture for 1 hour, followed by a 25/75% mixture for 1 hour and 2 changes of 100% epoxy resin for 1 and 2 hours, respectively, before being embedded in preformed beem capsules. The embedded samples were incubated at 37 °C for 2 hours before being placed into a 60 °C incubator for 48 hours.

4.2.2.3 Immuno-gold labelling

An Ultracut microtome (Reichert-Jung, Depew, NY) was used to cut 1 μm sections from embedded samples with the aid of a Histo Diatome knife and a DDK Delaware Diamond knife was used for cutting ultra thin sections (~700Å). 1 μm sections were placed on glass slides and stained with an aqueous solution of 1% toluidine blue and 1%

borax for 30 seconds on a hot plate in order to confirm the position of blood vessels in the section. The block was then trimmed to encompass the required structures and ultra thin sections then cut onto the water trough of the diamond knife. The sections were then placed onto 3.05 mm nickel 300 square mesh grids, which had been pre-treated with 10 % nitric acid. OsO_4 treated sections were used for morphological examination and non- OsO_4 treated sections were further processed for immuno-gold labelling with A1-1.

Throughout the procedures, TBS (pH 7.4) containing 1% BSA and 0.1% tween20 was used as a buffer. The non-OsO4 epoxy-resin sections were etched with two changes of 3% sodium meta-periodate for 20 minutes and heated in 0.01M citrate buffer (pH 6) at 90 °C for 10 minutes to increase the antigenicity. After blocking with 5% bovine serum albumin (BSA), 5% normal goat serum and 0.1% gelatine in TBS for 30 minutes, the grids were incubated in antibodies against A1-1 (1:4000), Jagged1 (1:1000; abcam, USA), ubiquitin (1:50; Dako, Denmark), heat shock protein 27 (HSP27, 1:100; abcam, USA), α-actin (1:100; Dako, Denmark) and collagen IV (1:30, abcam, USA) diluted in buffer for 2 hours at room temperature. They were rinsed in four changes of buffer and subsequently incubated in EM Goat anti-Rabbit IgG 5 nm Gold probes (1:30; BBInternational, UK) for one and a half hours. Sections, which were not treated with the primary antibodies, were stained with anti-human IgG-5nm gold conjugate (1:30, BBInternational, UK) to assess the involvement of immune response. To increase the visibility of the gold particles, the sections were further treated with a Silver Enhancing Kit for Light and Electron Microscopy (BBInternational, UK). Subsequently, the sections were post-fixed in 2% buffered glutaraldehyde for 5 minutes. They were contrasted with uranyl acetate saturated in 70% ethanol for 15 minutes at 60 °C and then with aqueous lead citrate for 5 minute at room temperature. EM images were taken

using a Philips 201 transmission electron microscope coupled to a Gatan multiscan camera, model 791 (Gatan, Pleasanton, CA).

4.3 Results

4.3.1 NOTCH3 ECD accumulation in CADASIL microvasculature

Figure 4.2 and **Table 4.1** summarize the light microscopic observation of A1-1 stained brain tissues. Distinct staining patterns, which were consistent with those by another N3ECD antibody (N2) described previously (Low et al., 2007), were observed in CADASIL tissue compared to all other groups. Except for CAD9, all CADASIL cases exhibited strong immunoreactivity in the vessel walls, although there was a slight difference in the size of the immunoreactive vessels and in stain intensity (**Figure 4.2 A** and **B**). Almost all small to large arterioles in both WM and GM were stained in CADASIL cases except for CAD4 and CAD8, in which small vessels in GM were negative for N3ECD or only faintly stained. The weak or no staining in CAD8 and CAD9, respectively, was probably due to the long fixation of the brain and consequent loss of antigenicity. The most distinctive difference was found in GM, where small vessels were still immunoreactive to N3ECD. The discontinuous, granular staining was found along the vessel walls of capillaries containing pericyte-like cells, which were also stained with A1-1 (**B** inset). Although most of the vessels were negative for N3ECD in controls, partial immunoreactivity was occasionally found in the wall of small vessels, possibly from pericytes or perivascular macrophages (**C** and **D**). Some, but very few, small vessels or larger arterioles in controls were stained in a similar pattern and always to a lesser extent than those in CADASIL (**E** and **F**). The number and the intensity of the microvascular staining in controls seemed to increase with age though such staining was rarely observed in a single isolated small vessel even in the controls aged over 100 years. Similarly, some VaD cases showed a few stained small

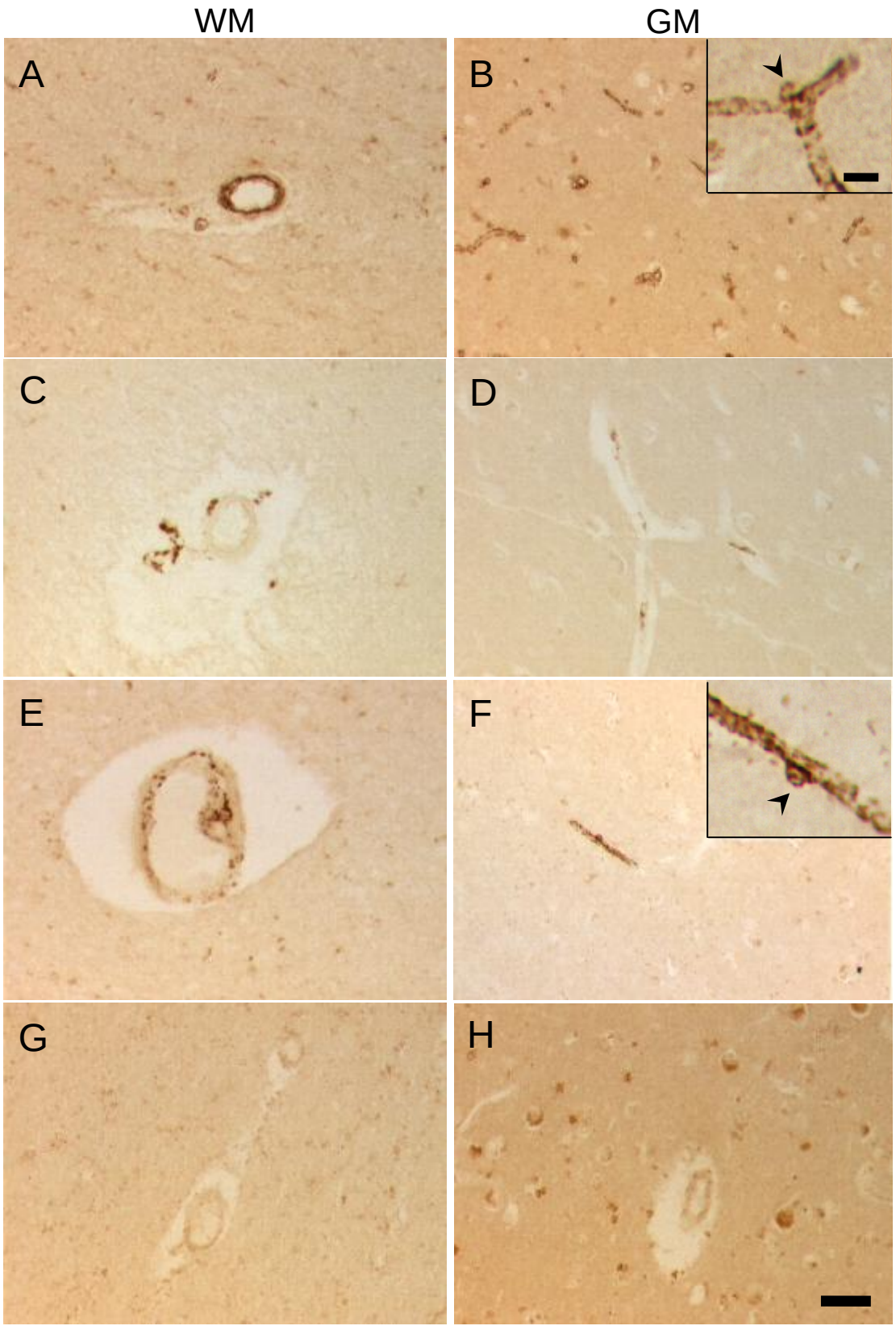

Figure 4.2. N3ECD accumulation in CADASIL vasculature. Large arterioles in WM (A) and small capillaries/arterioles in GM (B) of CADSIL were strongly stained with A1-1 (images from CAD7). The immunostaining in capillaries was granular with immunoreactive pericytes (B inset, arrowhead). Vessels in controls were mostly negative for N3ECD with stained macrophage-like cells, which may also be the source of partial immunoreactivity in small vessels (C and D from Ycont). A few arterioles of varying size in some of Ocont cases showed similar immunoreactivity as in CADASIL (E and F). Vasculature in VaD WM was also negative for N3ECD (G and H). Bars represent 50 μm, and 10 μm for insets.

Case (n)	Age (yrs)	Distribution in vascular profiles			Other comments
		Arteries	Arterioles	Capillaries	Perivascular cells
CADASIL (9)	58				yes(4)/no(5)
CAD1	44	+++	+++	+++	yes
CAD2	52	++	++	+	yes
CAD3	53	++	++	++	yes
CAD4	55	++	++	–	no
CAD6	59	+++	+++	++	no
CAD7	61	+++	+++	+++	yes
CAD8	63	+	+	+/–	no
CAD9	65	–	–	–	no
CAD11	68	+++	+++	++	no
Ycont (8)	58	–	–	–	yes(4)/no(4)
Mcont (7)	75	–	–	–	yes(5)/no(2)
Ocont (6)	97	–	– (/+)	– (/+)	yes(6)/no(0)
Young VaD (7)	66	–	–	–	yes(4)/no(3)
Old VaD (7)	92	–	–	– (/+)	yes(7)/no(0)

Table 4.1. Immunoreactivity of N3ECD antibody in CADASIL, controls and VaD. Score symbols show no (–), mild/slight (+), moderate (++) and frequent/abundant (+++) immunoreactivity. Only CADASIL cases exhibited extensive vascular immunoreactivity. A1-1 stained capillaries appeared more frequent in older cases in non-CADASIL cases. Immunoreactive perivascular cells were also more common among older cases. Ycont: young control, Mcont: middle-range age control and Ocont: old control.

vessels in GM, more in old than young, though most vessels were unstained (**G** and **H**). Neuronal staining was observed in many of the cases and the intensity and number increased with age. Strongly stained macrophage-like cells were observed around large arteries/arterioles in many cases, more common in older cases (**Table 4.1**). The above observations indicate that NOTCH3 accumulation in vasculature, especially in small vessels, is a CADASIL specific feature.

4.3.2 Distribution of ubiquitin and Jagged1 in CADASIL vasculature

We hypothesized that ubiquitin and Jagged1, which are both known to bind to a Notch receptor at some point in the Notch signalling pathway, are the other components of GOM. Light microscopic observation revealed ubiquitin immunoreactivity in the tunica media of arterioles in CADASIL but not in the capillaries (**Figure 4.3**). Similar VSMC layer staining was present in controls but in notably fewer arterioles. The capillary

immunoreactivity was same for controls and CADASIL; some of the pericytes and perivascular cells, possibly macrophages, were strongly stained for ubiquitin. Jagged1 immunoreactivity, on the other hand, was absent from the VSMC layer. The Jagged1 staining was present in neurons and perivascular cells, which were significantly increased

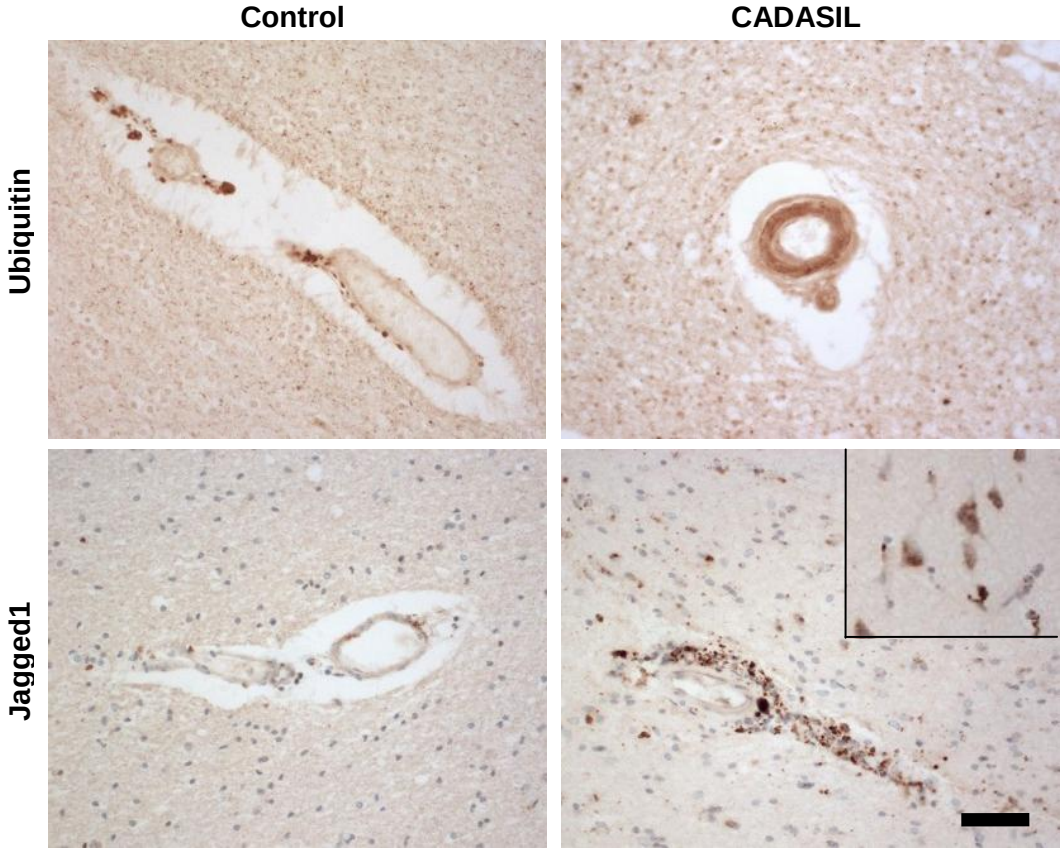

Figure 4.3. Ubiquitin and Jagged 1 immunoreactivity in CADASIL and control brain tissues. Vascular smooth muscle layer of arterioles was stained for ubiquitin in CADASIL whereas it was negative in controls. Jagged1 immunoreactivity was found mostly in neurons (inset) and perivascular cells. Bar represents 50 μm and 40μm for inset.

4.3.3 Colocalisation of NOTCH3 ECD and GOM in small vessels

As described in the previous section, IHC revealed N3ECD accumulation in brain arteries/arterioles as well as capillaries, which do not have VSMC. To determine the exact location of N3ECD accumulation in the cerebral vasculature, GM, WM and meninges samples from a CADASIL patient (CAD12) were processed for EM. The examination of 1 μm epoxy embedded tissue sections using light microscopy showed

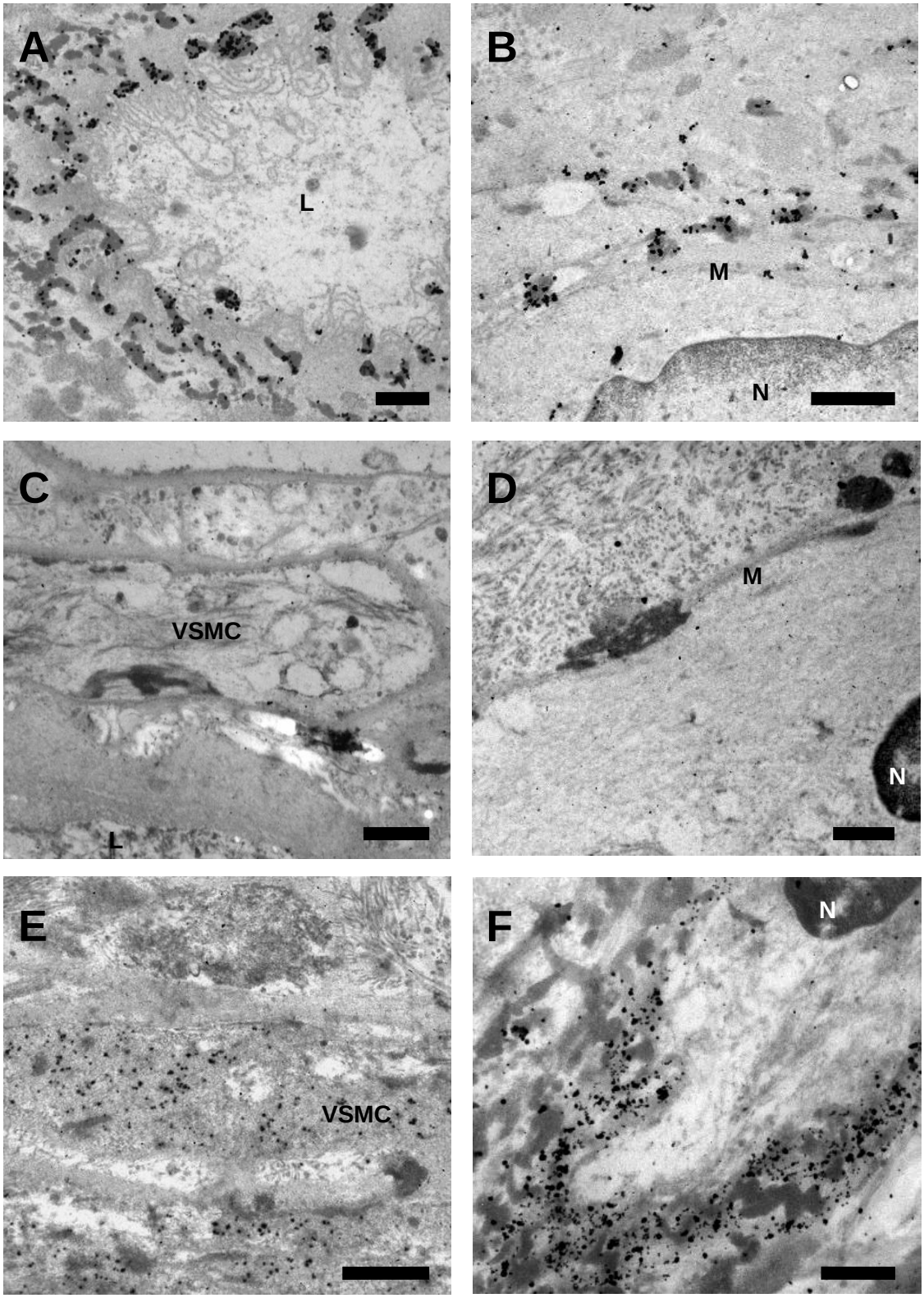

Figure 4.4. Specificity of A1-1 antibody. A1-1 immuno reactivity was found almost exclusively inside GOM depositions around vascular smooth muscle cells (VSMC) (A and B). No labelling was observed in GOM in control and negative control tissues stained for N3ECD (C and D), α-actin (E) or collagen IV (F) stained sections whereas antibody-specific staining was present for the latter two. L: lumen, M: plasma membrane, N: nucleus. Bars represent 1 μm.

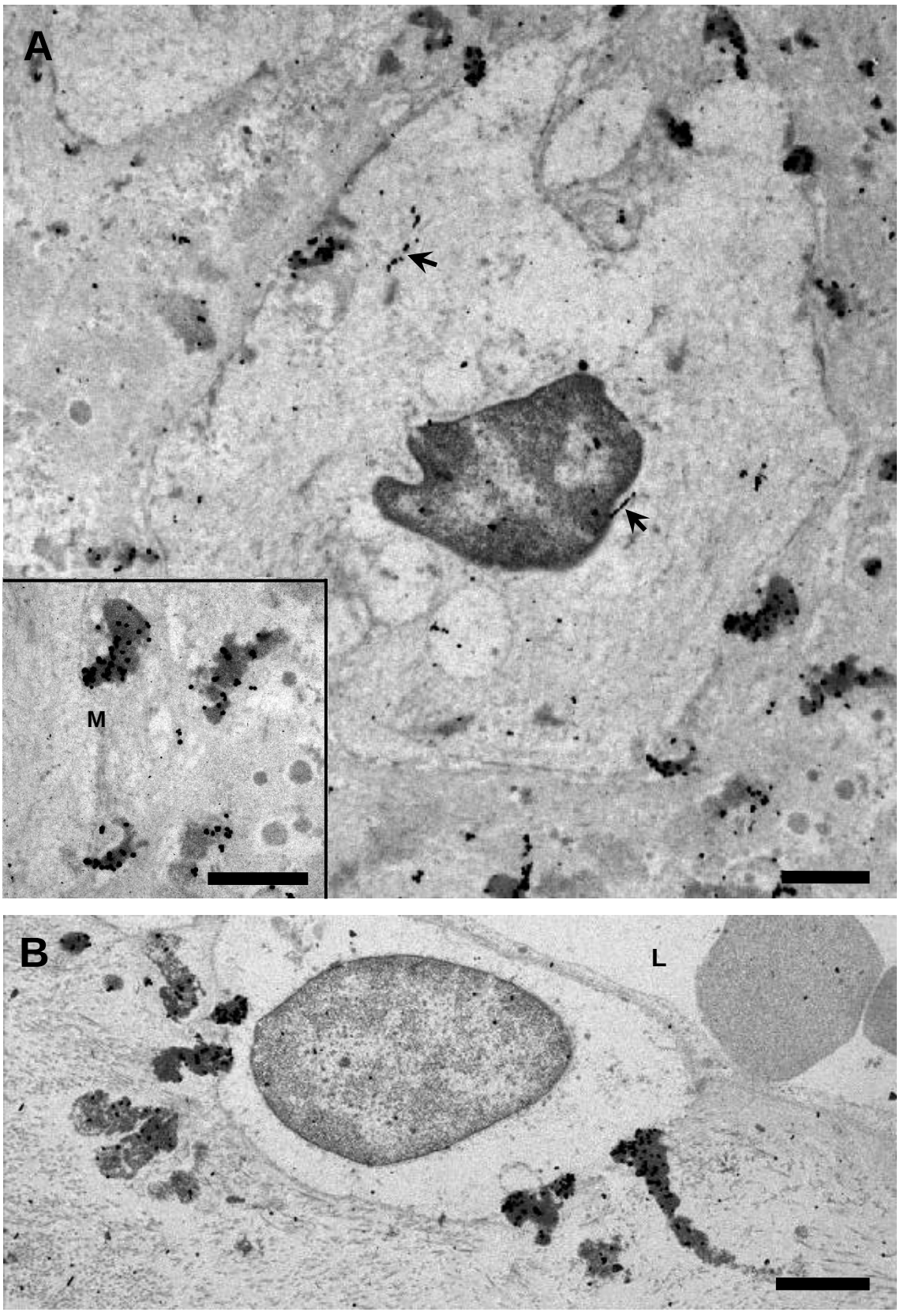

Figure 4.5. GOM depositions observed around VSMC in a meningeal artery. N3ECD-containing GOM was abundantly found in the close proximity of VSMC (A). In addition, a linear labelling pattern was occasionally observed in the cytoplasm (arrows). B shows the heterogeneousity of GOM; the farther from the plasma membrane, the more loosely the granules were associated, which was also evident from the distribution of gold particles. L: lumen, M: plasma membrane. Bars represent 1 μm (A) and 2μm (B).

severe tissue disruption, possibly due to the extensive trauma of the stroke the patient suffered prior to death. A large amount of corpora amylacea was also observed in the WM.

At EM level, some of the intracellular components, e.g. mitochondria, Golgi apparatus and ER, were damaged or completely lost in the blood vessels in GM and WM as expected, but the structural components of meningeal arteries were relatively well-preserved. EM examination also revealed abundant deposition of 0.2-2 μm GOM within the vasculature. The electron-dense material was immunoreactive to the immuno-gold staining with A1-1 antibody (**Figure 4.4 A, B** and **Figure 4.5**). Such labelling of GOM was not observed in control (**C**) and negative control tissues (**D**) or when the sections were stained for α-actin (**E**) and collagen IV (**F**), confirming the specificity of A1-1 immunoreactivity and thus the presence of N3ECD in GOM. N3ECD containing GOM were found not only around VSMCs in arteries and arterioles but also within basement membrane or around pericytes in the capillaries from GM (**Figure 4.5**, **Figure 4.6** and **Figure 4.7**). Most of the GOM deposits were heterogeneously stained with uranyl acetate and lead citrate; the granular component of GOM were more loosely associated as distanced from the plasma membrane of VSMCs as if they are dispersed into ISF (**Figure 4.5 B**). Where the staining was darker, the more gold particles were attached, which suggests a concentration gradient of N3ECD within GOM. No clusters of gold particles unassociated with GOM were found on the plasma membrane.

Interestingly, linearly arranged intracellular gold labelling was observed in the several arterial VSMCs in meninges, which relatively retained the structure of cell organelle (**Figure 4.5 A** arrows). They appear to be associated with disrupted membranous structure. Some pericytes contained several kinds of 0.1-0.3-μm inclusion bodies

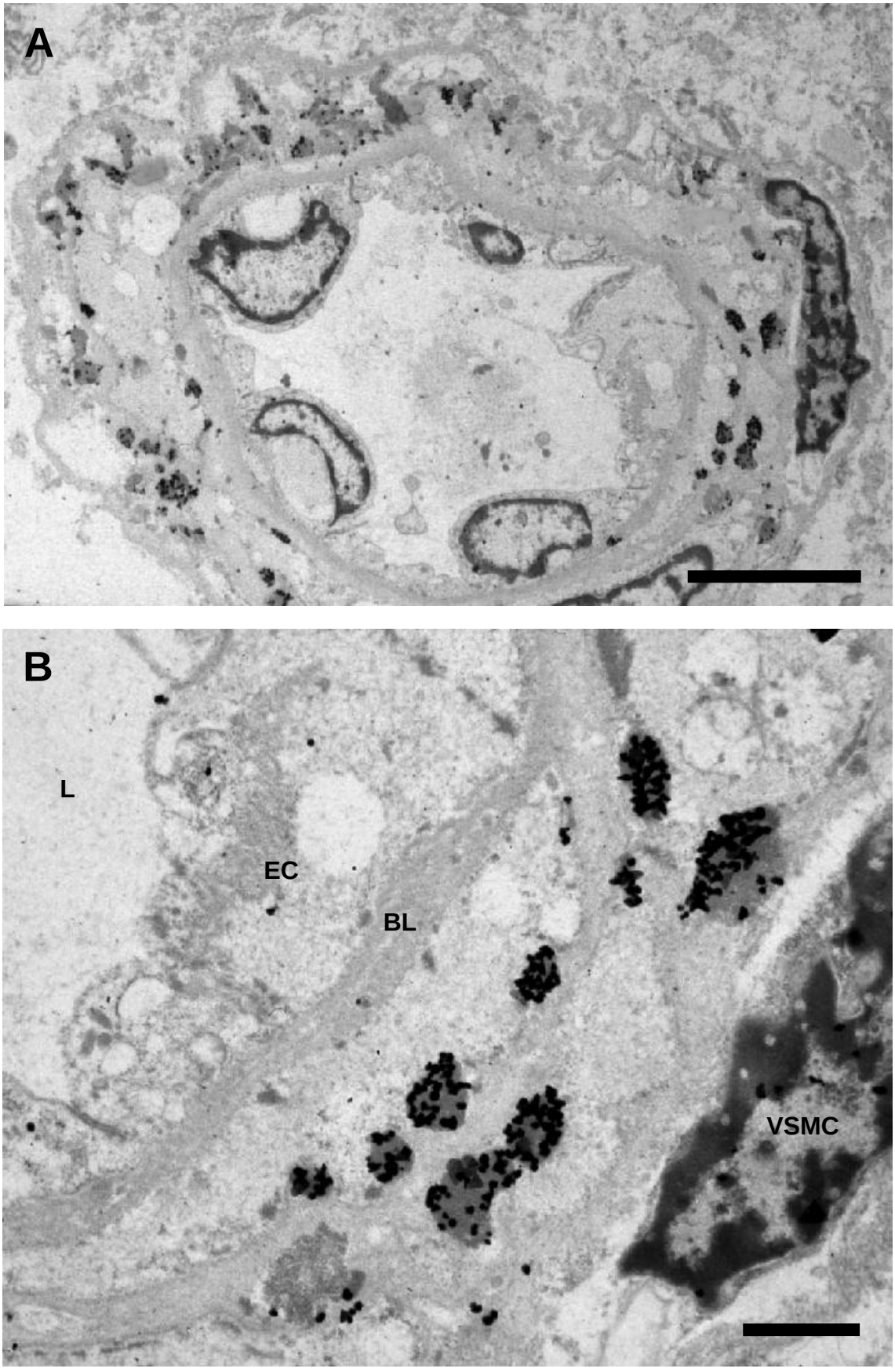

Figure 4.6. N3ECD-labeled GOM depositions found in the tunica media of a small arteriole in GM. L: lumen, EC: endothelial cell, BL: basal lamina, VSMC: vascular smooth muscle cell. Bars represent 5 μm (A) and 1 μm (B), respectively.

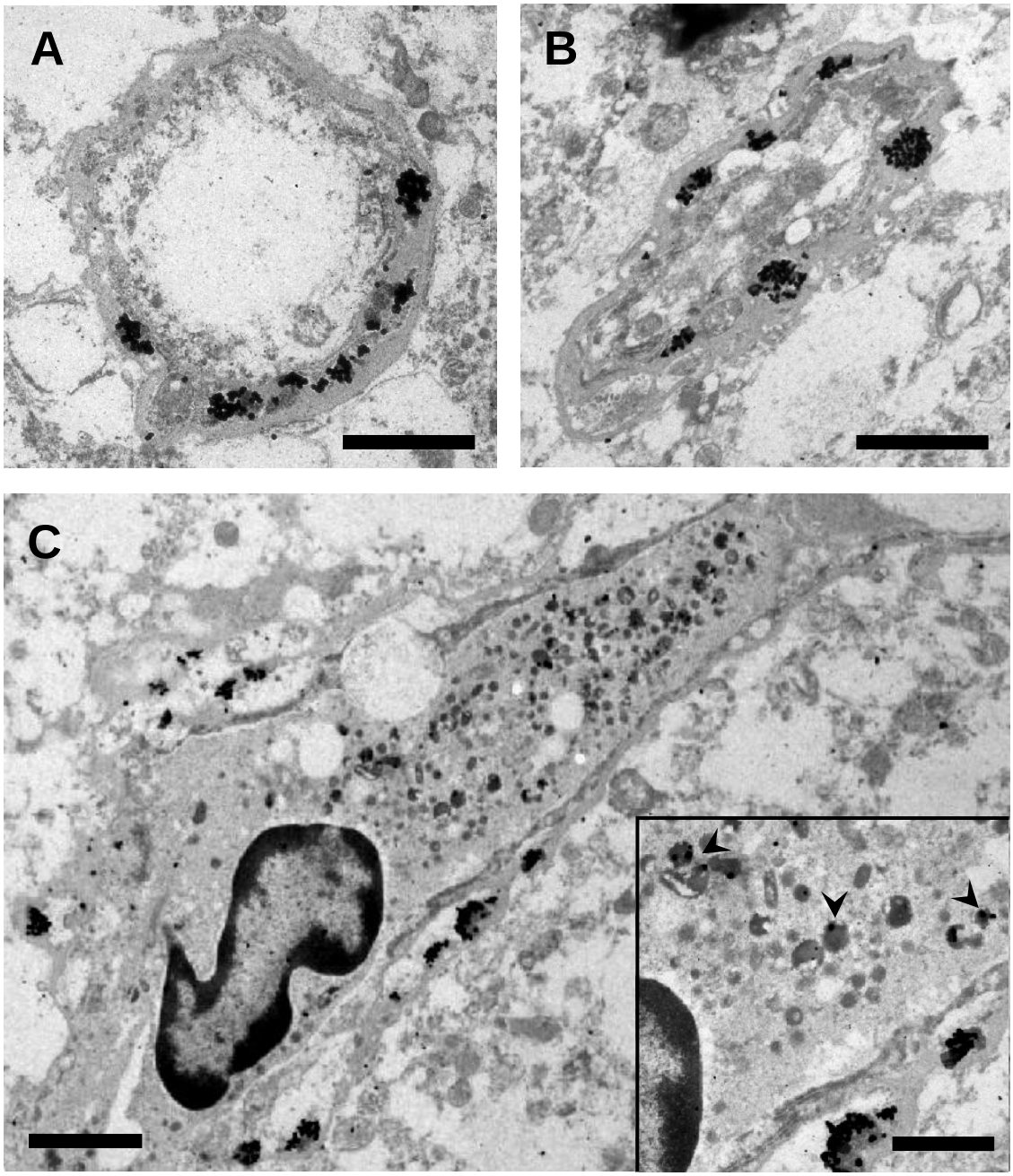

Figure 4.7. Capillaries in GM. N3ECD-labeled GOM were found in the basement membrane of capillaries (A and B) and also around pericytes (C). A few gold particles were also associated with some of the vesicles in pericytes (arrowheads). Bars represent 2 μm (A, B and C) and 1 μm (C inset), respectively.

distributed throughout the cytoplasm, some of which were opaque while others were more electron dense (granular pericyte, **Figure 4.7 C**). A few gold particles were attached to the darkly stained vesicles in the pericytes while almost none were found in the cytoplasm (**C inset)**.

To identify other components of GOM, we stained ultra thin sections with antibodies for Jagged1, ubiquitin and HSP27. The background staining was slightly high with Jagged1 antibody, but no significant amount of gold particles was specifically attached to GOM with any of the antibodies. Immunostaining for human IgG also showed no attachment of gold particles to GOM, suggesting lack of antibody production against mutant Notch3 within GOM.

4.3.4 Immune response in CADASIL

Percentage of CD45 and CD68 immunoreactivity (%Area), which are the markers of neucleated hematopoietic cells (*e.g.* B- and T cell) and monocytes/macrophages, respectively (Donovan and Koretzky, 1993, Holness and Simmons, 1993), was quantified to assess the involvement of immune response in the CADASIL pathology. Most of the CD45-positive cells were found around vessels whereas CD68-positive cells were abundantly found in the WM of CADASIL brains as shown in **Figure 4.8**. The significant difference was observed between CADASIL and age-matched controls for the CD45 %Area ($p = 0.004$) but not for CD68.

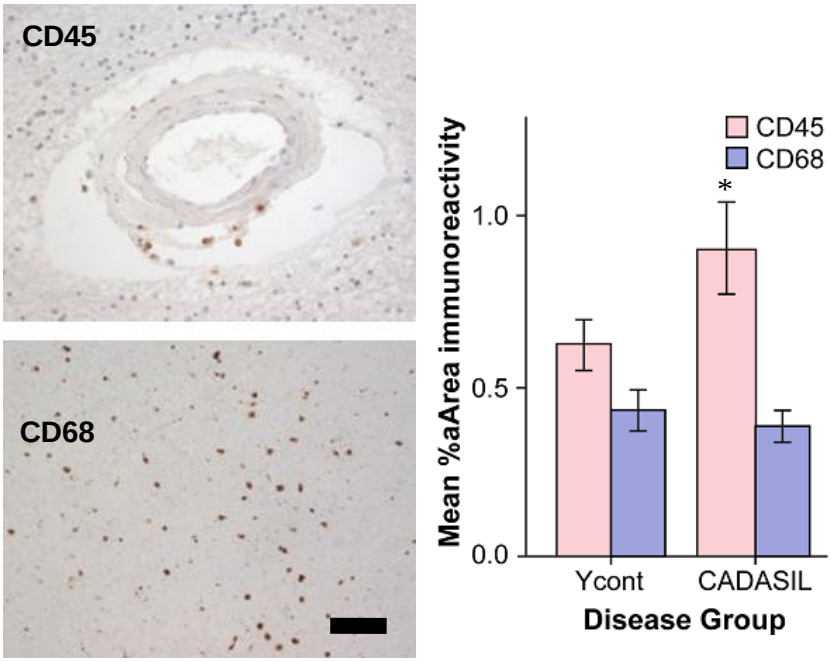

Figure 4.8. CD45 and CD68 immunoreactivities in the white matter of CADASIL brain. There was a significant increase in the percentage of CD45 immunoreactivity between CADASIL and young controls (marked with *). Bar represents 50 μm.

4.4 Discussion

Since the report of the N3ECD accumulation in the vasculature of CADASIL patients, it has been thought that N3ECD accumulates on the plasma membrane adjacent to, but not within GOM until challenged by a study showing the existence of N3ECD within skin GOM (Joutel et al., 2000, Ishiko et al., 2006). Since no study has followed to confirm either of the results, we examined the presence of N3ECD in GOM using postmortem brain tissue from a CADASIL patient. Here, we confirmed that N3ECD in fact accumulates inside GOM deposits located at the basement membrane of arteries, arterioles and capillaries in the brain for the first time. GOM deposits, sized 0.5-2 μm, were found in close proximity to either VSMCs or pericytes, consistent with a recent observation by Lewandowska et al. (2010) in skin biopsies.

The differences between our observations and that in Joutel's study may be attributed to the methodology used to demonstrate the localisation of GOM. The major problem in Joutel et al.'s study (2000) was the use of pre-embedding method on paraffin embedded postmortem brain tissues fixed in buffered formalin. The method greatly limits the accessibility of antibody to the antigen and reduces antigenicity, which could explain the partial immunoreactivity adjacent to GOM (Ishiko et al., 2006). On the other hand, Ishiko's group (2006) used skin biopsy samples prepared using cryofixation and freeze substitution, which require several tissue-embedding processes at -60 to -80 °C but preserve the antigenicity. We sought an easier method that we could use on brain tissues fixed in paraformaldehyde at room temperature, but without false negative result, and optimised the post-embedding immunogold staining method. Our method successfully maximised the immunoreactivity by the combination of double etching and antigen retrieval in citrate buffer while reducing non-specific background staining as

demonstrated by the lack of staining in GOM in negative controls and collagen IV stained sections.

The heterogeneous distribution of N3ECD suggested the presence of other components, and thus this study also attempted to demonstrate the involvement of other Notch-related proteins in GOM deposition, namely Jagged1 and ubiquitin. Jagged1 is a major NOTCH3 ligand expressed in VSMCs and its interaction with NOCTH has been demonstrated to induce VSMC differentiation (Hofmann and Iruela-Arispe, 2007, Doi et al., 2006). We hypothesized that Jagged1, ubiquitin and/or HSP27 were inherent in GOM with N3ECD, as ligand-N3ECD complex is reported to be endocytosed by ligand-presenting cells destined for lysosomal degradation, which involves the process of ubiquitination (Sorkin and Von Zastrow, 2009). Contrary to the expectations, however, GOM was completely devoid of Jagged1, ubiquitin and HSP27, though there still is a possibility that other Notch3 ligands expressed in VSMC, *i.e.* Jagged2 and Delta1, are expressed in GOM. In addition to those ligands, other DSL ligands, as well as non-DSL ligands such as Y-box protein-1, should also be tested as it has been suggested that *NOTCH3* mutations alter Fringe glycosylation, which determines ligand preference of the receptor (Rauen et al., 2009, Arboleda-Velasquez et al., 2005).

The other interesting observation of the present study was weak intracellular immunoreactivity in VSMCs and granular pericytes: slightly curved lines of gold probes in VSMCs and a few isolated gold probes on vesicles in pericytes, which have never been described previously. Although they have potentially valuable implications supporting gain-of-toxic-function (or ER stress) hypothesis (Takahashi et al., 2010), their reliability should be carefully considered for two reasons. One of the reasons is the major tissue disruption due to the patient's advanced disease state. The cyto-architecture

is normally disrupted in postmortem human material due to several factors inclusive of agonal state, extensive postmortem delay and immersion fixation but the consistency of the brain appeared flaccid and did not exhibit the normal rigidity associated with post mortem brain tissue. The tissue had clearly lost much of its morphological integrity and extensive vacuolation as well as corpora amylacea were evident. However, the vascularity appeared to be reasonably preserved. Close examination of the EM images revealed membrane-like structures underlying the linearly arranged gold particles in VSMCs. However, the loss of integrity of the structure does not allow further interpretation of possible labelled sites such as exposed ER, or VSMC plasma membrane invagination with GOM, which may be transected and appearing as unconnected islands within the cytoplasm. These structures can appear in TEM, as the sections are extremely thin and have little depth to follow continuity of membranes. In regard to the vesicular labelling in granular pericytes, the relative lack of clustered gold probes limits clear conclusion. More than 15 vesicles in the pericyte cytoplasm were labelled with a few probes in contrast to the rarely observed cytoplasmic staining. Although weak, the frequent staining implies the presence of N3ECD within the electron-dense vesicles. The vesicles are presumed to be endosomes or secondary lysosomes from their morphology, but their origin is difficult to ascertain from the EM image alone. There are two possible sources of N3ECD in those endosomes, either endogenous or exogenous. Surface expression of NOTCH3 receptor is regulated by its endocytosis from plasma membrane and the recycling or lysosomal degradation that follows (see **Figure 1.2**). The weak immunoreactivity of the vesicles may be due to the fact that N3ECD are not aggregated at that stage. However, it raises a question why such vesicles were not observed in VSMCs. Pericyte is known to have not only vasoconstrictive ability similar to VSMC but also macrophage-like properties, *i.e.* phagocytosis and pinocytosis (Thomas, 1999). It is plausible that N3ECD in the vesicles

were derived from GOM. In support of the notion, the phagocytic activity was reported in a previous EM study in our laboratory, which found a macrophage engulfing a GOM-like electron-dense material (Low RC, unpublished data). Both pericytes and macrophage are important initiators of inflammatory response (Thomas, 1999), thus the above observations may not only imply clearance activity in the perivascular drainage system but also the involvement of inflammatory/immune responses in CADASIL pathology. Indeed, the observed marked increase of inflammatory cells, as indicated by CD45 immunoreactivity (Voskuhl et al., 2009), may corroborate the notion. However, if there is phagocytic activity, it does not seem to induce antibody production. Thus, questions remain with regard to the toxicity of GOM. To further pursue this issue, it would be interesting to examine cervical lymph nodes, where ISF drains into via perivascular drainage pathway to be filtered and GOM may activate immune system.

A number of important limitations in the current study need to be considered. Firstly, limited availability of properly-fixed human brain tissue, suitable for immuno EM, only allowed us to examine one case each for CADASIL and control. Even though the specificity of N3ECD antibody and the identical staining pattern among CADASIL cases were confirmed at light microscopic level, it would have strengthened the arguments if more CADASIL cases and at least one control cases could be included. Secondly, the widespread ischemic changes impacted on the tissue integrity of the CADASIL brain as reflected by its postmortem gelatinous state. The vascular morphology was disturbed and many of the cell organelles were destroyed, which sometimes made it difficult to identify the further intracellular structures associated with the immunogold staining. Lastly, our optimised immuno-gold EM method significantly improved immunoreactivity, but often failed to detect lower concentration of antigens. Further studies using better morphologically preserved tissue, either from humans or Tg

mice, should be conducted to confirm the above findings of intracellular ultrastructural N3ECD gold labelling.

Chapter 5. Neuronal and Vascular Pathology in CADASIL Compared to Sporadic Vascular Dementia

5.1 Introduction

The profile of cognitive impairment in CADASIL is similar to sporadic subcortical VaD and appears to start with impairment in processing speed and executive function, eventually leading to more widespread cognitive decline as the disease progresses (Dichgans, 2009). Cognitive function domains, *e.g.* reasoning, attention, memory, planning, recognition, speaking and perception, are managed by several different areas of the brain and the cross-interactions between them. Among those areas, the hippocampal formation including the subiculum and the entorhinal cortex, is essential for memory consolidation, attention and orienting reactions (Sweatt, 2004, Joseph, 1996). Entorhinal cortex is a main interface connecting hippocampus and various cortical areas, including prefrontal cortex, cingulate cortex, temporal cortex, parietal areas and pyriform cortex (O'Keefe and Nadel, 1978). The inputs from cortical areas are sent to the dentate gyrus, CA3, CA1 and subiculum via the superficial layers (layer II and III) of entorhinal cortex, and are further conveyed to CA2, CA1, subiculum and back to the deep layers (layer V and VI) of the entorhinal cortex (**Figure 5.1**).

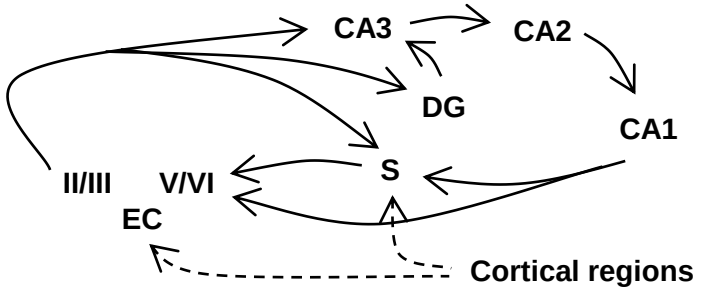

Figure 5.1. Proposed neuronal inputs between hippocampal areas and adjacent areas.
DG: dentate gyrus, S: subiculum and EC: entorhinal cortex

Pathological changes in the hippocampal formation have been reported in mild cognitive impairment and several forms of dementia. Atrophy of the entorhinal cortex and hippocampus - the former precedes the latter - is one of the most common changes in mild cognitive impairment and mild AD (Stoub et al., 2006, Pennanen et al., 2004). Loss of neurons is suggested as the cause of atrophy (Zarow et al., 2005), but the most affected areas (or subtypes of neurons) seem to differ depending on the disease pathology. Decreased neuronal density in the entorhinal cortex and hippocampal regions is implicated in cognitive decline in mild cognitive impairment and mild AD (Kordower et al., 2001, Gómez-Isla et al., 1996, Kril et al., 2002a) while DLB showed loss of lower presubiculum pyramidal neurons only and not in the CA1 or entorhinal cortex (Harding et al., 2002, Gómez-Tortosa et al., 2000). The neuronal changes in VaD remain unclear. Two studies have measured hippocampal neuronal density in VaD using a stereological method. Zarow et al.(2005) reported that brains from ischemic vascular dementia patients retained neuronal number in CA1 and CA2. On the other hand, Kril et al. (2002b) found that the number of CA1 pyramidal neurons was substantially decreased in SVD with dementia. The contradicting results may stem from the difference in the criteria used for the selection of the dementia groups; the former study selected samples based on the number and location of infarcts, and the latter used demented group with significant vascular pathology (*e.g.* vessel wall thickening and PVS dilation) but no AD or other degenerative pathology (Zarow et al., 2005, Kril et al., 2002b). In addition to the problem with VaD criteria, the lack of sufficient data on neuronal density in VaD has limited us in drawing any conclusions. To our knowledge, no study has investigated the neuronal density changes in CADASIL. As the pathology underlying the cognitive dysfunction in CADASIL is rather uniform than in sporadic VaD or SVD, a study in neuronal density of the hippocampus and entorhinal cortex in CADASIL may provide clear insight into the cognitive impairment in SVD.

The cause of neuronal loss in the hippocampal formation may vary between diseases reflecting upon different degradative processes: abnormal protein deposition is the most likely candidate for both AD and DLB, and vascular factors for VaD and CADASIL. Cortical or subcortical microinfarcts or BBB breakdown in subcortical structures causing disruption to the limbic circuits, as suggested in chapter 3, may be the primary cause in CADASIL. Another possibility is the decreased CBF to the temporal lobe (Chabriat et al., 2000). Joutel and her group (2010) reported the rarefaction of capillaries in the corpus callosum but not in the cortex of the transgenic *NOTCH3* (Arg169Cys) mice. Our previous findings (Yamamoto Y and Kalaria RN, unpublished observations) indicated that the density of Glut-1 positive vasculature was decreased, albeit in frontal lobe, in CADASIL also support the notion that microvascular abnormality may contribute to the neuronal loss in the hippocampal formation.

Therefore, in this chapter, we assessed density changes of neuronal population and vasculature in the hippocampus and entorhinal cortex to evaluate the neurovascular pathology in CADASIL. In addition, the density of a neuronal subpopulation immunoreactive to SMI32 antibody, a sensitive marker of ischemic insult (Leifer and Kowall, 1993), was assessed in order to examine the damage to the pyramidal neurons. The analysis was conducted using a three dimensional stereological system, which is the most reliable and accurate density estimation method currently available.

5.2 Materials and Methods

5.2.1 Subjects and IHC

Formalin fixed, paraffin-embedded hippocampus blocks containing the anterior hippocampal formation from 8 CADASIL cases (mean age = 58, SD = 7.6), 10 CADASIL age-matched controls (Ycont, mean age = 61, SD = 8.3), 7 older controls

(Ocont, mean age = 79, SD = 4.2), and 8 post-stroke demented COGFAST cases (mean age = 85, SD = 4.2, as described in chapter 2) were cut into 10- and 30-µm sections. Postmortem delay ranged from 14 to 72 hours and length of tissue fixation was an average of 6 months. There was no significant difference in fixation length and postmortem delay between groups. The 30-µm sections were stained with anti-non-phosphorylated neurofilament H (mouse anti-SMI32/TBS 1:500, Covance, USA) to identify large pyramidal projecting neurons, and then counterstained with CFV to visualize all the neurons and glial cells present. During IHC, the sections were microwaved twice for 10 minutes for antigen retrieval. The 10-µm sections were stained with anti-glucose transporter-1 (rabbit anti-GLUT-1/PBS 1:200, Thermo Fisher Scientific Inc., USA) and CFV to identify vasculature for the quantification of the microvascular density in the hippocampal formation.

5.2.2 Three dimensional stereology

5.2.2.1 Principles

In the past few decades, stereology has been increasingly recognised as an essential tool for the more precise quantification of geometrical properties in a three-dimensional structure. The keys to the accurate stereological estimation are uniform and random sampling and unbiased systematic interrogation. In principle, the sum of the probe dimensions and the parameter dimensions have to be larger than 3, *e.g.* area probe (dimensions, dim = 2) is used for length estimation (dim = 1) and volume probe (dim = 3) for numbers (dim = 0) (Calhoun and Mouton, 2001). The density of linear objects, such as blood vessels and axons can be measured as length density since the number of the objects per volume strongly depends on the directionality of the object to the section surface. The length density of linear biological objects, which is the total length of the objects within a unit volume, is estimated based on the probability of intersections

between probes and the objects as first proposed by George L. Buffon (1777) and later by Smith and Guttman (1953) for 3D application. Length per unit volume (length density, Lv) is related to two times the number of random intersections and area of sampling probe (plane).

$$Lv = 2 \cdot \sum Q / \sum A$$

ΣQ: number of random intersections
ΣA: area of sampling probe

For the estimation of object density, on the other hand, volume (3D) probes (dissector box) are randomly placed on the image of thin sections for the number of object within to be counted. The density is calculated using the following formula.

$$Nv = \frac{\sum Q^{-}}{P \cdot V}$$

Nv: Numerical density
$\sum Q^{-}$: Total counts of object
P: Total number of dissectors
V: Disector box volume

The volume of objects (VN), in number-weighted distribution, is estimated using the 'nucleator' method developed by Gundersen (1988). The unique point (*e.g.* nucleolus) of the object within the dissector box is defined by the researcher and distances to the boundary of cell membrane are used to calculate the volume.

$$\hat{\bar{V}}_N = \frac{4\pi}{3} \cdot \bar{l}_n^3 = \frac{4\pi}{3 \cdot n} \sum_{i=1}^{n} l_{n,i}^3$$

l_n: Distance from sampling point

n is the total number of point-sampled linear intercepts and l3n,$_i$ is the cube of the *i*th point-sampled intercept length. Larger number of random distance measurements improves the efficiency and accuracy of the volume estimation.

5.2.2.2 Estimation of neuronal and glial densities and neuronal size

The immunostained 30-µm brain sections were analyzed using the computer assisted stereology toolbox (Visiopharm Integrator System; Visiopharm, Denmark). Each region

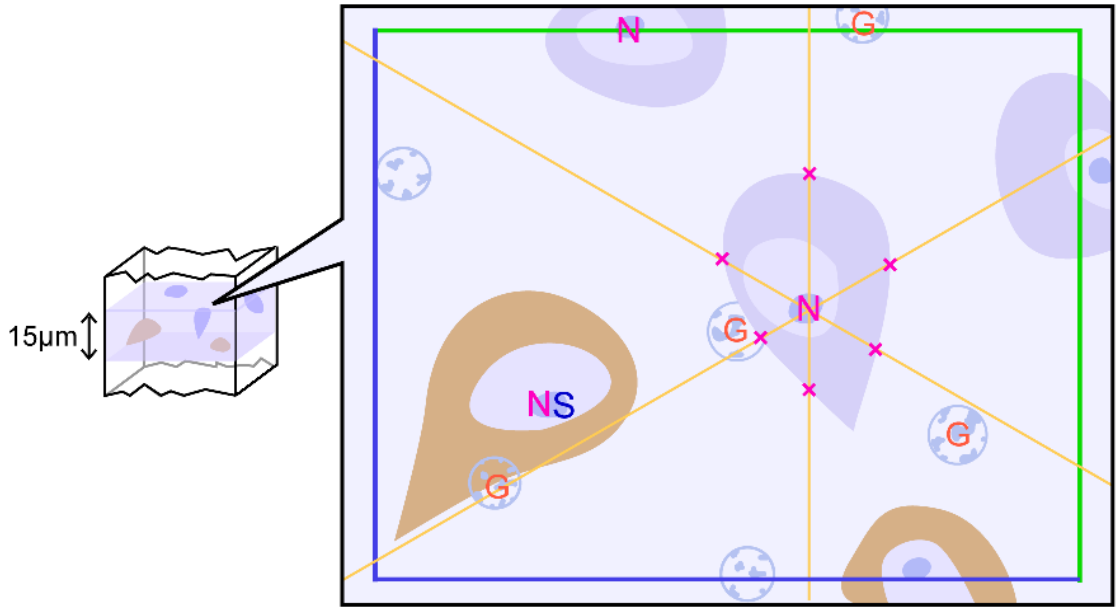

Figure 5.2. 3D stereology: counting rules and the volume estimation method. The middle 15-µm depth was scanned through to identify neurons and glial cells within the dissector box. Glial cells and neurons with a nucleolus inside or touching the green lines were counted and measured for volume estimation. Neurons were marked with N, SMI32 positive neurons (coloured brown) with S and glial cells with G. The intersections of lines with cell membrane were marked by the researcher for volume estimation.

of interest (ROI), *i.e.* entorhinal cortex layer V (ECV) and hippocampus regions (CA1 and CA2) defined as described in chapter 2, was outlined using a Zeiss Axioplan Photomicroscope coupled to a Pixelink PL-B623CF colour digital video camera (Pixelink U.K.) at x2.5 objective magnification. Cell counts and volume estimation were conducted under x100 magnification while the XY and Z motorised stage (Prior ProScan II, Prior Scientific Instruments Ltd, Cambridge, U.K.) provided systematic random sampling of the field to be analysed. The unbiased dissector and nucleator methods were used to estimate density and size of neurons and glial cells. The thickness of the tissue was measured using a Heidenhain gauge (Heidenhain GB Ltd, London, U.K.) for one in every ten fields during analysis to correct for artificial damage and shrinkage during tissue processing. There was no significant difference in mean section thickness between groups. Approximately 40 to 80 fields per ROI were analysed to

achieve the same sampling fraction for each ROI between sections. Each dissector box measured 56.43 μm long x 45.14 μm wide. CFV staining revealed purple neurons with a pale nucleus and a single darker-shade nucleolus, as well as glial cells, of which nucleus only was heterogeneously stained. Neurons were counted and measured only when the nucleolus came into focus either fully inside the dissector box or touching one of the three non-forbidden planes (green lines; right, top and upper side) within the dissector height, which was set at 15 μm (see **Figure 5.2**). SMI32 positive (+) neurons were separately counted from the total number of neurons (SMI32(+) and negative (-)) which was also counted. Volumes of neurons were estimated based on six randomly projected lines extended from a point defined by the researcher, which in this case was the nucleolus. For glial cells, of which cytoplasm was unstained with CFV, only density was measured following the same counting rules. Coefficient of error was calculated using the Gundersen-Jensen method (Gundersen and Jensen, 1987).

5.2.2.3 Estimation of vascular density

Glut1 immunostained brain sections were analyzed using the Visiopharm Integrator System. The ROIs in CA1, CA2 and whole entorhinal cortex (layer II to VI) were outlined using a Zeiss Axioplan Photomicroscope coupled to a Pixelink PL-B623CF colour digital video camera (Pixelink U.K.) at x2.5 objective magnification. 60, 100 and 40% of CA1, CA2 and entorhinal cortex, respectively, were analysed under x25 magnification. A dissector box of 571.12 μm long x 456.93 μm wide was placed on an image at each sampling point, and the number of intersections between the dissector box (area probe) and the spine of vessels were counted following the same counting rules as neurons: vessels fully inside the dissector box or their spine touching green lines were counted. The length density was calculated as described in 5.2.2.1.

5.2.3 Statistical analysis

Cell counts were divided by ROI volume, derived from ROI area multiplied by ROI depth 15 μm, to obtained density. Neuronal/glial densities and neuronal volume were compared between groups using both Kruskal-Wallis and Mann-Whitney U tests. Correlation was tested using Pearson's correlation test.

5.3 Results

There were no significant changes in the density of glial cells between groups, except in CA1 and CA2 between Ocont and Ycont, which had fewer cells ($p = 0.040$ and 0.072). There was no correlation between neuronal densities and fixation length or postmortem delay. The SMI32 and CFV staining pattern of representative areas for each disease group is presented in **Figure 5.3**. In general, control tissues had stronger immunoreactivity and more SMI32(+) neurons compared to CADASIL and COGFAST.

5.3.1 Neuronal density changes

Figure 5.4 shows the total neuronal density in each disease group as well as the SMI(+/-) density. Unexpectedly, there was no significant difference between Ycont and CADASIL in total neuronal density, defined as all CFV(Nissl) stained neurons, but only trends of decreases in CA1 and CA2 ($p = 0.101$ and 0.073) (**A**). The COGFAST also showed marginal decrease in total neuronal density in the ECV ($p = 0.053$) and not in the other regions. The statistical difference is partly derived from higher density in Ocont than Ycont, which may be accounted for by the biological variability among controls. Moreover, the total neuronal density did not correlate with either CAMCOG or MMSE scores.

On the other hand, the density of SMI32(+) and (-) neurons showed dramatic changes (**Figure 5.4 B**). Although statistically not significant due to the large variation in the

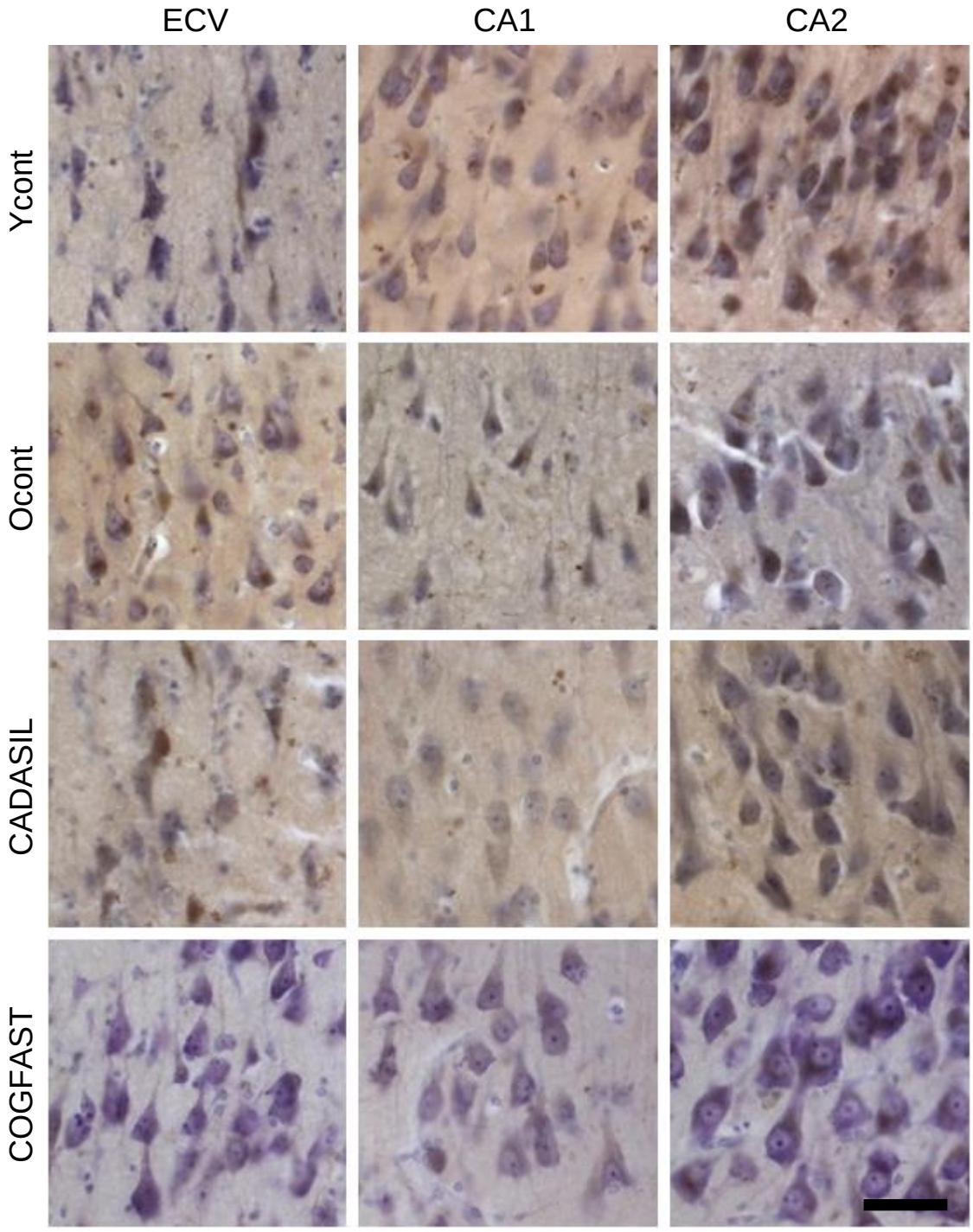

Figure 5.3. Representative images for each ROI in brain tissues stained with CFV and SMI32 antibody. Controls had more SMI32 staining in neurons than CADASIL or COGFAST groups. ECV: entorhinal cortex layer V. Bar represents 50 μm.

Ycont group, CADASIL brains had 40.4, 28.8 and 40.1 % lower density of SMI32(+) neurons compared to Ycont in the ECV ($p = 0.055$), CA1 and CA2, respectively. Significant difference between Ocont and COGFAST cases in SMI32(+) ($p = 0.004$) but

not SMI32(-) density was also noted in the ECV, suggesting a greater insult in the area in COGFAST and loss of large pyramidal neurons, which are immunoreactive to SMI32. The effect of ageing was limited to loss of SMI32 expression as indicated by the notable increase of SMI32(-) neuronal density in ECV in Ocont (p = 0.042) and slight increase in CA1 (p = 0.109) compared to Ycont.

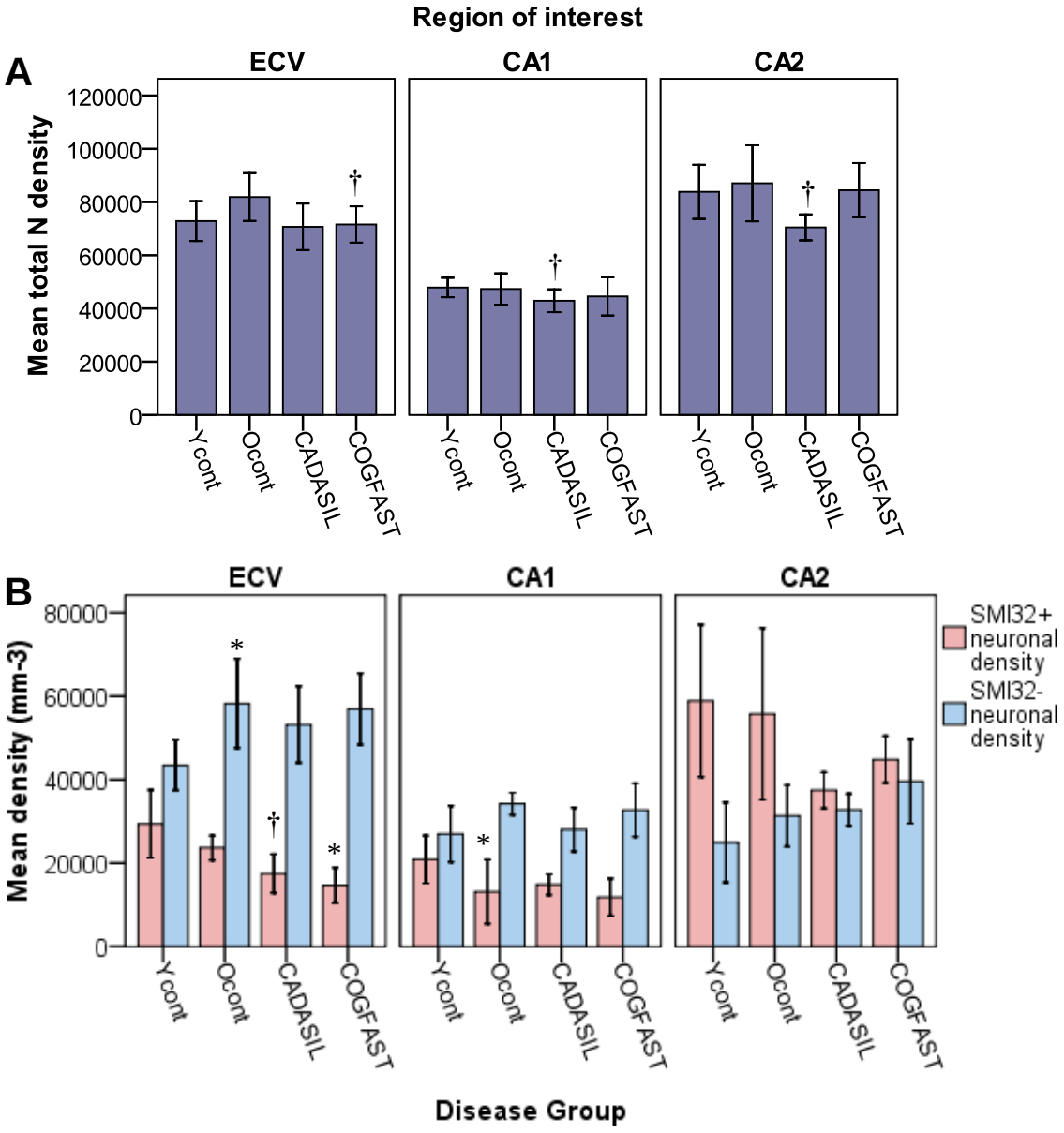

Figure 5.4. Neuronal density changes in entorhinal cortex layer V (ECV) and hippocampus regions CA1 and CA2. The total neuronal density (mm^{-3}) was relatively preserved in CADASIL and COGFAST (A). SMI32 positive neuronal density was decreased in CADASIL while SMI32 negative neuronal density was slightly increased (B). *: Significance (P < 0.05) and †: trend (P < 0.1) vs. age-matched controls or between controls. Error bars ± 2SE

Correlation analysis between SMI32(+) and SMI32(-) neuronal densities was performed to note if the decrease in the density of SMI32 positive neurons in Ocont, CADASIL and COGFAST is a true reflection of large pyramidal neuronal loss or merely the loss of SMI32 immunoreactivity. As expected, controls showed negative correlation between SMI32(+) and (-) neurons (Ycont and Ocont combined; ECV: R = -0.495, p = 0.051; CA1: R = -0.777, p = 0.0001; CA2: R = -0.884, p = 0.0001). However, there was no significant correlation in any of the regions in CADASIL (ECV: R = -0.338, CA1: R = -0.578, CA2: R = -0.046) and COGFAST (ECV: R = -0.613, CA1: R = -0.151, CA2: R = -0.257), suggesting imbalances between the decrease of SMI32(+) and the increase of SMI32(-) densities. These results indicate that while the expression of SMI32 was reduced in Ocont, only small numbers of large pyramidal neurons (SMI32(+) neurons) were lost in CA1 and CA2 of CADASIL (coinciding with decreased SMI32 expression), and in ECV of COGFAST (**Table 5.1**).

	CADASIL			**COGFAST**		
	ECV	CA1	CA2	ECV	CA1	CA2
Total N	→	↓	↓	↓	→	→
SMI32 (+)	↓	→ (↓)	→ (↓)	↓↓	→	→
SMI32 (-)	→ (↑)	→	→ (↑)	→	→	→

Table 5.1. Summary of neuronal density changes in CADASIL and COGFAST compared to age-matched controls. →: no change, ↑↑/↓↓: statistically significant increase/decrease, ↑/↓: trend of increase/decrease, (↓) decreased mean. Decreased total neuronal density (Total N) coincided with decreased SMI32(+) density indicates loss of SMI32(+) neurons, while spared Total N and decreased SMI32(+) but increased SMI32(-) mean loss of SMI32 expression. Imbalance between SMI32(+) decline and SMI32(-) increase may suggest slight neuronal loss.

5.3.2 Neuronal volume

In general throughout all the groups, the volume of SMI32(+) neurons was larger by 6.88-37.90% than that of SMI32(-) neurons in ECV and CA2. There were no significant changes apparent in neuronal volumes between CADASIL and Ycont.

However, neurons in COGFAST showed significantly increased volumes in the ECV compared to age-matched controls (p = 0.038) (**Figure 5.5**). The volume change was greater in SMI32(+) neurons than in SMI32(-) neurons (data not shown).

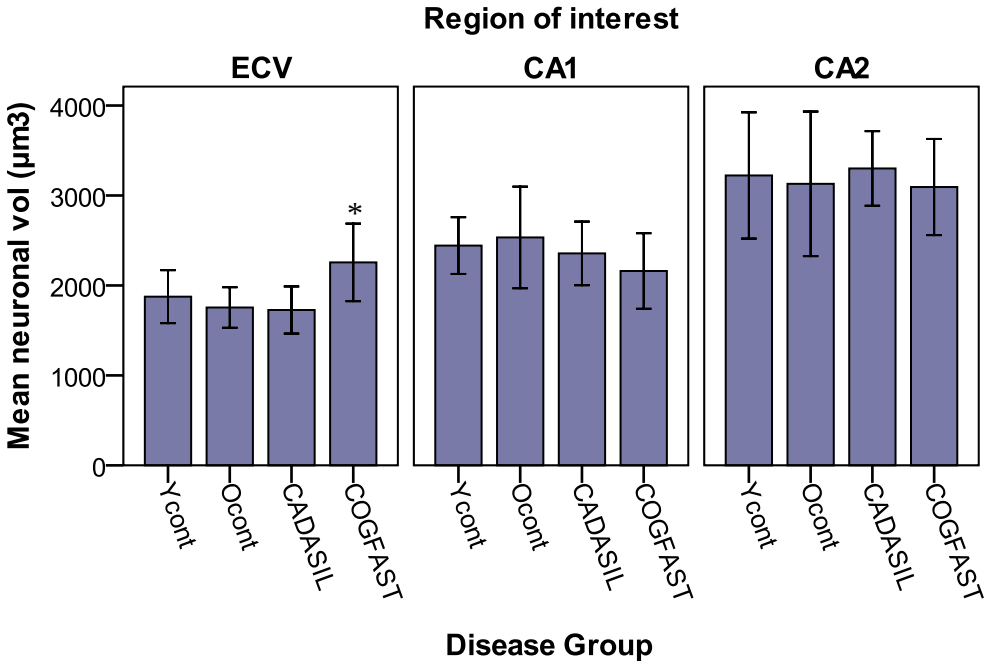

Figure 5.5. Neuronal volumes in entorhinal cortex layer V (ECV) and hippocampus regions CA1 and CA2. There was no significant difference in volume except between Ocont and COGFAST in ECV. Error bars ± 2SE.

5.3.3 Vascular density

Length density of Glut-1 immunoreactive small vessels was estimated to evaluate the microvascular changes in relation to neuronal changes. Although CADASIL samples compare to Ycont showed 12.1% decrease in length density in CA1 region, the Kruskal-Wallis test indicated no significant differences between the groups in any of the ROI (**Figure 5.6**). The lack of significance may be partly accounted for by small sample size. Neuronal density correlated (controls: R = 0.365, p = 0.034; CADASIL: R = 0.637, p = 0.014; COGFAST: R = 0.685, p = 0.001) with vascular length density when ROIs were combined, confirming the close relationship between neurons and vasculature. In general, length density was CA2= ECV >CA1.

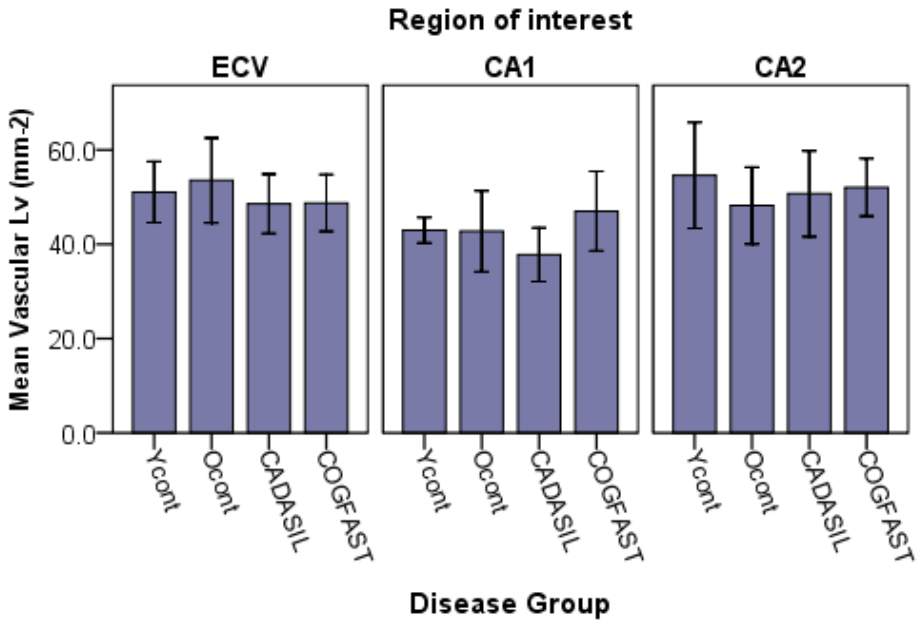

Figure 5.6. Mean length density of Glut-1 immunoreactive vasculature. There were no significant differences between the groups. Error bars ± 2SE

5.4 Discussion

This study provided the first quantitative data in relation to cognitive dysfunction in CADASIL. Hippocampal atrophy and neuronal density changes in mild cognitive impairment and mild AD have been described previously (Kordower et al., 2001, Gómez-Isla et al., 1996, Kril et al., 2002a), while results for sporadic VaD varied possibly due to the differential underlying pathology in VaD (Zarow et al., 2005, Kril et al., 2002b). CADASIL brain pathology is relatively uniform in this regard, being largely described to be SVD type, and thus suitable to explore the degree of hippocampal changes with respect to cognitive dysfunction in VaD.

Our results showed that total neuronal density is relatively preserved in CADASIL and COGFAST though the number of neurons was slightly decreased in hippocampus (CA1 and CA2) in CADASIL and in ECV in COGFAST. These results partially agree with the findings from the two previous studies on sporadic VaD. Kril et al.'s study (2002b),

which included only SVD cases without other neuropathological abnormalities, demonstrated loss of pyramidal neurons in CA1. The lack of significant neuronal loss in the CADASIL group may be due to the significant age difference between CADASIL (mean age = 58 years in this study) and sporadic SVD (mean age = 86 years in Kril's study) though such age effect was not observed among our CADASIL cases. COGFAST, on the other hand, included largely but not exclusively SVD cases with post-stroke dementia as in Zarow et al.'s study (2005) (mean age = 81), which showed no change in CA1 and CA2 neuronal densities. The different patterns of neuronal loss may stem from the difference in their pathogenesis; chronic or acute hypoperfusion, micro- or macro- infarcts and global or focal insult. In fact, the hypertrophy of ECV SMI32(+) neurons in COGFAST seems to indicate the acute and early stage of damage. In addition to the data from sporadic cases, the observation by Viswanathan et al. (2006) is in agreement with the lack of significant neuronal density changes in the CADASIL hippocampal regions. The authors described an increased number of apoptotic neurons in the various areas of cerebral cortex including frontal and occipital cortices, and glial cells in WM of four CADASIL cases, but minimal neuronal apoptosis in the hippocampus. Another CADASIL patient study also pointed out that cholinergic axons were relatively spared in the hippocampus, entorhinal cortex and temporal neocortex whereas cholinergic denervation is extensive in posterior parietal, dorsal frontal, and occipital cortices (Mesulam et al., 2003).

Our study not only quantitatively corroborated the above previous studies but also provided a further insight into the neuronal changes in the hippocampus of CADASIL by focusing on a specific subtype of neurons, namely SMI32(+) neurons. SMI32, which is non-phosphorylated neurofilament-M and -H, is found in pyramidal projecting neurons (type I) and its depletion is a sensitive marker of chronic ischemic stress (Leifer

and Kowall, 1993, Voelker et al., 2004). Higher susceptibility of SMI32(+) neurons has also been reported in AD and DLB (Thangavel et al., 2008). Although not significant, the observed decrease in SMI32(+) but not SMI32(-) density confirmed SMI32 depletion and the minor loss of pyramidal neurons in hippocampal formation, suggesting that the hippocampal formation is not completely spared from hypoxic/ischemic damage in CADASIL and COGFAST. The damage, however, is probably not the result of decreased microvascular density, at least in the hippocampal formation as suggested by this study, as opposed to a Tg mice study showing microvascular rarefaction (Joutel et al., 2010). Whether SMI32 immunoreactivity can indicate functional integrity of neurons is unknown, but functional or structural disruption of the connectivity between hippocampal formation and other regions of the brain may underlie the impaired episodic memory retrieval in CADASIL as the SMI32(+) neuronal subpopulation consists of long projecting neurons with heavily myelinated axons responsible for subcortical and corticocortical connections (Voelker et al., 2004, Hof et al., 1995).

Collectively, our data provided the neuronal basis for the intact memory encoding and storage processes in CADASIL. One source of weakness in this study which could have affected the results was the number of samples used. Although our sample size was no smaller than those in the previous stereological studies on hippocampal neuronal density (Harding et al., 2002, Kril et al., 2002a, Kril et al., 2002b, Zarow et al., 2005), it is possible that there were insufficient statistical power to detect the milder neuronal loss in CADASIL compared to other forms of dementia. Depending on the availability, analysis of additional CADASIL cases will strengthen our findings. Further research is also needed to provide complete picture of cognitive impairment in CADASIL in terms of the locations of damaged area and the pathogenesis. It is of interest to ascertain

whether neuronal density changes in frontal cortex (*e.g.* BA9), representative of executive function, or the disconnection of cortical areas and the hippocampal formation due to axonal damage is a cause of executive dysfunction.

Chapter 6. Severity and Distribution of Axonal Damage in CADASIL

6.1 Introduction

The hippocampal formation is an essential part of the brain and is responsible for memory functions; however, it is not the only structure that is associated with memory, or cognitive function (Warburton and Browna, 2010, Chayer and Freedman, 2001). The previous chapter discussed the possibility of pathologies other than neuronal loss in the hippocampal formation being implicated in cognitive decline in CADASIL, *i.e.* neuronal loss in other areas of the brain and disrupted corticocortical, cortico-subcortical communication due to WM damage (O'Sullivan et al., 2005). Although WM abnormalities alone may not cause cognitive decline, its substantial effects on cognitive functions cannot be ignored (Deary et al., 2003).

The disconnection syndrome, in which brain dysfunction at least in part, resulted from disrupted associative connections between various brain regions by WM abnormality, has recently regained the interest of researchers (Catani and Ffytche, 2005). Disconnection of different circuits resulting in cognitive dysfunction has been suggested to occur in AD, frontotemporal dementia, multiple sclerosis and cognitive impairment after traumatic brain injury (Collette et al., 2007, Dineen et al., 2009, Stoub et al., 2006, Kato et al., 2007). In AD, for example, the functional anterior-posterior disconnection (prefrontal cortex - hippocampus and visual area) together with damage to medial temporal structures was associated with delayed memory (Grady et al., 2001). On the other hand, studies in multiple sclerosis related worse working memory and processing speed to disruption of the splenium of the corpus callosum, superior longitudinal fasciculus (SLF), BA40 and BA4 (Dineen et al., 2009, Ranjeva et al., 2005). CADASIL

subjects exhibit rather specific spatial distribution of WM lesions as shown by MRI (Coulthard et al., 2000), and thus it is plausible that disrupted connectivity of specific brain regions underlie the profile of cognitive deficits. Indeed, Tatsch et al. (2003) considered disconnections by subcortical lesions as one of the causes of reduced cortical metabolism and cognitive dysfunction in CADASIL. The neuropsychological manifestations also suggest the disconnection of prefrontal cortex from thalamus and basal ganglia: CADASIL patients exhibit mild cognitive impairment, psychomotor retardation, executive dysfunctions but not dementia until the later stage of the disease (Amberla et al., 2004, Blanco Menéndez et al., 2001). It should be noted that while lacunar infarcts have been associated with cognitive dysfunction in CADASIL (Viswanathan et al., 2007), WM hyperintensities on MRI did not correlate with cognitive function in CADASIL (Liem et al., 2007, Scheid et al., 2006). However, abnormalities in normal-appearing WM, which are not detectable with conventional MRI but DTI or magnetization transfer imaging, have been shown to contribute to the impairment of cognitive function, especially of executive function (Vernooij et al., 2009, O'Sullivan et al., 2001, Dineen et al., 2009), suggesting the significance of subtle changes in WM.

In this chapter, we aimed to reveal the distribution and significance of axonal damage in CADASIL by quantifying SMI32 immunoreactive axons using a recently developed 3D stereological method. We also propose a novel 2D method for the estimation of axonal density as a part of this analysis. SMI32 abundantly exists in neuronal cell bodies and dendrites but is absent in normal myelinated axons unless they are damaged and dysmyelinated (Trapp et al., 1988). As SMI32 staining, which appears as continuous lines, small dots or ovoids (retraction bulbs), is detected in axons only after a longer dysmyelination periods unlike the amyloid precursor protein, used as a marker for acute

injury, it is a useful indicator of chronic axonal damage and possibly axonal degeneration (Lindner et al., 2009). Since the WM hyperintensity on T_2-weighted MRI does not necessarily indicate axonal dysfunction, the evaluation of SMI32 positive axonal density in various parts of the brain WM would provide a new insight into WM disconnectivity in CADASIL.

6.2 Materials and Methods

6.2.1 Brain samples IHC

For the analysis, we used 4 controls (Cont1, 2, 3 and 4; age = 68, 69, 72 and 78 years old) and 3 CADASIL cases (CAD1, CAD 11 and CAD12 in Table 2.1, age = 44, 68 and 68 years old), which had appropriate fixed blocks of tissue for the areas of interest. The blocks included A, B, C, G, K, R, S, Z, AD, AE, AG, AI, AJ and AK as marked on the Newcastle Brain Map (**Figure 2.1**). Formalin fixed, paraffin-embedded blocks were cut to produce 10 and 30 µm sections. The sections were stained with anti-non-phosphorylated neurofilament H (mouse anti-SMI32 1:500, Covance, CA) and CFV to visualize damaged axons. Each set of slides was randomly labelled with number and corresponding block code by a technician blind to the researcher.

6.2.2 Length density estimation

6.2.2.1 Principle of 'space balls' method

As described in 5.2.2.1, the length density, which is total length per unit volume, is estimated from the number of intersections between probes and objects of interest. The probes used for the length density estimation include line probes as in chapter 5 and cycloids. The disadvantage of these probes is the absolute requirement of isotropic object-probe intersections by complete randomisation of the inherent object orientation. That is, the ROI in the tissue needs to be extracted and randomly rotated before being

sectioned, which is not always possible in a human study due to the often limited availability of the tissue. The most recent and now widely accepted spherical probes, also referred to as space balls, provides a good solution; the surface of a sphere covers all possible orientations and thus does not require complicated randomized sectioning methods or counting rules (Mouton et al., 2002). The total length is estimated using the following formula

$$L = 2 \cdot \sum Q \cdot \frac{v}{a} \cdot \frac{1}{ssf} \cdot \frac{1}{asf} \cdot \frac{1}{tsf}$$

v: volume of a sampling box
a: surface area of a sphere probe

where ∑Q = sum of the intersections between sphere probes and liner objects, ssf = the fraction of the total number of sections analysed, asf = the fraction of the sampled area and tsf = the fraction of the sampled thickness. The unbiased sampling is achieved only if the diameter of the probe is larger than two-fifths of the object diameter (Mouton et al., 2002). Therefore, in practice, hemispherical probes are used to increase the diameter of the probe relative to the diameter of the objects.

6.2.2.2 Axonal length density estimation

The stained 30-µm brain sections, two adjacent sections per sample, were first examined using a light microscope to exclude the slides without quantifiable amounts of axonal staining in the WM from further analysis. Where a notable amount of staining was present, the staining pattern and location were recorded prior to the axonal length density measurement. A sampling area of approximately 10 x 12 mm was marked on the slides so that corresponding areas of the WM was examined for each case. The sections were then viewed under an Olympus BX51 upright microscope coupled with mbf Bioscience CX9000 camera and analysed using StereoInvestigator (MBF Bioscience, VT, USA). The XYZ motorized stage was controlled by a Modular Automation Controller 6000 (Ludl Electronic Products Ltd., USA). The ROI was

outlined at x2 magnification and then switched to x100 magnification for axonal counting. The sampling grid size (distance between the centres of hemispherical probes) was set to 902 x 751 μm to acquire an average of 150-200 counts per ROI in a sample with moderate axonal density. The thickness of the tissue was measured at each sampling point using a Heidenhain gauge (Heidenhain GB Ltd, London, UK) in order to place the hemispherical probe at the centre of the section thickness (**Figure 6.1**). The radius of the probe was set to 12 μm taking the tissue shrinkage and guard volume into consideration. At each sampling point, the sampling depth was scanned through and the intersections between the hemispherical probes (appears as a circle on screen) and the SMI32 axons in focus were marked for counting. The length density was calculated by dividing the total axonal length by the sampled reference volume.

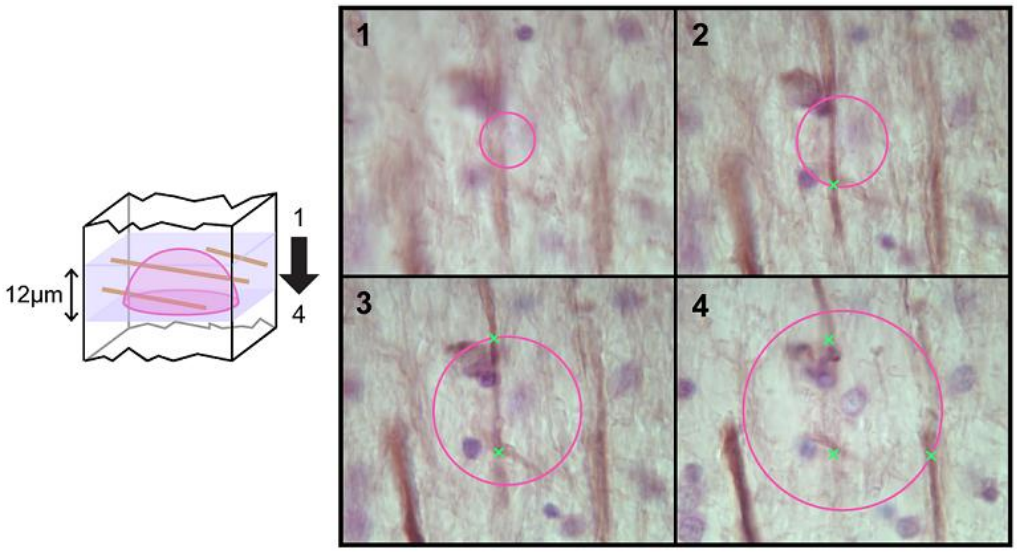

Figure 6.1. Length density estimation using the space balls method. Hemispherical probes were placed at the centre of tissue thickness. The intersections between probes (appear as circles with changing size) and focused axons were counted (marked with x).

6.2.3 New approach for the quantification of axonal density

6.2.3.1 Principle of cutting plane angle correction

The comparison of axonal densities between sections is only possible if the cutting plane angle (θ) is the same and thus θ was normalized to 0 degree as follows (**Figure 6.2**). θ was estimated from the mean apparent length of the axons (mL), which was attained by measuring length (L) of 10 randomly-selected axons, and section thickness T. The estimated θ was then used to calculate width of sampling frame (W) using the formulae below.

$$\theta = \tan^{-1}(T / mL)$$
$$W = T / \sin(\theta)$$

Axons contained fully inside the counting frame, touching both or either of the green lines (top and right) but not blue lines (bottom and left) or ones running through the counting frame were counted. The number of axons in the sampling fame is equivalent to that in the T-µm section when cut completely parallel to the axonal tract. The axonal density was calculated by dividing the number of axons per sampling frame by the area derived from T and height of sampling frame (H).

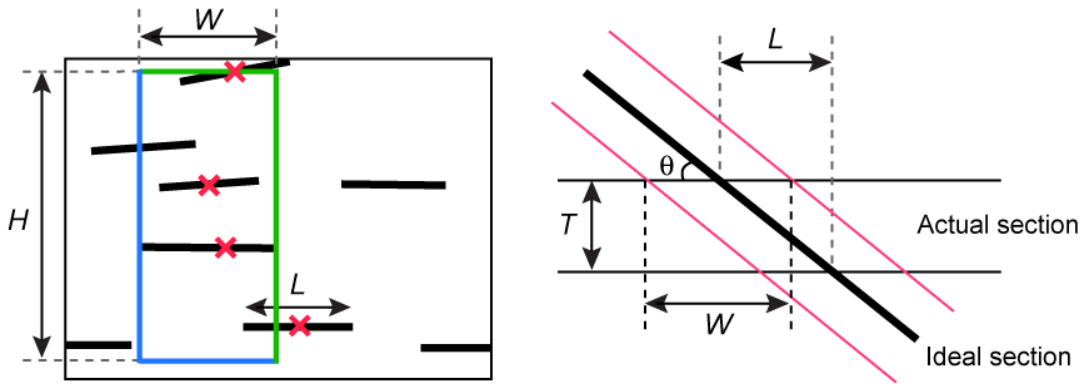

Axonal density (μm^{-2}) = Number of axons

Figure 6.2. Quantification of axonal density by cutting angle correction. Cutting plane angle θ and W were calculated from mean apparent length of axons (mL). The number of axons in the sampling frame with W was divided by area derived from section thickness (T) and sampling frame height (H).

6.2.3.2 Computer software design

Computer software named AxoCounter was created to simplify the axonal density quantification procedure using Microsoft Visual Basic 2008 Express Edition (the main source code is presented in Appendix 0). As all the calculations were performed in pixel, calibration factor was calculated by dividing the length of user defined calibration line in pixel by actual length of the line in μm prior to the experiments.

mL, θ and *W* were calculated subsequently after drawing 10 lines along axons of interest. When 'Start Experiment' button was pressed, the user was prompted to draw the ROI. *H* was defined as the height of ROI minus guarding length of 10 pixels (5 each from top and bottom). The position of sampling frames was determined depending on whether the sampling frames overlap or not, which was judged by dividing width of ROI by sampling number (Sn) and comparing to W. Sn was set so that the overlap width did not exceed one third of *W*.

The mean (μ), standard deviation (SD) and coefficient of error (CE) were calculated from axonal density per sampling frame at the end of the experiment using the following formulae.

$$SD = \sqrt{\frac{1}{Sn-1}\sum_{i=1}^{Sn}(ArrDi-\mu)^2}$$

$$CE = \frac{SD}{\sqrt{Sn}\cdot\mu}$$

6.2.3.3 Model images

Model images of WM with known axonal density (0.00025, 0.0005, 0.00075 and 0.0010 /μm2) and *θ* (15, 30, 45, 60 and 75 degree) with scales equivalent to x20 and

x40 magnifications were analyzed to test the accuracy of the angle correction method. 10 and 20 model images of 30 µm sections were computer generated by Model Image Generator (MiG) for x20 and x40, respectively. The program aligned rows of axons with length L (= 30/tan(θ)) with gap between rows (g) = 30/sin(θ) – L, and then randomly moved up to Lshift = ± L/2 to transverse direction (**Figure 6.3**).

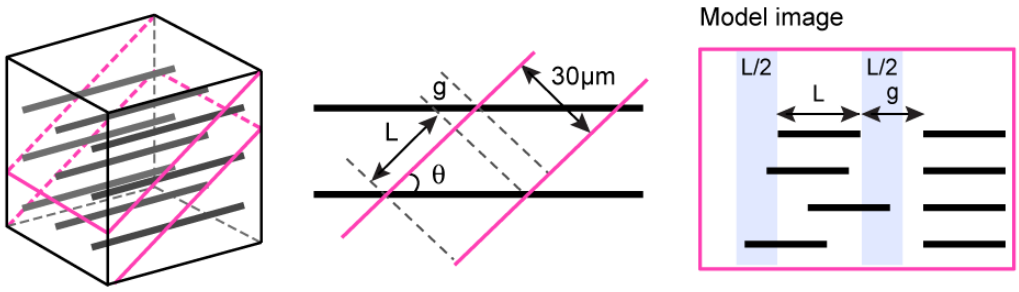

Figure 6.3. Model image generation. The apparent length of axons (L) was calculated from section thickness (T) and cutting plane angle (θ). Axons with L were aligned with gap between rows g and then randomly moved up to L/2.

6.3 Results

Intense and abundant SMI32 staining was observed in the WM of CADASIL cases while controls, especially Cont2 and Cont4, had significantly less staining. Certain brain regions had substantially more axonal staining in WM when compared to the other tissue blocks from the same case: the most extensive staining by eye was in WM near BA4 (primary motor cortex) and BA6 (premotor cortex/ supplementary motor area). Close examination of the sections revealed microinfarcts and markedly enlarged PVSs in block Z in CAD1 and CAD11. The representative staining pattern in CADASIL is illustrated with images in **Figure 6.4**. SMI32 immunoreactive axons in controls, most abundant in block AD and AE, were often thick in diameter, whereas many of those in CADASIL cases were thin and twisted, or segmented, showing a sign of degeneration.

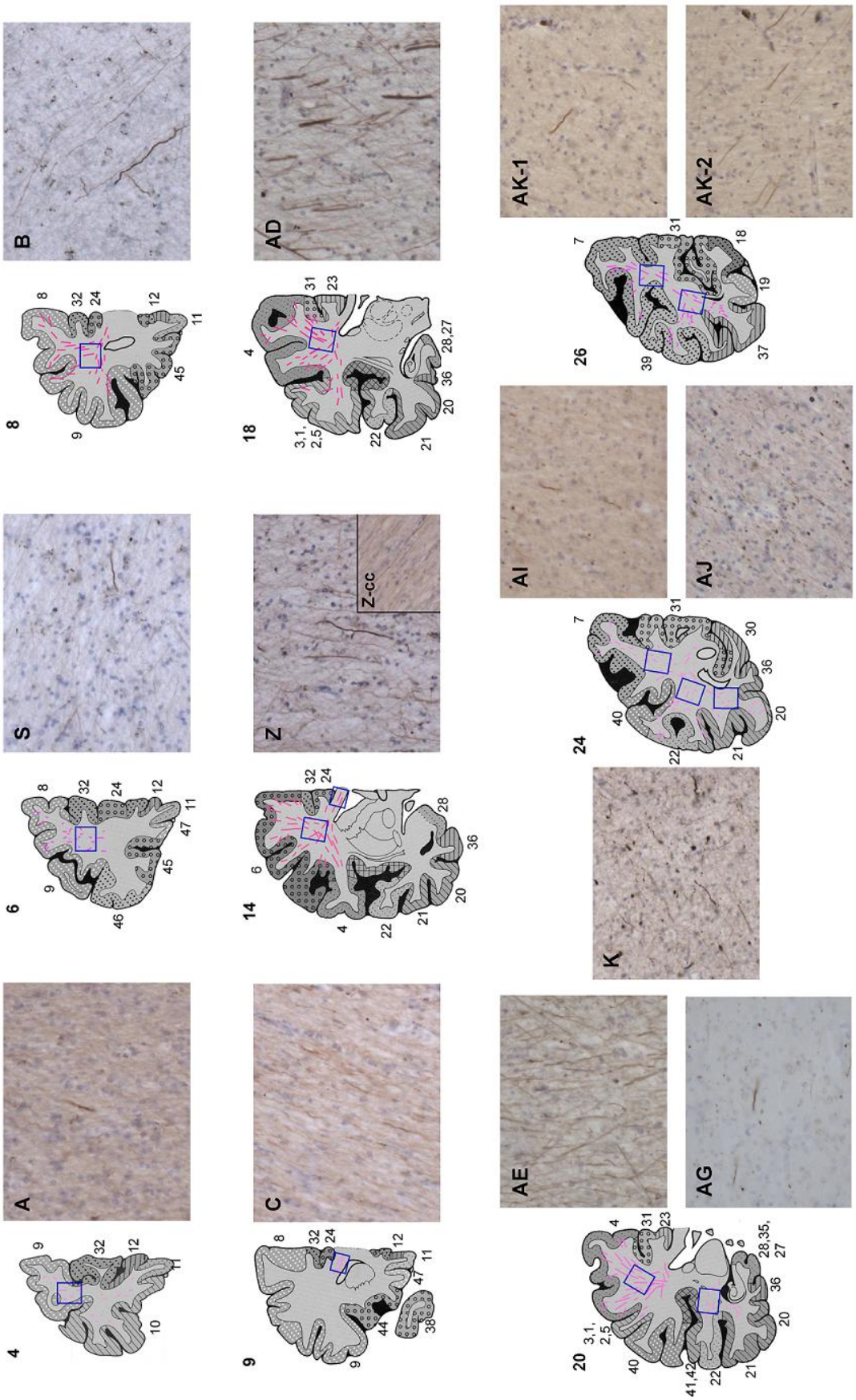

Figure 6.4. Typical staining pattern of SMI32 positive axons in CADASIL brain. Extensive staining was found in block Z, AD and AE. Blue boxes indicate examined areas. Z-cc: corpus callosum region in the block Z.

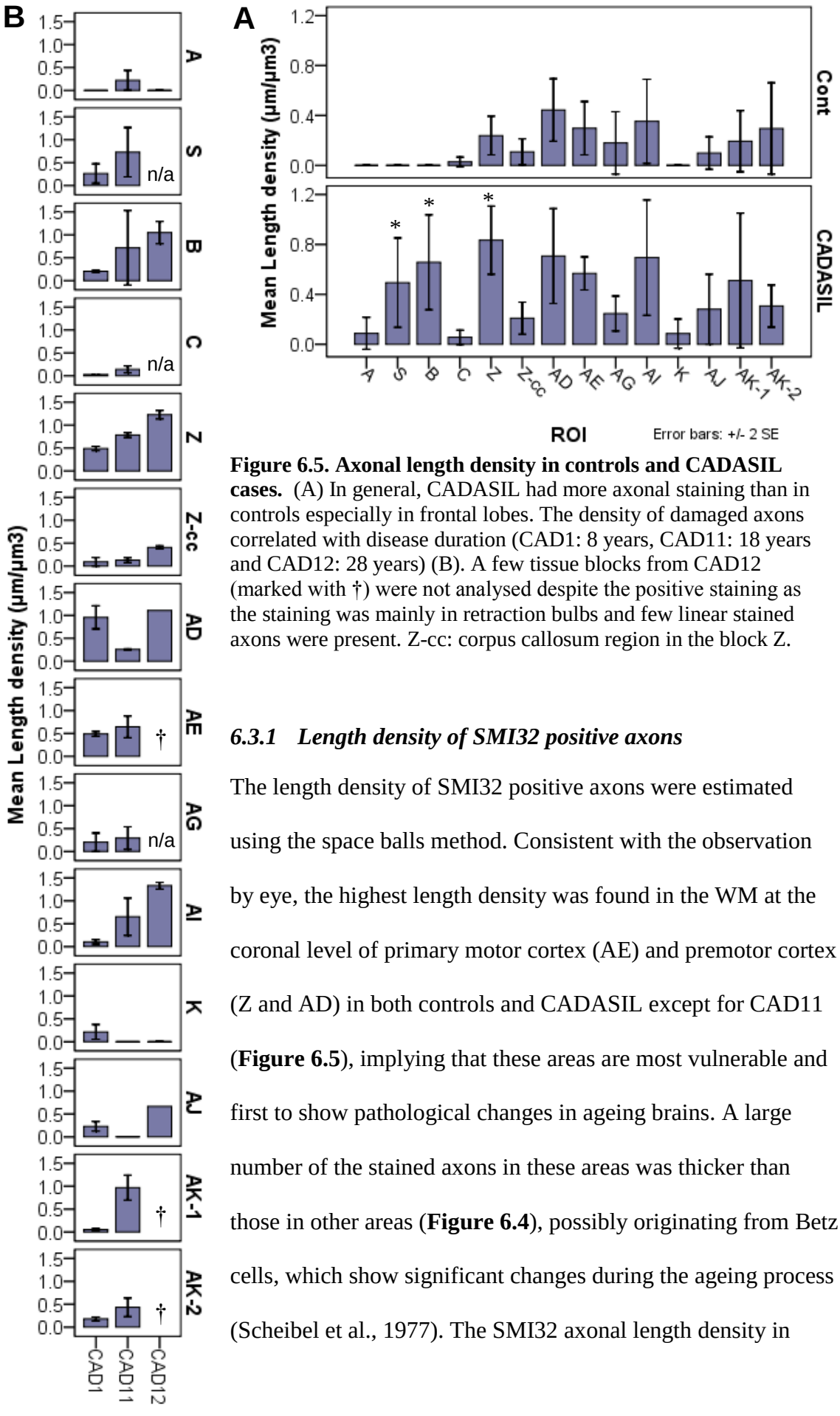

Figure 6.5. Axonal length density in controls and CADASIL cases. (A) In general, CADASIL had more axonal staining than in controls especially in frontal lobes. The density of damaged axons correlated with disease duration (CAD1: 8 years, CAD11: 18 years and CAD12: 28 years) (B). A few tissue blocks from CAD12 (marked with †) were not analysed despite the positive staining as the staining was mainly in retraction bulbs and few linear stained axons were present. Z-cc: corpus callosum region in the block Z.

6.3.1 Length density of SMI32 positive axons

The length density of SMI32 positive axons were estimated using the space balls method. Consistent with the observation by eye, the highest length density was found in the WM at the coronal level of primary motor cortex (AE) and premotor cortex (Z and AD) in both controls and CADASIL except for CAD11 (**Figure 6.5**), implying that these areas are most vulnerable and first to show pathological changes in ageing brains. A large number of the stained axons in these areas was thicker than those in other areas (**Figure 6.4**), possibly originating from Betz cells, which show significant changes during the ageing process (Scheibel et al., 1977). The SMI32 axonal length density in

temporal lobe (AG) was not as high as in the WM regions at the level of premotor cortex (Z, AD and AE). Signs of degenerating axons, which are swollen fragments of axons and 'retraction bulbs,' were found in AG, K and AJ. Axonal fragmentation reduces the possibility of intersections with probes. It may underlie the lower length density of SMI32 axons in those areas. Although extensive axonal staining was observed in the WM near motor cortices, it was frontal lobe (blocks S, B and Z) where the significant differences between controls and CADASIL were found ($p = 0.029$, 0.010 and 0.002, respectively). The severity of the damage differed even between CADASIL cases. CAD11 and CAD12, which experienced longer disease duration than CA1 (18 and 28 vs. 8 years), had more severe damage in frontal and parietal lobes (B: $R = 0.811$, $p = 0.050$; Z: $R = 0.987$, $p = 0.001$, AI: $R = 0.970$, $p = 0.001$ and AK: $R = 0.978$, $p = 0.022$). Generally, the staining intensity in the AD sections from CAD11 was weak and few retraction bulbs were observed in WM. The damage to the axons in corpus callosum remained negligible in all of the CADASIL cases. It should also be noted that the SMI32 staining was rather restricted to the upper part of the brain.

6.3.2 Model image study

The accuracy of axonal density quantification by angle correction was assessed by analyzing model images with known axonal density and θ. Density measurement by AxoCounter was shown to be accurate both at x20 and x40 magnification (**Figure 6.6**). The estimated density was significantly different from actual values only at two points, 0.00025/μm2 at 45˚ ($p = 0.018$) and 0.001/μm2 at 30˚ ($p = 0.021$). To assess whether the significant error was caused by faults in AxoCounter or in MiG, different sets of images and images generated using modified random shifting were analyzed. The error changed in both of the cases, indicating statistical (Type I) and systematic error of MiG (data not shown). Although the difference in magnification, in other words, difference

in size and number of axons per image, did not affect the accuracy of quantification, it was better at x20 magnification as indicated by the mean error percentages (8.66 for x20 and 11.44 for x40).

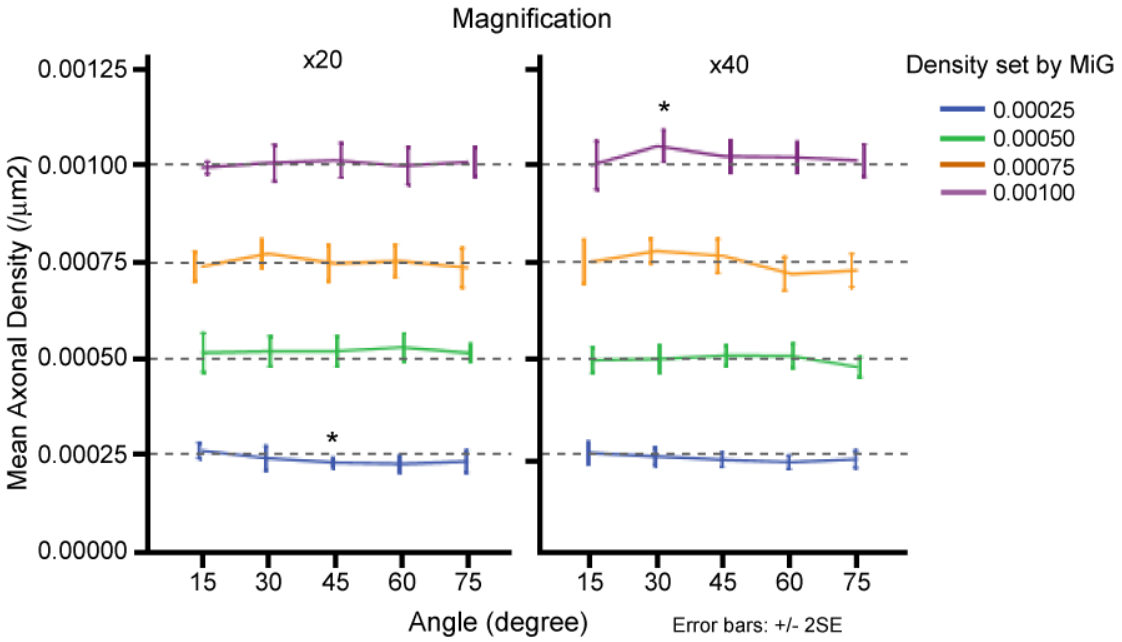

Figure 6.6. Summary of model image analysis. AxoCounter successfully quantified density correctly at all the densities and θ with the exception of two (indicated with *).

6.4 Discussion

WM integrity has been linked to cognitive function, and the disconnection of brain regions has been suggested in various disorders with cognitive impairment (Dineen et al., 2009, Hannesdottir et al., 2009, Grady et al., 2001). This small-scale study was designed to determine the extent of WM damage in postmortem brains and its relation to cognitive dysfunction in CADASIL. When quantifying the SMI32 immunoreactive axons, we found that there was widespread decrease in the integrity of the WM in CADASIL, possibly affecting corticocortical association pathways. In contrast, control cases showed limited axonal damage, and most of the immunoreactivity was restricted to the WM near premotor/motor cortices. The comparison of axonal damage distribution

in controls and CADASIL cases implies that the affected area spreads from areas above the ventricle at the level of premotor and motor cortices, where small infarcts were found, to frontal and parietal lobes. The distribution of the axonal damage is consistent with those described in the previous MRI studies, which located T_2-weighted WM hyperintense lesions in frontal, parietal and temporal lobes (Yousry et al., 1999, Coulthard et al., 2000, Singhal et al., 2005). We failed to detect damage in the corpus callosum in contrast to a previous report, but this could be largely attributed to its low frequency in CADASIL (Coulthard et al., 2000, Yousry et al., 1999).

The most important finding in the current study, however, is the significant axonal damage in the frontal/prefrontal WM compared to other areas in brains of CADASIL subjects. The extent of WM damage significantly correlated with the disease duration in frontal lobes as well as in parietal lobes. It is interesting to compare the findings of cognitive profiles in CADASIL. As described in 1.3.1.3, the early cognitive impairment in CADASIL is mainly executive dysfunction, and other cognitive dysfunctions, such as impaired episodic memory retrieval, slow processing speed and impaired visuospatial ability, manifest as the disease progresses with age (Buffon et al., 2006, Amberla et al., 2004, Peters et al., 2005c). Executive functions are largely attributed to the frontal lobes, but the communication with other areas of the brain, such as motor and sensory cortices (parietal lobes) as well as limbic and midbrain regions greatly contributes to the "top-down control," which interprets sensory input, monitors activity, sends feedback and maintains the cognitive control (Miller and Cohen, 2001, Stoet and Snyder, 2009). Frontal lobes are also suggested to be involved in the formation of working memory and the retrieval of long-term memory (Miller and Cohen, 2001, Chayer and Freedman, 2001), whereas parietal lobes have been associated with visuomotor transformations, spatial perception and episodic retrieval (Wagner et al., 2005, Fogassi and Luppino,

2005). The increasing axonal damage in the frontal and parietal WM with disease progression suggests that the disconnection of the frontal lobe from other part of the brain, for example the parietal lobes, may explain the executive dysfunction in CADASIL. Similar results were reported by a DTI study which demonstrated the correlation between executive function and various frontal WM regions in CADASIL patients (O'Sullivan et al., 2005). The list of the WM structures includes internal capsule, cingulum bundle, SLF and inferior longitudinal fasciculus (ILF).

Although we had the advantage of observing each single degenerating axon and not diffuse damaged areas as seen on MRI, the data must be interpreted with caution because different axonal tracts can be intermingled with each other in WM. Of all the WM tracts listed by O'Sullivan et al. (2005) to be correlated with executive functions, the anatomical distribution of the SMI32 immunoreactive axons seem to suggest the involvement of SLF (especially II), which connects frontal, parietal, occipital and temporal lobes (Makris et al., 2005). The other listed WM structures, cingulum bundle and internal capsule, were absent from axonal damage in our study, but ILF may comprise a part of the damaged axons in the occipital lobes (block AK). SLF would provide a good explanation for the frequently observed ataxia and hemiparesis in CADASIL patients as well as some of the cognitive dysfunction (Yousry et al., 1999, Chabriat et al., 1995), as it is responsible for associative motor behaviour, spacial attention and somatosensory input and has been linked to spacial working memory, verbal task and attention skills (Karlsgodt et al., 2008, Frye et al., 2010, Schmahmann et al., 2008, Vestergaard et al., 2010). The result may also corroborate the previous reports of cholinergic impairment in motor cortex, parietal and occipital lobes (Manganelli et al., 2008, Mesulam et al., 2003). ILF, on the other hand, is a bundle of association fibres connecting temporal and occipital lobes and is associated with visual memory

(Schmahmann et al., 2008, Shinoura et al., 2007). Considering the lack of significant difference in SMI32 axonal density in CADASIL occipital lobes as well as a report that showed worse visual memory in patients over the age of 60 (Buffon et al., 2006), the current findings suggest SLF is the first to be affected and ISF may be damaged only after certain disease duration (>8 years).

Together with the previous neuroimaging studies (Tatsch et al., 2003, Blanco Menéndez et al., 2001), our results support the notion that disconnection of corticocortical or subcortical-cortical network is involved in cognitive dysfunction in CADASIL. Further experimental investigations including the collection of more CADASIL cases are needed to estimate the correlation between axonal damage and cognitive dysfunction.

Chapter 7. General Discussion

7.1 Introduction

Various studies have investigated the cerebral pathology of CADASIL (Cumurciuc et al., 2006, Viswanathan et al., 2006, O'Sullivan et al., 2005, Miao et al., 2004, Lewandowska et al., 2010, Chabriat et al., 1999), but a lot of quantitative evaluations of those changes, which enable the characterisation of CADASIL in relation to sporadic VaD, are still insufficient. The main aim of the programme of the study was to quantify and differentiate the morphological pathology of CADASIL vasculature and their effect on neuronal population in order to elucidate the pathology underlying the clinical manifestations. In chapter 3, vascular and related WM pathology was characterised by measuring SI and PVS using newly designed computer programme, which enabled faster and more accurate measurement than the previous method by hand. Chapter 4 identified the distribution and the localisation of mutant N3ECD in small vessels using immunogold EM. The following chapter 5 and 6 quantified neuronal density in the hippocampal formation and axonal damage in the WM, respectively, in order to elucidate the substrate of cognitive impairment in CADASIL. The main findings in this study, listed below and discussed in detail in the following sections, were concordant with the clinical findings and further provided important implications for future research.

- Vascular wall thickness was significantly increased in CADASIL even compared to sporadic SVD. The severity of wall thickening correlated with the extent of PVS dilatation, a profound feature in CADASIL.

- N3ECD was detected within GOM deposited in the basement membrane of arteries/arterioles/capillaries. Some EM immunoreactivity was found associated

with membranous cytoplasmic structures in VSMCs, and vesicular inclusions in granular pericytes. In addition, there was a marked increase of nucleated hematopoietic cells, which is an indication of inflammatory response.

- Overall neuronal density in hippocampal formation (CA1, CA2, ECV) were relatively preserved in CADASIL though minor loss of neurons was indicated with preference to projecting pyramidal neurons.

- WM tracts were severely damaged in the frontal lobes of CADASIL compared to controls. The extent of damage significantly correlated with disease duration in the frontal and parietal lobes.

Our findings are subject to at least three limitations. Firstly, the relative small sample size, particularly for the damaged axonal density study, could have affected the statistical power and resulted in the false negative results. Secondly, the limited availability of neuropsychometric scores for CADASIL cases prevented us to relate the cerebral pathologies to cognitive features. Lastly, the lack of quantitative MR imaging of the cases limited the association of damage as shown by neuroimaging method and actual structural changes. In the present project, we obtained total of 12 CADASIL brain tissues from several resources in Newcastle, Oxford, London, Bristol, USA and Germany, which inevitably resulted in the inconsistency in diagnostic criteria, neuroimaging method, neuropsychological tests and postmortem processing protocols. Establishing large prospective studies of CADASIL by collaborating centres would greatly help reduce the above limitations and thus understanding of CADASIL as a model of sporadic SVD causing dementia. For this reason, clinical and neuropsychological testing, imaging protocols and postmortem brain processing methods should be clearly defined as proposed by Hachinski et al. (2006).

7.2 Relationship between vascular pathology and WM changes

The study on the vascular and perivascular pathology revealed significant vascular wall thickening and enlarged PVS in CADASIL. PVS is a normal anatomical structure surrounding a penetrating vessel and considered pathological when its diameter exceeds 2-3 mm on MRI (Wang, 2009). Nevertheless, an MRI study in healthy elderly population sample without any vascular or neurological disorders linked the number of small PVS (< 1-2mm) with severity of WM lesion and cognitive function (MacLullich et al., 2004). Enlarged PVS is frequently observed in SVD and was linked to the severity of SVD (Rouhl et al., 2008, Doubal et al., 2010). These data indicate that a common factor underlies the formation of dilated PVS, WM lesion and silent infarct, but the mechanism remains yet to be determined.

Lack of significant pathology other than in brain strongly suggests the involvement of cerebrovasculature-specific function. Three main factors have been suggested so far: BBB disruption, hypoxia/ischemia and obstructed perivascular drainage pathway, which are closely related to each other, appear to contribute to the dilation of PVS (Roher et al., 2003, Wardlaw, 2010) (**Figure 7.1**). BBB is a unique structure existing only in the brain and various mechanisms are known to be involved in its disruption, of which consequence is a leakage of blood proteins and neurotoxic substances into the brain parenchyma. Hypoxia and inflammation, for instance, are known to induce BBB breakdown. Hypoxia associated to lacunar infarcts damages endothelial cells and thus their structural integrity and function, subsequently destructing the surrounding structures starting from glial endfeets, and promoting ischemia-induced inflammation and oxidative stress (Eisert and Schlachetzki, 2008, Sandoval and Witt, 2008, Wardlaw, 2010, Ueno et al., 2002). SVD characteristic vascular pathology, such as atherosclerosis

and abnormal autoregulation, further promote oxygen depletion in the lesion and exacerbates the tissue destruction (Wardlaw, 2010). BBB breakdown and the following PVS dilation in multiple sclerosis have also been speculated to be related to inflammatory response (Wuerfel et al., 2008, Inglese et al., 2005). CADASIL characteristic vascular pathology includes sclerosis (vessel wall thickening), impaired cerebrovascular tone, chronic hypoperfusion and subcortical infarcts (Stenborg et al., 2007, Scheid et al., 2006, Coulthard et al., 2000). Thus, hypoxia is undoubtedly contributing to the disruption of endothelium structure (Brulin et al., 2002), enlarged PVS and related WM damage in CADASIL, but immune response-related inflammation may also be involved. Similar to the picture in AD, abnormal deposition of proteins, such as mutant N3ECD-containing GOM in arteries, arterioles and capillaries in case of

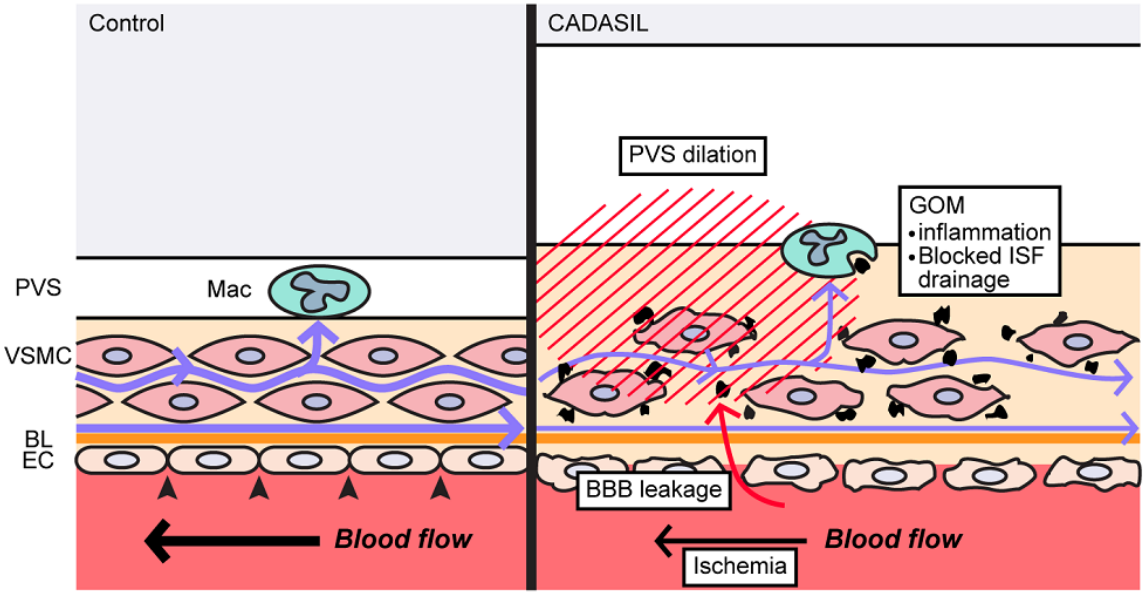

Figure 7.1. Proposed pathogenesis in CADASIL. Tight junctions (arrowheads) between endothelial cells (EC) form blood-brain barrier (BBB) to protect brain from cytotoxic substances, whereas solutes in interstitial fluid (ISF) drain out of brain through perivascular drainage pathway driven by vascular tone. Reduced vascular tone, vascular thickening and BBB breakdown in CADASIL result in the reduced efficiency of drainage pathway. Granular osmiophilic material (GOM) deposits surrounding VSMCs may disrupt ISF drainage or cause inflammation, which contribute to perivascular space (PVS) enlargement and WM damage. BL, basal lamina; Mac, perivascular macrophage.

CADASIL, can activate immune system and cause chronic inflammation (Salminen et al., 2009). In fact, we observed weak N3ECD immunoreactivity in the vesicular inclusions in granular pericytes, which are known for its capacity to uptake solutes and small molecules from ISF and have macrophage-like functions including phagocytosis, antigen presentation and prostaglandin production (Thomas, 1999). The increased CD45 immunoreactivity in CADASIL brain and a previous study in our laboratory, which found phagocytosis of an electron-dense material – presumably GOM – by a macrophage-like cell (unpublished data by Low WC), also point to the involvement of immune responses.

The deposition of GOM, which may trigger immune response, can be closely related to the functionality of perivascular drainage pathway. As described in 1.4.3, ISF is cleared through the lymphatic drainage route within the capillary/arterial wall driven by vascular pulsation (Weller et al., 2009). Impaired vascular reactivity is a characteristic feature of CADASIL, possibly caused by Notch3 signalling dysfunction with contribution of the accumulation of extracellular matrix proteins, which thicken and stiffen the arterial wall(Lacombe et al., 2005, Hussain et al., 2004, Dubroca et al., 2005a). Vascular dysfunction impedes the clearance of proteins via perivascular drainage pathway, resulting in their accumulation within vessel wall and subsequent damage to the vessel wall and then surrounding tissues (PEFA) (Weller et al., 2010). In support of the notion, our result demonstrated the correlation between vessel wall thickening and PVS enlargement. A good example of PEFA is VSMC-derived Aβ deposition within blood vessel wall in AD patients (cerebral amyloid angiopathy). There are three main clearance mechanisms of Aβ: protease degradation in the parenchyma, absorption into blood by low-density lipoprotein receptor-related protein-1, and perivascular drainage (Weller et al., 2008). As the vascular pulsation is reduced and

vessel stiffen with age, Aβ42 followed by Aβ40 accumulate along the drainage route, forming insoluble fibrillar deposits (Weller et al., 2008). The Aβ deposition alters composition of basement membrane, destructs VSMCs and causes fibrinoid necrosis, eventually increasing susceptibility to haemorrhage and ischemia (Weller et al., 2008, Weller et al., 2010). In fact it was previously suggested to correlate with the increase of PVS size and number (Roher et al., 2003). Considering the similarity in protein activation between NOTCH and amyloid precursor protein (Wolfe, 2002), it is tempting to relate the CADASIL pathology to the same pathogenesis, but a few facts should be noted and carefully evaluated. In contrast to fibrillary Aβ deposit, mutant N3ECD is confined to a relatively large (0.5-2 μm) granular formation (GOM) without forming any clearly-distinguishable structure. Some of GOM even appeared to be partly dispersed in ISF, implying it is not a rigid structure. Our result indicated that Jagged1 and ubiquitin are not present in GOM, but it does not exclude the possibility of other proteins entrapped in the structure, which may prevent extreme multimerization of mutant N3ECD. The difference in the nature of deposition can result in the difference in toxicity, as suggested by the EM observation of Tg mice that the amount of GOM does not correlate with VSMC degeneration (Ruchoux et al., 2003). Moreover, the authors noted that vascular morphological changes – *e.g.* increased intracellular dense bodies, wider intrasmooth muscle and subendothelial space, and cellular deformation – precede the appearance of GOM. Hence, GOM may be a consequence of the reduced vascular functionality and its pathogenic significance, if there is any, may rather be in its mass, which physically obstructs the ISF drainage and further exacerbates perivascular damage. The hypothesis is supported by a study which showed that the mechanical obstruction of lymphatic drainage system, by macroadenoma, can cause PVS enlargement, which can be improved by removal of the cause (Cerase et al., 2009).

Quantification of N3ECD (GOM) accumulation in relation to PVS enlargement would be the best way to test the hypothesis.

Other implications of our study are a possible intracellular accumulation and scavenging activity of mutant N3ECD. A few intracellular immunoreactivities were detected in ER-like structure in VSMCs, or vesicles in granular pericytes as mentioned earlier. Although the result was rather suggestive and not sufficient to conclude the presence of N3ECD within those structure, future study using human samples with less tissue destruction or Tg mice arteries would be beneficial to support or oppose the ER stress hypothesis and the involvement of immune responses in CADASIL.

7.3 Loss of hippocampal neurons and white matter disconnection

Neuronal density in the hippocampal formation in CADASIL and COGFAST was quantified to elucidate the contribution of hippocampal pathology in cognitive dysfunction in those disorders. Several studies have demonstrated decreased neuronal density in hippocampus in various dementias including AD and mild cognitive impairment whereas two previous studies on sporadic VaD reported opposing results (Kril et al., 2002a, Kril et al., 2002b, Zarow et al., 2005, Gómez-Isla et al., 1996, Kordower et al., 2001). Our hypothesis was that CADASIL and COGFAST groups, which were both demented at the time of death, would show reduced neuronal density in the hippocampal areas, at least in CA1 where the vascular density is the lowest and experience severer BBB leakage after ischemia (Schmidt-Kastner and Hossmann, 1988, Cavaglia et al., 2001).

Contrary to the expectation, however, the overall neuronal density in the hippocampus and entorhinal cortex of CADASIL was relatively preserved showing only mild (not

statistically significant) loss of neurons in CA1 and CA2. It is interesting to compare the result with the cognitive profile of CADASIL, which is characterized by executive dysfunction with preserved hippocampal functions (*e.g.* episodic memory) until the later stage of the disease (Amberla et al., 2004). The minor neuronal change in the hippocampus confirms that the hippocampus is the last to be affected and may suggest the minimal involvement of hippocampal dysfunction even when the patients were clinically demented. Our results provided quantitative evidence to the observation by Viswanathen et al. (2006) who reported an increased number of apoptotic neurons in the cerebral cortex and glial cells in WM, but minimal neuronal apoptosis in the hippocampus. It is also in accordance with another study, which demonstrated that cholinergic axons were relatively spared in the hippocampus, entorhinal cortex and temporal neocortex whereas cholinergic denervation is extensive in posterior parietal, dorsal frontal, and occipital cortices (Mesulam et al., 2003). It should be noted that the majority of the neuronal loss in hippocampus appeared to be selectively of SMI32(+) neurons. SMI32, a 200kDa nonphosphorylated neurofilament, is expressed in large pyramidal projecting neurons as confirmed by the volume difference between SMI32(+) and SMI32(-) neurons in chapter 5. Those SMI32 positive pyramidal neurons are most abundantly found in the long association pathway connecting frontal, temporal and parietal cortices (Hof et al., 1995). The vulnerability of the SMI32(+) neurons have been previously reported in AD and ischemia (Leifer and Kowall, 1993, Bussière et al., 2003, Thangavel et al., 2008). Our result not only confirmed the vulnerability of these pyramidal neurons to ischemic stress but also revealed the difference in the distribution of neuronal damage in CADASIL and sporadic VaD: CA1 and CA2 were affected in CADASIL while it was ECV in COGFAST. The different patterns of neuronal loss could stem from the difference in their pathogenesis, but considering the diverse

pathology of COGFAST cases, analysis of larger samples is necessary to determine the difference between CADASIL and sporadic VaD.

The above findings led us to hypothesize that WM disconnection underlies the cognitive impairment in CADASIL. The disconnection syndrome is a theory that brain dysfunction can be, at least in part, attributed to disrupted associative connections between various brain regions by WM abnormality (Catani and Ffytche, 2005). The involvement of disconnection in cognitive dysfunction has been suggested in various forms of dementia including AD (Collette et al., 2007, Dineen et al., 2009, Stoub et al., 2006, Kato et al., 2007). Since the spatial distribution of WM hyperintensity in CADASIL is rather specific involving anterior temporal poles, frontal lobes, external capsules and periventricular WM (Singhal et al., 2005), it is plausible that the disconnection of specific WM tracts, either by small infarcts, BBB breakdown or other factors discussed in the previous section, causes characteristic cognitive impairment in CADASIL. The distribution and severity of axonal damage in CADASIL were assessed by quantifying SMI32 immunoreactive axons, which indicate chronic axonal damage and degeneration (Lindner et al., 2009). The difference between controls and three CADASIL cases were rather striking, with greater number of damaged axon covering a larger area of WM in CADASIL whereas controls showed less in a restricted area. The affected area appeared to be originated from areas above the ventricle at the level of premotor and motor cortices, where small infarcts were found, and spread to frontal and parietal lobes. The distribution is consistent with those described in the previous MRI studies, which located T_2-weighted WM hyperintense lesions in frontal, parietal and temporal lobes (Yousry et al., 1999, Coulthard et al., 2000, Singhal et al., 2005). However, in the current study, the significant difference in WM damage was only detected in the frontal lobes, where the extent of the damage correlated with the disease

duration, compare to controls. It is not only concordant with the observation from MRI studies, which showed the increased frequency of T_1-weighted hypointensity and T_2-weighted hyperintensity with age (Chabriat et al., 1998), but also the clinical observations that CADASIL is characterised with executive dysfunction (Buffon et al., 2006).

The distribution and the directionality of the damaged axons suggested the involvement of a few tracts; since the SMI32 axonal density in corpus callosum remained minimal, SLF and a bundle of fibres passing the internal capsule are the likeliest to be disrupted in the two CADASIL cases. SLF connects frontal, parietal, occipital and temporal lobes and responsible for associative motor behaviour, special attention and somatosensory input (Makris et al., 2005, Schmahmann et al., 2008). The projection fibres in the internal capsule includes the pyramidal tracts originating from motor and somatosensory cortex and projecting to the brain stem and the spinal cord (Heimer, 1983). They would provide a good explanation for the frequently observed ataxia and hemiparesis in CADASIL patients as well as some of the cognitive dysfunction (Yousry et al., 1999, Chabriat et al., 1995), as disruption of SLF has been linked to dysfunction of spacial working memory, verbal task and attention skills (Karlsgodt et al., 2008, Frye et al., 2010, Vestergaard et al., 2010) while damage in internal capsule were associated with motor deficit (Pendlebury et al., 1999). The result is in agreement with the previous reports of cholinergic impairment in motor cortex, parietal and occipital lobes (Manganelli et al., 2008, Mesulam et al., 2003). In contrast to the motor areas, axonal damage in frontal lobes, which play a major role in executive functions, greatly differed between CA1 and CA11, possibly reflecting the severity of executive dysfunction in these cases.

Taken together, our results and the previous neuroimaging studies (Tatsch et al., 2003, Blanco Menéndez et al., 2001) support the hypothesis that cognitive dysfunction in CADASIL stem from the disconnection of corticocortical or subcortical-cortical network. In future investigations, it would be interesting to evaluate the neuronal density in other areas of the brain, for example, frontal cortex (layer III and V) where the loss of pyramidal neurons have been reported in AD (Hof et al., 1990, Bussière et al., 2003).

7.4 Conclusions

The experiments in this thesis were designed to establish vascular and related neuronal pathology in CADASIL in the hope it would provide clues to elucidate its pathophysiology. In this regard, the findings from this study made several contributions to the current literature as follows.

- Chapter 3 investigated the vascular and perivascular changes in CADASIL. The newly developed computer programme for the experiment greatly helped to improve the accuracy of the analysis and to reduce analysis time, and will be a useful tool for future studies examining SI and PVS. The quantitative data revealed extensive wall thickening and PVS enlargement in CADASIL, which were shown to be closely related to each other. The finding suggested either that vascular thickening contribute to the perivascular tissue destruction or that same factor underlies their pathogenesis.

- Chapter 4 was dedicated to the examination of another CADASIL characteristic vascular pathology, GOM deposition. We demonstrated the presence of N3ECD within GOM in the wall of cerebral arteries, arterioles as well as capillaries in

postmortem brain tissues, providing strong support for a previous study by Ishiko et al., which reported N3ECD in GOM using skin biopsy samples (Ishiko et al., 2006). In addition, we found weak intracellular N3ECD immunoreactivities in the ER-like structures in VSMCs and vesicular inclusions in pericytes for the first time. Together with the increased CD45 immunoreactivity in the WM of CADASIL brains, the results of EM provided important implications for future studies: involvement of ER stress and inflammation/immune response in CADASIL pathogenesis.

- Chapter 5 evaluated neuronal density in the hippocampal formation, which is often decreased in various forms of dementias, in CADASIL and sporadic VaD using a 3D stereological method. Unexpectedly, overall neuronal density in hippocampal formation (CA1, CA2, ECV) were relatively preserved in CADASIL though minor loss of neurons were observed with preference to pyramidal projecting neurons. The result led to a hypothesis that the cognitive impairment in CADASIL is rather due to the disrupted corticocortical connectivity than hippocampal dysfunction, which is also in line with its executive dysfunction.

- The following chapter 6 therefore assessed the distribution and severity of axonal damage in CADASIL using the newest stereological method that enables unbiased length density estimation without complicated random tissue sectioning. WM tracts were severely damaged especially in the frontal lobes of CADASIL. The density of damaged axon significantly correlated with disease duration in frontal and parietal lobes, suggesting that the disrupted connectivity of frontal lobes from other areas of the brain is the cause of executive dysfunction, slow processing speed and memory retrieval impairment in CADASIL.

Collectively, the present project revealed a close relationship between vascular pathology and neuronal/axonal damage, which underlies the cognitive impairment in CADASIL. This research has also thrown up many questions in need of further investigation as described in detail in the following section.

7.5 Future directions

7.5.1 N3ECD-GOM deposition

The present study demonstrated the presence of N3ECD but not Jagged1 and ubiquitin in GOM. Moreover, we found possible involvement of ER stress and inflammation in the pathogenesis of CADASIL. An issue that was not addressed in this study was the relationship between N3ECD accumulation, inflammatory response and WM damage (PVS enlargement). Future research should therefore concentrate on the following topics to elucidate the mechanism of how vascular pathology leads to WM pathology.

- 10 μm brain tissue sections double stained with A1-1 antibody and CD45 (or other inflammatory cell-related antigen) antibody are used for the study. The amount of GOM deposition is measured as the density of N3ECD immunoreactivity per vessel and compared with the number of CD45-positive perivascular cells and the size of PVS to evaluate the relationships between N3ECD accumulation, inflammation/immune response and PVS enlargement.

- The suggested intracellular N3ECD accumulation should be re-examined using more human and mutant *NOTCH3* Tg mice samples to confirm the accumulation in ER and phagocytosis by pericytes. We have stained Tg mice (R91C, equivalent of human R90C) brains with N3ECD antibody, which showed little staining in the cerebral vasculature. On the basis of the fact that tail arteries show severer vascular

pathology (Ruchoux et al., 2003), it may be better to include tail samples in addition to brain tissues.

- More information on the components of GOM would also help us to elucidate the mechanism in its formation. The distribution and amount of Notch3 related proteins other than Jagged1 and ubiquitin need to be examined. The list of proteins includes Notch ligands (*e.g.* Jagged 2, Delta 1-4 and YB-1) (Rauen et al., 2009, Kopan and Ilagan, 2009), exosome markers (*e.g.* heat shock protein 8 and CD63) (Mathivanan and Simpson, 2009) and molecular chaperons.

7.5.2 Neuronal density in the frontal and parietal lobes

The results of this study indicated that the neuronal densities in the hippocampal formation are relatively preserved and that frontal-parietal connection is disrupted in CADASIL. It is therefore important to quantify the neuronal density, especially of pyramidal neurons, using the same experimental set up as in chapter 5. The regions of interest include prefrontal (BA9) and parietal cortices (BA39/40), which play important roles in executive functions and episodic memory retrieval (Wagner et al., 2005, Chayer and Freedman, 2001).

7.5.3 Notch3 signalling activity in the mutant NOTCH3 transfected cells

Due to the time constraint, cell-culture study on the Notch3 signalling activity under stress was not completed. The working hypothesis was that Notch3 signalling show defects when VSMCs are under a stressful environment, such as hypoxia/ischemia. The study was design to incubate mutant *NOTCH3*-transfected VSMCs in hypoxic environment achieved by AnaeroPack for cell culture (Mitsubishi Gas Chemical Co., Tokyo, Japan) and analyze morphological and protein expression changes using fluorescent immunocytochemistry and Western blotting. So far, HA-tagged plasmid

DNA (*NOTCH3* wildtype, R90C, R133C, and R449C) were constructed and transfection methods were tested. Human primary VSMC were transfected with the *NOTCH3* plasmid using FuGENE® HD Transfection Reagent (Roche Applied Science, Cat. No. 04709691001) and Nucleofector™ Kits for Primary Smooth Muscle Cells (amaxa), but both methods yielded less than 5% transfection rate even with β-galactosidase control vector. A possible explanation for the low transfection rate is that primary VSMCs are sensitive to insults and resulting in cell death. A collaborating laboratory faced same problem with a VSMC cell line (personal communication) and thus it is recommended to use either viral vectors or other cell lines.

Appendix

The following sections contain the source code of the computer programmes designed and used for analysis in chapter 3 and 6. VasCalc measures Dint, Dext and Dpvs of blood vessels and estimates SI, Vwall and PVSc. Axocounter is a programme to calculate the density of linear objects from their length and number.

I. VasCalc main source code

```
Public ImageName As String
Public CalF As Double '1um = xxx pixel
Public Dint(LineNo - 1) As Double
Public Dext(LineNo - 1) As Double
Public Dpvs(LineNo - 1) As Double
Public mDint As Double
Public mDext As Double
Public mDpvs As Double
Public SI As Double
Public LArea As Double
Public VArea As Double
Public PvsArea As Double
Public LineNo As Integer 'number of lines used to measure diameter
Public Counter As Integer 'Mouse click counter
Private PicWidth As Integer  'width of pictureboc
Private PicHeight As Integer 'height of pictureboc
Private DrawLineStart As Boolean 'Line drawing mode control
Private CalibMode As Boolean 'Calibration mode control
Private CalibLength As Double
Private pStart(Counter - 1) As Point 'The position where the mouse button went 'down'.
Private pStop(Counter - 1) As Point 'The position where the mouse button went 'up'.
Private pCurr As New Point 'The current mouse location to make the shape appear to follow the mouse cursor.
Private centerp As Point
Private Lastline As Boolean

Private Sub btnSI_Click(ByVal sender As System.Object, ByVal e As System.EventArgs) Handles btnSI.Click
    If btnSI.Text = "SI PVS" Then
        DrawLineStart = True
        Me.PicBox.Cursor = Cursors.Cross

        LineNo = nudLine.Value
        Counter = 0

        cmbSetting.Enabled = False
        cmbCalib.Enabled = False
        nudLine.Enabled = False

        'button controls
        btnSave.Enabled = False
        btnSaveAs.Enabled = False
        btnSetDelete.Enabled = False
        btnNewCalib.Enabled = False
        btnDelCalib.Enabled = False
        btnOpen.Enabled = False

        'disable SIPVS button till line-drawing finishes
        btnSI.Enabled = False
        btnSI.Text = "Dint OK"
        btnUndo.Enabled = True
        btnAbort.Enabled = True
        txtInstruction.Text = "Analysing '" & ImageName & "'. Measure the internal diameters of a blood
        vessel (Dint)."
```

```
        ReDim pStart(0)
        ReDim pStop(0)
        ReDim Dint(LineNo - 1)
        ReDim Dext(LineNo - 1)
        ReDim Dpvs(LineNo - 1)

    ElseIf btnSI.Text = "Dint OK" Then 'If pressed after measuring Dint

        'Calculate each line length and mean internal diameter
        For i = 0 To LineNo - 1 'in micron
            Dint(i) = Math.Sqrt((pStop(i).X - pStart(i).X) ^ 2 + (pStop(i).Y - pStart(i).Y) ^ 2) / CalF
        Next

        Me.PicBox.Cursor = Cursors.Cross

        'mean calculation
        Dim sum As Double
        For Each item As Double In Dint
            sum += item
        Next
        mDint = sum / LineNo 'Mean internal diameter

        'Disable the SIPVS button till line-drawing finishes
        btnSI.Enabled = False
        btnSI.Text = "Dext OK"
        txtInstruction.Text = "Analysing '" & ImageName & "'. Measure the external diameters of the  blood
      vessel (Dext)."

        Counter = 0
        ReDim pStart(0)
        ReDim pStop(0)
        PicBox.Refresh()

    ElseIf btnSI.Text = "Dext OK" Then 'If pressed after measuring Dext
        'Calculate each line length and mean external diameter
        For i = 0 To LineNo - 1 'in micron
            Dext(i) = Math.Sqrt((pStop(i).X - pStart(i).X) ^ 2 + (pStop(i).Y - pStart(i).Y) ^ 2) / CalF
        Next

        Me.PicBox.Cursor = Cursors.Cross

        'mean calculation
        Dim sum As Double
        For Each item As Double In Dext
            sum += item
        Next
        mDext = sum / LineNo 'Mean external diameter

        'Disable the SIPVS button till line-drawing finishes
        btnSI.Enabled = False
        btnSI.Text = "Dpvs OK"
        txtInstruction.Text = "Analysing '" & ImageName & "'. Measure the diameters of the perivascular
        spaces (Dpvs)."

        Counter = 0
        ReDim pStart(0)
        ReDim pStop(0)
        PicBox.Refresh()

    Else
        'Calculate each line length and mean perivascular space diameter
        For i = 0 To LineNo - 1 'in micron
            Dpvs(i) = Math.Sqrt((pStop(i).X - pStart(i).X) ^ 2 + (pStop(i).Y - pStart(i).Y) ^ 2) / CalF
        Next

        'Mean calculation
        Dim sum As Double
        For Each item As Double In Dpvs
            sum += item
        Next

        mDpvs = sum / LineNo 'Mean internal diameter

        'Disable the SIPVS button till line-drawing finishes
        btnSI.Text = "SI PVS"
        txtInstruction.Text = "'" & ImageName & "' loaded: Start Analysis."
```

```
        Counter = 0
        ReDim pStart(0)
        ReDim pStop(0)
        PicBox.Refresh()

        '**********Calculate SI
        SI = 1 - (mDint / mDext)
        LArea = Math.PI * (mDint / 2) ^ 2
        VArea = Math.PI * (mDext / 2) ^ 2 - LArea
        PvsArea = Math.PI * ((mDpvs / 2) ^ 2 - (mDext / 2) ^ 2)

        'Open a result window.
        If Result.ResultLoaded = True Then
            Result.DataShow()
            Result.Visible = True
        Else
            Result.Show()
        End If

        DrawLineStart = False
        Me.PicBox.Cursor = Cursors.Default()

        cmbSetting.Enabled = True
        cmbCalib.Enabled = True
        nudLine.Enabled = True

        'Button controls
        btnSave.Enabled = True
        btnSaveAs.Enabled = True
        btnSetDelete.Enabled = True
        btnNewCalib.Enabled = True
        btnDelCalib.Enabled = True
        btnOpen.Enabled = True
        btnUndo.Enabled = False
        btnAbort.Enabled = False
        btnResult.Enabled = True
        btnSI.Focus()
    End If
End Sub

'*************** Drawing tool macros ***************

Private Sub PicBox_MouseDown(ByVal sender As Object, ByVal e AsSystem.Windows.Forms.
MouseEventArgs) Handles PicBox.MouseDown

    'If the drawing mode is on
    If DrawLineStart = True Or CalibMode = True Then
        If DrawLineStart = True Then
            If Counter = LineNo Then 'Drawing mode end point
                Lastline = True
                Exit Sub
            End If

            Counter = Counter + 1
            If Counter = 1 Then
                btnUndo.Enabled = True
                centerp.X = 0
                centerp.Y = 0
            End If

            'Redefine the array
            ReDim Preserve pStart(Counter - 1)
            ReDim Preserve pStop(Counter - 1)
        End If

        If CalibMode = True Then
            Counter = 1
            ReDim pStart(Counter - 1)
            ReDim pStop(Counter - 1)
        End If

        pStop(Counter - 1).X = 0
        pStop(Counter - 1).Y = 0

        ' Save the mouse's start postition
        If e.X < 0 Then
```

```
            pStart(Counter - 1).X = 0
        ElseIf e.X > PicWidth Then
            pStart(Counter - 1).X = PicWidth
        Else
            pStart(Counter - 1).X = e.X
        End If

        If e.Y < 0 Then
            pStart(Counter - 1).Y = 0
        ElseIf e.Y > PicHeight Then
            pStart(Counter - 1).Y = PicHeight
        Else
            pStart(Counter - 1).Y = e.Y
        End If

        'Save the current location for the immediate drawing
        pCurr = pStart(Counter - 1)
    End If

    Me.Invalidate()
End Sub

Private Sub PicBox_MouseMove(ByVal sender As Object, ByVal e As System.Windows.Forms.
MouseEventArgs) Handles PicBox.MouseMove
    If Counter > 0 Then
        If Lastline = True Then
            Exit Sub
        End If
        'If mouse down outside the PicBox and mousemove inside the PicBox
        If Counter = 0 Then
            Exit Sub
        End If

        'If the drawing mode is on, set the current location, and force the redraw.
        If Me.DrawLineStart = True Or CalibMode = True Then
            If Not pStart(Counter - 1) = Nothing Then
                ' Save the current location for the immediate drawing
                If e.X < 0 Then
                    pCurr.X = 0
                ElseIf e.X > PicWidth Then
                    pCurr.X = PicWidth
                Else
                    pCurr.X = e.X
                End If

                If e.Y < 0 Then
                    pCurr.Y = 0
                ElseIf e.Y > PicHeight Then
                    pCurr.Y = PicHeight
                Else
                    pCurr.Y = e.Y
                End If

.
                Me.Invalidate()
            End If
        End If
    End If
End Sub

Private Sub PicBox_MouseUp(ByVal sender As Object, ByVal e As System.Windows.Forms.
MouseEventArgs) Handles PicBox.MouseUp

    If DrawLineStart = True Or CalibMode = True Then
        If DrawLineStart = True Then
            If Lastline = True Then
                Exit Sub
            End If
        End If

        'If mouse down outside the PicBox and up inside the PicBox
        If Counter = 0 Then
            Exit Sub
        End If

        ' Save the mouse's End postition
        If e.X < 0 Then
```

```
            pStop(Counter - 1).X = 0
        ElseIf e.X > PicWidth Then
            pStop(Counter - 1).X = PicWidth
        Else
            pStop(Counter - 1).X = e.X
        End If

        If e.Y < 0 Then
            pStop(Counter - 1).Y = 0
        ElseIf e.Y > PicHeight Then
            pStop(Counter - 1).Y = PicHeight
        Else
            pStop(Counter - 1).Y = e.Y
        End If

        'Invalidate and for the paint method to be called.
        Me.Invalidate()

        If DrawLineStart = True Then

            'If first line
            If Counter = 1 Then
                    Dim xlength As Integer = Math.Round(Math.Sqrt((pStart(0).X - pStop(0).X) ^ 2) / 2)
             'Calculate the center point
                Dim ylength As Integer = Math.Round(Math.Sqrt((pStart(0).Y - pStop(0).Y) ^ 2) / 2)

                If pStart(0).X > pStop(0).X Then
                    centerp.X = pStop(0).X + xlength
                Else
                    centerp.X = pStart(0).X + xlength
                End If

                If pStart(0).Y > pStop(0).Y Then
                    centerp.Y = pStop(0).Y + ylength
                Else
                    centerp.Y = pStart(0).Y + ylength
                End If
            End If

            'If all the lines were drawn, stop drawing
            If Counter = LineNo Then
                Me.PicBox.Cursor = Cursors.Default
                btnSI.Enabled = True
                btnSI.Focus()
                Exit Sub
            End If

            btnUndo.Focus()
        End If

        If CalibMode = True Then
            If Counter = 1 Then
                btnNewCalib.Enabled = True
                btnNewCalib.Focus()
            End If
        End If

        PicBox.Refresh()
    End If
End Sub

Private Sub PicBox_Paint(ByVal sender As Object, ByVal e As System.Windows.Forms.
PaintEventArgs) Handles PicBox.Paint
    Dim g As Graphics = e.Graphics
    '**************Draw line mode
    If DrawLineStart = True Or CalibMode = True Then
        If Counter > 0 Then
            Dim pts() As Point =

            Using cap_path As New Drawing2D.GraphicsPath
                cap_path.AddLines(pts)

                Using LineCap As New Drawing2D.CustomLineCap(Nothing, cap_path)
                    Dim Pen As New Pen(Color.GreenYellow)
                    Pen.Width = 3
                    Dim PenwCap As New Pen(Brushes.GreenYellow)
```

```
                PenwCap.CustomStartCap = LineCap
                PenwCap.CustomEndCap = LineCap

                If DrawLineStart = True Then
                    PenwCap.Width = 1
                ElseIf CalibMode = True Then
                    PenwCap.Width = 2
                End If

                Using Pen
                    If pStop(Counter - 1).X = 0 And pStop(Counter - 1).Y = 0 Then 'While still drawing
                        g.DrawLine(PenwCap, pStart(Counter - 1).X, pStart(Counter - 1).Y, pCurr.X,
                            pCurr.Y)

                        For i = 0 To Counter - 2
                            g.DrawLine(Pen, pStart(i).X, pStart(i).Y, pStop(i).X, pStop(i).Y)
                        Next
                    Else 'drawing stopped
                        For i = 0 To Counter - 1
                            g.DrawLine(Pen, pStart(i).X, pStart(i).Y, pStop(i).X, pStop(i).Y)
                        Next
                    End If
                End Using

                'Display centre point
                If Counter > 0 Then
                    If CalibMode = False Then
                        Dim Pen2 As New Pen(Color.Cyan)
                        Pen2.Width = 2
                        Using Pen
                            g.DrawLine(Pen2, centerp.X - 4, centerp.Y, centerp.X + 4, centerp.Y)
                            g.DrawLine(Pen2, centerp.X, centerp.Y - 4, centerp.X, centerp.Y + 4)
                        End Using
                    End If
                End If
            End Using
        End Using
    Else
        Exit Sub
    End If
End If
End Sub
```

I. AxoCounter main source code

```
Private Sub btnAngle_Click(ByVal sender As System.Object, ByVal e As System.EventArgs) Handles
btnAngle.Click
    If btnAngle.Text = "Measure mL" Then
        '**************************Define Thickness
        Thickness = txtT.Text
        '*********************************

        'Activate line drawing mode, change cursor, disable angle button
        DrawLineStart = True
        Lastpoint = False
        Me.PicBox.Cursor = Cursors.Cross
        btnAngle.Text = "Calc Angle"
        btnAngle.Enabled = False
        btnUndoLine.Enabled = True
        btnStart.Enabled = False 'Disable start button to avoid error
        DeleteToolStripMenuItem.Enabled = False
        lblInstruction.Text = "Draw 10 lines over randomly-selected axons. Press 'Calc Angle' when finished."
        txtmL.Text = ""
        txtAngle.Text = ""
        txtW.Text = ""
        cmbSetting.Enabled = False
        txtT.Enabled = False
        txtMag.Enabled = False
        nudSn.Enabled = False
        W = 0
        ReDim pStart(0)
        ReDim pStop(0)
```

```
        Else 'If pressed after drawing 10 mL lines
            'Calculate mL, angle and W
            Dim Length(9) As Double
            For i = 0 To 9
                Length(i) = Math.Sqrt((pStop(i).X - pStart(i).X) ^ 2 + (pStop(i).Y - pStart(i).Y) ^ 2)
            Next

            'mL calculation
            Dim sum As Double
            For Each item As Double In Length
                sum += item
            Next

            mL = sum / 10
            txtmL.Text = Math.Round(mL / CalF, 3)

            'Radian calculation
            Dim Radian As Double
            If mL > PicWidth - 10 Then 'If cutting plane is parallel to the axonal tract
                MsgBox("Is cutting angle 0 degree?", MsgBoxStyle.YesNo)
                If MsgBoxResult.Yes Then
                    Radian = 0
                    txtAngle.Text = 0
                Else
                    GoTo RadianDef
                End If

            Else
                '************************************************
RadianDef:      Radian = Math.Atan(Thickness * CalF / mL)
                '************************************************
                txtAngle.Text = Math.Round(180 * Radian / Math.PI, 2)
            End If

            If Radian = 0 Then 'If cutting plane is parallel to the axonal tract, use couting line rather than frame
                W = 1
                txtW.Text = 1
            Else
                'W calculation
                '******************* Obtain a public variable Sampling width (W) in pixel
                W = Thickness * CalF / Math.Sin(Radian)
                '*********************************************************************
                txtW.Text = Math.Round(W / CalF, 3)
            End If

            'Delete all the mL lines, reset all the variables
            Array.Clear(pStart, 0, 10)
            Array.Clear(pStop, 0, 10)
            Counter = 0
            Lastpoint = False
            DrawLineStart = False
            btnAngle.Text = "Measure mL"
            btnStart.Enabled = True
            btnUndoLine.Enabled = False
            cmbSetting.Enabled = True
            txtT.Enabled = True
            txtMag.Enabled = True
            nudSn.Enabled = True
            DeleteToolStripMenuItem.Enabled = True
            lblInstruction.Text = "Click 'Start Experiment' to start counting."
            btnStart.Focus()
            PicBox.Refresh()
        End If
    End Sub

    Private Sub btnStart_Click(ByVal sender As System.Object, ByVal e As System.EventArgs) Handles btnStart.Click
        If btnStart.Text = "Start Experiment" Then
            'Disable lad image
            OpenImageToolStripMenuItem.Enabled = False
            DeleteToolStripMenuItem.Enabled = False
            Sn = nudSn.Value
            btnStart.Text = "ROI OK"
            btnStart.Enabled = False
            btnAngle.Enabled = False
            btnUndoLine.Enabled = False
            btnAddM.Enabled = False
```

```
        btnDelM.Enabled = False
        btnReset.Enabled = True
        txtT.Enabled = False
        txtMag.Enabled = False
        nudSn.Enabled = False
        'disble seting combo box
        cmbSetting.Enabled = False
        lblInstruction.Text = "Define region of interest."

        'Clear previous arrays
        ReDim ArrM1C(0)
        ReDim ArrM1D(0)

        'Draw rectangle to define ROI
        DrawLineStart = True
        Rectangle = True 'Draw rectangle mode ON
        Me.PicBox.Cursor = Cursors.Cross

    ElseIf btnStart.Text = "ROI OK" Then 'ROI defined
        'If valid ROI not drawn
        If Rheight < 10 Or Rwidth < 0 Then
            MsgBox("Define valid ROI")
            Exit Sub
        End If

        Rectangle = False 'Draw rectangle mode OFF
        Marker = True 'Draw marker mode ON
        Me.PicBox.Cursor = Cursors.Default
        btnStart.Text = "End Experiment"
        btnStart.Enabled = False
        lblInstruction.Text = "Press Next to move to the next frame."

        'Marker buttons enable
        If btnMark1.Text <> "" Then
            btnMark1.Enabled = True
            Mc1 = 0
            M1 = True 'Activate marker 1
        End If

        Counter = 1 'Sampling frame number

        '******************************************** Calculate Area
        Area = Thickness * (Rheight - 10) / CalF 'Area in um2
        '*****************************************************************

        'Define sampling frame top left position. Take gurd volum of 5 pixels
        If (Rwidth - 10) / Sn > W Then 'Sampling frames do not overlap
            'Draw first sampling frame
            Sframe.X = Math.Round(ROIStart.X + (Rwidth - 10) / (2 * Sn) - W / 2 + 5, 0)
            Sframe.Y = ROIStart.Y + 5

        Else 'Sampling frames overlap
            OL = (Sn * W - Rwidth + 10) / (Sn - 1) 'Overlap width
            If OL > W / 3 Then 'If counting frames overlat more than 1/3 of frame width
                Dim dlg As DialogResult = MsgBox("Too many sampling number." & vbCrLf & "Recommended Sn = " &
                Int((3 * Rwidth - W) / (2 * W)) & "." & vbCrLf & "Proceed anyway?", MsgBoxStyle.YesNo)

                If dlg = MsgBoxResult.Yes Then
                    GoTo OLposition

                Else 'reset start button. Ask user to change sampling number
                    Marker = False
                    DrawLineStart = False
                    btnStart.Text = "Start Experiment"
                    btnStart.Enabled = True
                    btnAngle.Enabled = True
                    nudSn.Enabled = True
                    'clear ROI position
                    Erase pStart
                    Erase pStop
                    ReDim pStart(1)
                    pStart(0).X = 0
                    pStart(0).Y = 0
                    PicBox.Refresh()
                    lblInstruction.Text = "Reduce sampling number."
                    nudSn.Focus()
```

```
                    Exit Sub
                End If
            End If
OLposition:
            Sframe.X = ROIStart.X + 5
            Sframe.Y = ROIStart.Y + 5
        End If

        If Sn = 1 Then 'If sampling number is 1
            btnStart.Enabled = True
            btnStart.Focus()
        Else 'If more than one, enable next button
            btnNext.Enabled = True
            btnNext.Focus()
        End If
        PicBox.Refresh()

    Else 'If the end of the experiment
        'Store counts, clear current mark counts display and marks, reset mark counter
        CountStorage()

        'Deactivate marker mode (all the shapes are deleted)
        Marker = False
        DrawLineStart = False
        PicBox.Refresh()

        'Calculate the mean density etc
        For i = 0 To Sn - 1
            ReDim Preserve ArrM1D(Sn - 1)
            ArrM1D(i) = ArrM1C(i) / Area 'Mean density of marker 1 axons (/um2)
        Next

        'Reset counter
        Counter = 0
        M1 = False
        'Clear counts
        lblC1.Text = ""
        lblMC1.Text = ""

        'disable buttons
        btnUndo.Enabled = False
        btnClear.Enabled = False
        btnReset.Enabled = False
        btnAngle.Enabled = True
        btnAddM.Enabled = True
        btnDelM.Enabled = True
        cmbSetting.Enabled = True
        txtT.Enabled = True
        txtMag.Enabled = True
        nudSn.Enabled = True
        btnStart.Text = "Start Experiment"
        lblInstruction.Text = "Load next image and press 'Measure mL'"

        'Enable load image and delete setting
        OpenImageToolStripMenuItem.Enabled = True
        DeleteToolStripMenuItem.Enabled = True

        'Open result window.
        If Result.ResultLoaded = True Then
            Result.DataShow()
            Result.Visible = True
        Else
            Result.Show()
        End If
    End If
End Sub
```

References

ABBOTT, N. J., RÖNNBÄCK, L. & HANSSON, E. (2006) Astrocyte-endothelial interactions at the blood-brain barrier. *Nat Rev Neurosci,* 7**,** 41-53.

ABRAHAMS, S., LEIGH, P. N., HARVEY, A., VYTHELINGUM, G. N., GRISÉ, D. & GOLDSTEIN, L. H. (2000) Verbal fluency and executive dysfunction in amyotrophic lateral sclerosis (ALS). *Neuropsychologia,* 38**,** 734-747.

ABU-AMERO, K. K., HELLANI, A. & BOHLEGA, S. (2008) Absence of mtDNA mutations in leukocytes of CADASIL patients. *BMC Res Notes,* 1**,** 16.

ADACHI, Y., HAYASHI, M. & NAKASHIMA, K. (2006) Examination of Notch3 mutations in Japanese patients with leukoaraiosis without hypertension. *Jpn J Stroke,* 28**,** 585-589.

ADIB-SAMII, P., BRICE, G., MARTIN, R. J. & MARKUS, H. S. (2010) Clinical spectrum of CADASIL and the effect of cardiovascular risk factors on phenotype: Study in 200 consecutively recruited individuals. *Stroke,* 41**,** 630-634.

AMARAL, D. & LAVENEX, P. (2006) Hippocampal Neuroanatomy. IN ANDERSEN, P., MORRIS, R., AMARAL, D., BLISS, T. & O'KEEFE, J. (Eds.) *The Hippocampus Book.* Oxford University Press.

AMARAL, D. G. & INSAUSTI, R. (1990) Hippocampal formation. IN PAXINOS, G. (Ed.) *The Human Nervous System.* Academic Press.

AMBERLA, K., WÄLJAS, M., TUOMINEN, S., ALMKVIST, O., PÖYHÖNEN, M., TUISKU, S., KALIMO, H. & VIITANEN, M. (2004) Insidious cognitive decline in CADASIL. *Stroke,* 35**,** 1598-1602.

ANNUNEN-RASILA, J., KÄRPPÄ, M., FINNILÄ, S., YLÄ-OUTINEN, H., VEIJOLA, J., TUOMINEN, H., PELTONEN, J. & MAJAMAA, K. (2007) Cytoskeletal structure in cells harboring two mutations: R133C in NOTCH3 and 5650G>A in mitochondrial DNA. *Mitochondrion,* 7**,** 96-100.

ARBOLEDA-VELASQUEZ, J. F., LOPERA, F., LOPEZ, E., FROSCH, M. P., SEPULVEDA-FALLA, D., GUTIERREZ, J. E., VARGAS, S., MEDINA, M., MARTINEZ DE ARRIETA, C., LEBO, R. V., SLAUGENHAUPT, S. A., BETENSKY, R. A., VILLEGAS, A., ARCOS-BURGOS, M., RIVERA, D., RESTREPO, J. C. & KOSIK, K. S. (2002) C455R notch3 mutation in a Colombian CADASIL kindred with early onset of stroke. *Neurology,* 59**,** 277-279.

ARBOLEDA-VELASQUEZ, J. F., MARTINEZ, M. C., DONAHUE, C. P., NAVARRO-GONZALEZ, M. F., KOSIK, K. S., FUNG, E., LIBBY, P., AIKAWA, M., RAMPAL, R., HALTIWANGER, R. S., DARLAND, D. C., D'AMORE, P. A. & LIU, M. (2005) CADASIL mutations impair Notch3 glycosylation by Fringe. *Hum Mol Genet,* 14**,** 1631-1639.

ARBOLEDA-VELASQUEZ, J. F., ZHOU, Z., HWA, K. S., LOUVI, A., KIM, H.-H., SAVITZ, S. I., LIAO, J. K., SALOMONE, S., AYATA, C., MOSKOWITZ, M. A. & ARTAVANIS-TSAKONAS, S. (2008) Linking Notch signaling to ischemic stroke. *P Natl Acad Sci USA,* 105**,** 4856-4861.

ARIMA, K., YANAGAWA, S., ITO, N. & IKEDA, S. (2003) Cerebral arterial pathology of CADASIL and CARASIL (Maeda syndrome). *Neuropathology,* 23**,** 327-334.

ARTAVANIS-TSAKONAS, S., RAND, M. D. & LAKE, R. J. (1999) Notch signaling: Cell fate control and signal integration in development. *Science,* 284**,** 770-776.

BAARS, M. A. E., VAN BOXTEL, M. P. J. & JOLLES, J. (2010) Migraine does not affect cognitive decline: Results from the Maastricht aging study: Research submission. *Headache,* 50**,** 176-184.

BAUDRIMONT, M., DUBAS, F., JOUTEL, A., TOURNIER-LASSERVE, E. & BOUSSER, M. G. (1993) Autosomal dominant lenkoencephalopathy and subcortical ischemic stroke. A clinicopathological study. *Stroke,* 24**,** 122-125.

BEATUS, P., LUNDKVIST, J., OBERG, C. & LENDAHL, U. (1999) The notch 3 intracellular domain represses notch 1-mediated activation through Hairy/Enhancer of split (HES) promoters. *Development,* 126**,** 3925-3935.

BELIN DE CHANTEMÈLE, E. J., RETAILLEAU, K., PINAUD, F., VESSIÈRES, E., BOCQUET, A., GUIHOT, A. L., LEMAIRE, B., DOMENGA, V., BAUFRETON, C., LOUFRANI, L., JOUTEL, A. & HENRION, D. (2008) Notch3 is a major regulator of vascular tone in cerebral and tail resistance arteries. *Arterioscler Thromb Vasc Biol,* 28**,** 2216-2224.

BELL, R. D. & ZLOKOVIC, B. V. (2009) Neurovascular mechanisms and blood-brain barrier disorder in Alzheimer's disease. *Acta Neuropathol,* 118**,** 103-113.

BELLAVIA, D., CHECQUOLO, S., CAMPESE, A. F., FELLI, M. P., GULINO, A. & SCREPANTI, I. (2008) Notch3: From subtle structural differences to functional diversity. *Oncogene,* 27**,** 5092-5098.

BENHAÏEM-SIGAUX, N., GRAY, F., GHERARDI, R., ROUCAYROL, A. M. & POIRIER, J. (1987) Expanding cerebellar lacunes due to dilatation of the perivascular space associated with Binswanger's subcortical arteriosclerotic encephalopathy. *Stroke,* 18**,** 1087-1092.

BLAIR, S. S. (2000) Notch signaling: Fringe really is a glycosyltransferase. *Curr Biol,* 10**,** R608-R612.

BLANCO MENÉNDEZ, R., AGUADO BALSAS, A. M., BLANCO, E., LOBO RODRÍGUEZ, B. & VERA DE LA PUENTE, E. (2001) The CADASIL syndrome: a model of subcortical-cortical disconnection. *Rev Neurol,* 32**,** 750-754.

BORDERS JR., C. L., BROADWATER, J. A., BEKENY, P. A., SALMON, J. E., LEE, A. S., ELDRIDGE, A. M. & PETT, V. B. (1994) A structural role for arginine in proteins: Multiple hydrogen bonds to backbone carbonyl oxygens. *Protein Sci* 3**,** 541-548.

BOZKULAK, E. C. & WEINMASTER, G. (2009) Selective use of ADAM10 and ADAM17 in activation of Notch1 signaling. *Mol Cell Biol,* 29**,** 5679-5695.

BRAAK, H. & BRAAK, E. (1991) Neuropathological stageing of Alzheimer-related changes *Acta Neuropathol,* 82**,** 239-259.

BRUENING, R., DICHGANS, M., BERCHTENBREITER, C., YOUSRY, T., SEELOS, K. C., WU, R. H., MAYER, M., BRIX, G. & REISER, M. (2001) Cerebral Autosomal dominant arteriopathy with subcortical Infarcts and leukoencephalopathy: decrease in regional cerebral blood volume in hyperintense subcortical lesions inversely correlates with disability and cognitive performance. *Am J Neuroradiol,* 22**,** 1268-1274.

BRULIN, P., GODFRAIND, C., LETEURTRE, E. & RUCHOUX, M.-M. (2002) Morphometric analysis of ultrastructural vascular changes in CADASIL: Analysis of 50 skin biopsy specimens and pathogenic implications. *Acta Neuropathol,* 104**,** 241-248.

BUCCIANTINI, M., GIANNONI, E., CHITI, F., BARONI, F., FORMIGLI, L., ZURDO, J., TADDEI, N., RAMPONI, G., DOBSON, C. M. & STEFANI, M. (2002) Inherent toxicity of aggregates implies a common mechanism for protein misfolding diseases. *Nature,* 416**,** 507-511.

BUFFON, F., PORCHER, R., HERNANDEZ, K., KURTZ, A., POINTEAU, S., VAHEDI, K., BOUSSER, M. G. & CHABRIAT, H. (2006) Cognitive profile in CADASIL. *J Neurol Neurosur Ps,* 77**,** 175-180.

BUFFON, G. L. C. (1777) Essai d'arithmétique morale. *Histoire naturelle,* Supplément 4.

BÜSSEMAKER, E., PISTROSCH, F., FÖRSTER, S., HERBRIG, K., GROSS, P., PASSAUER, J. & BRANDES, R. P. (2007) Rho kinase contributes to basal vascular tone in humans: role of endothelium-derived nitric oxide. *Am J Physiol Heart Circ Physiol,* 293**,** H541-547.

BUSSIÈRE, T., GIANNAKOPOULOS, P., BOURAS, C., PERL, D. P., MORRISON, J. H. & HOF, P. R. (2003) Progressive degeneration of nonphosphorylated neurofilament protein-enriched pyramidal neurons predicts cognitive impairment in Alzheimer's disease: Stereologic analysis of prefrontal cortex area 9. *J Comp Neurol,* 463**,** 281-302.

CALHOUN, M. E. & MOUTON, P. R. (2001) Length measurement: new developments in neurostereology and 3D imagery *J Chem Neuroanatomy,* 21**,** 257-265.

CAMPOS, A. H., WANG, W., POLLMAN, M. J. & GIBBONS, G. H. (2002) Determinants of Notch-3 receptor expression and signaling in vascular smooth muscle cells: implications in cell-cycle regulation. *Circ Res,* 91**,** 999-1006.

CATANI, M. & FFYTCHE, D. H. (2005) The rises and falls of disconnection syndromes. *Brain,* 128**,** 2224-2239.

CAVAGLIA, M., DOMBROWSKI, S. M., DRAZBA, J., VASANJI, A., BOKESCH, P. M. & JANIGRO, D. (2001) Regional variation in brain capillary density and vascular response to ischemia. *Brain Res,* 910**,** 81-93.

CERASE, A., VENTURI, C., RUBENNI, E., TARANTINI, B. & PACINI, F. (2009) Complete Regression of a Temporal Stem Dilated Perivascular Space Following Resection of a Pituitary Nonfunctioning Macroadenoma. *Am J Neuroradiol,* 30**,** e4-e5.

CHABRIAT, H., LEVY, C., TAILLIA, H., IBA-ZIZEN, M. T., VAHEDI, K., JOUTEL, A., TOURNIER-LASSERVE, E. & BOUSSER, M. G. (1998) Patterns of MRI lesions in CADASIL. *Neurology,* 51**,** 452-457.

CHABRIAT, H., PAPPATA, S., OSTERGAARD, L., CLARK, C. A., PACHOT-CLOUARD, M., VAHEDI, K., JOBERT, A., LE BIHAN, D. & BOUSSER, M. G. (2000) Cerebral hemodynamics in CADASIL before and after acetazolamide challenge assessed with MRI bolus tracking. *Stroke,* 31**,** 1904-1912.

CHABRIAT, H., PAPPATA, S., POUPON, C., CLARK, C. A., VAHEDI, K., POUPON, F., MANGIN, J. F., PACHOT-CLOUARD, M., JOBERT, A., LE BIHAN, D. & BOUSSER, M. (1999) Clinical severity in CADASIL related to ultrastructural damage in white matter: in vivo study with diffusion tensor MRI. *Stroke,* 30**,** 2637-2643.

CHABRIAT, H., VAHEDI, K., IBA-ZIZEN, M., JOUTEL, A., NIBBIO, A., NAGY, T. G., KREBS, M. O., JULIEN, J., DUBOIS, B., DUCROCQ, X., LEVASSEUR, M., HOMEYER, P., MAS, J. L., LYON-CAEN, O., TOURNIER-LASSERVE, E. & BOUSSER, M.-G. (1995) Clinical spectrum of CADASIL: a study of 7 families. *Lancet,* 346**,** 934-939.

CHARLTON, R. A., MORRIS, R. G., NITKUNAN, A. & MARKUS, H. S. (2006) The cognitive profiles of CADASIL and sporadic small vessel disease. *Neurology,* 66**,** 1523-1526.

CHAYER, C. & FREEDMAN, M. (2001) Frontal lobe functions. *Curr Neurol Neurosci Rep,* 1**,** 547-552.

CHEN, Y., CHEN, X., XIAO, W., MOK, V. C., WONG, K. S. & TANG, W. K. (2009) Frontal lobe atrophy is associated with small vessel disease in ischemic stroke patients. *Clin Neurol Neurosurg,* 111**,** 852-857.

CHITNIS, A. (2006) Why Is Delta Endocytosis Required for Effective Activation of Notch? *Dev Dynam,* 235**,** 886-894.

CLAPHAM, R., O'SULLIVAN, E., WELLER, R. O. & CARARE, R. O. (2010) Cervical lymph nodes are found in direct relationship with the internal carotid artery: Significance for the lymphatic drainage of the brain. *Clin Anat,* 23**,** 43-47.

COLLETTE, F., AMIEVA, H., ADAM, S., HOGGE, M., VAN DER LINDEN, M., FABRIGOULE, C. & SALMON, E. (2007) Comparison of inhibitory functioning in mild Alzheimer's disease and frontotemporal dementia. *Cortex,* 43**,** 866-874.

COULTHARD, A., BLANK, S. C., BUSHBY, K., KALARIA, R. N. & BURN, D. J. (2000) Distribution of cranial MRI abnormalities in patients with symptomatic and subclinical CADASIL. *Br J Radiol,* 73**,** 256-265.

CRUM, R. M., ANTHONY, J. C., BASSETT, S. S. & FOLSTEIN, M. F. (1993) Population-based norms for the mini-mental state examination by age and educational level. *JAMA,* 269**,** 2386-2391.

CUMURCIUC, R., GUICHARD, J.-P., REIZINE, D., GRAY, F., BOUSSER, M. G. & CHABRIAT, H. (2006) Dilation of Virchow-Robin spaces in CADASIL. *Eur J Neurol,* 13**,** 187-190.

D'SOUZA, B., MIYAMOTO, A. & WEINMASTER, G. (2008) The many facets of Notch ligands. *Oncogene,* 27**,** 5148-5167.

DALKARA, T., NOZARI, A. & MOSKOWITZ, M. A. (2010) Migraine aura pathophysiology: the role of blood vessels and microembolisation. *Lancet Neurol* 9**,** 309-317.

DE CELIS, J. F. & BRAY, S. J. (2000) The Abruptex domain of Notch regulates negative interactions between Notch, its ligands and Fringe. *Development,* 127**,** 1291-1302.

DE CELIS, J. F., MARÍ-BEFFA, M. & GARCÍA-BELLIDO, A. (1991) Cell-autonomous role of Notch, an epidermal growth factor homologue, in sensory organ differentiation in Drosophila. *Proc Natl Acad Sci USA,* 88**,** 632-636.

DE KONING, I., VAN KOOTEN, F., DIPPEL, D. W., VAN HARSKAMP, F., GROBBEE, D. E., KLUFT, C. & KOUDSTAAL, P. J. (1998) The CAMCOG: a useful screening instrument for dementia in stroke patients. *Stroke,* 29**,** 2080-2086.

DE LA COSTE, A. & FREITAS, A. A. (2006) Notch signaling: distinct ligands induce specific signals during lymphocyte development and maturation. *Immunol Lett,* 102**,** 1-9.

DE LA PEÑA, P., BORNSTEIN, B., DEL HOYO, P., FERNÁNDEZ-MORENO, M. A., MARTÍN, M. A., CAMPOS, Y., GÓMEZ-ESCALONILLA, C., MOLINA, J. A., CABELLO, A. & ARENAS, J. (2001) Mitochondrial dysfunction associated with a mutation in the Notch3 gene in a CADASIL family. *Neurology,* 57**,** 1235-1238.

DEARY, I. J., LEAPER, S. A., MURRAY, A. D., STAFF, R. T. & WHALLEY, L. J. (2003) Cerebral white matter abnormalities and lifetime cognitive change: A 67-year follow-up of the Scottish Mental Survey of 1932. *Psychol Aging,* 18**,** 140-148.

DEL ZOPPO, G. J. (2009) Inflammation and the neurovascular unit in the setting of focal cerebral ischemia. *Neuroscience,* 158**,** 972-982.

DELBOSC, S., GLORIAN, M., LE PORT, A.-S., BÉRÉZIAT, G., ANDRÉANI, M. & LIMON, I. (2008) The benefit of docosahexanoic acid on the migration of vascular smooth muscle cells in partially dependent on Notch regulation of MMP-2/-9. *Am J Pathol,* 172**,** 1430-1440.

DESMOND, D. W., MORONEY, J. T., LYNCH, T., CHAN, S., CHIN, S. S. & MOHR, J. P. (1999) The natural history of CADASIL: a pooled analysis of previously published cases. *Stroke,* 30**,** 1230-1233.

DICHGANS, M. (2009) Cognition in CADASIL. *Stroke,* 40**,** S45-S47.

DICHGANS, M., FILIPPI, M., BRŨNING, R., IANNUCCI, G., BERCHTENBREITER, C., MINICUCCI, L., UTTNER, I., CRISPIN, A., LUDWIG, H., GASSER, T. & YOUSRY, T. A. (1999) Quantitative MRI in

CADASIL: Correlation with disability and cognitive performance. *Neurology,* 52**,** 1361-1367.

DICHGANS, M., HOLTMANNSPÖTTER, M., HERZOG, J., PETERS, N., BERGMANN, M. & YOUSRY, T. A. (2002) Cerebral microbleeds in CADASIL: a gradient-echo magnetic resonance imaging and autopsy study. *Stroke,* 33**,** 67-71.

DICHGANS, M., MARKUS, H. S., SALLOWAY, S., VERKKONIEMI, A., MOLINE, M., WANG, Q., POSNER, H. & CHABRIAT, H. S. (2008) Donepezil in patients with subcortical vascular cognitive impairment: a randomised double-blind trial in CADASIL. *Lancet Neurol,* 7**,** 310-318.

DICHGANS, M., MAYER, M., UTTNER, I., GASSER, T., BRŬNING, R., MŬLLER-HÖCKER, J., EBKE, M., KLOCKGETHER, T. & RUNGGER, G. (1998) The phenotypic spectrum of CADASIL: Clinical findings in 102 cases. *Ann Neurol,* 44**,** 731-739.

DINEEN, R. A., VILISAAR, J., HLINKA, J., BRADSHAW, C. M., MORGAN, P. S., CONSTANTINESCU, C. S. & AUER, D. P. (2009) Disconnection as a mechanism for cognitive dysfunction in multiple sclerosis. *Brain,* 132**,** 239-249.

DING, X.-Q., HAGEL, C., RINGELSTEIN, E. B., BUCHHEIT, S., ZEUMER, H., KUHLENBÄUMER, G., APPENZELLER, S. & FIEHLER, J. (2010) MRI features of pontine autosomal dominant microangiopathy and leukoencephalopathy (PADMAL). *J Neuroimaging,* 20**,** 134-140.

DOI, H., ISO, T., SATO, H., YAMAZAKI, M., MATSUI, H., TANAKA, T., MANABE, I., ARAI, M., NAGAI, R. & KURABAYASHI, M. (2006) Jagged1-selective notch signaling induces smooth muscle differentiation via a RBP-Jκ-dependent pathway. *J Biol Chem,* 281**,** 28555-28564.

DOMENGA, V., FARDOUX, P., LACOMBE, P., MONET, M., MACIAZEK, J., KREBS, L. T., KLONJKOWSKI, B., BERROU, E., MERICSKAY, M., LI, Z., TOURNIER-LASSERVE, E., GRIDLEY, T. & JOUTEL, A. (2004) Notch3 is required for arterial identity and maturation of vascular smooth muscle cells. *Gene Dev,* 18.

DONAHUE, C. P. & KOSIK, K. S. (2004) Distribution pattern of Notch3 mutations suggests a gain-of-function mechanism for CADASIL. *Genomics,* 83**,** 59-65.

DONOVAN, J. A. & KORETZKY, G. A. (1993) CD45 and the immune response. *J Am Soc Nephrol,* 4**,** 976-985.

DOTTI, M. T., DE STEFANO, N., BIANCHI, S., MALANDRINI, A., BATTISTI, C., CARDAIOLI, E. & FEDERICO, A. (2004) A novel NOTCH3 frameshift deletion and mitochondrial abnormalities in a patient with CADASIL. *Arch Neurol,* 61**,** 942-945.

DOUBAL, F. N., MACLULLICH, A. M. J., FERGUSON, K. J., DENNIS, M. S. & WARDLAW, J. M. (2010) Enlarged perivascular spaces on MRI are a feature of cerebral small vessel disease. *Stroke,* 41**,** 450-454.

DOWNWARD, J. (2004) PI 3-kinase, Akt and cell survival *Semin Cell Dev Biol,* 15**,** 177-182.

DUBROCA, C., LACOMBE, P., DOMENGA, V., MACIAZEK, J., LEVY, B., TOURNIER-LASSERVE, E., JOUTEL, A. & HENRION, D. (2005a) Impaired vascular mechanotransduction in a transgenic mouse model of CADASIL arteriopathy. *Stroke,* 36**,** 113-117.

DUBROCA, C., YOU, D., LÉVY, B. I., LOUFRANI, L. & HENRION, D. (2005b) Involvement of RhoA/Rho kinase pathway in myogenic tone in the rabbit facial vein. *Hypertension,* 45**,** 974-979.

DUYCKAERTS, C. & HAUW, J. J. (1997) Prevalence, incidence and duration of Braak's stages in the general population: can we know? *Neurobiol Aging,* 18**,** 389-392.

DZIEWULSKA, D. & RAFALOWSKA, J. (2008) Is the increased expression of ubiquitin in CADASIL syndrome a manifestation of aberrant endocytosis in the vascular smooth muscle cells? *J Clin Neurosci,* 15**,** 535-540.

EARLEY, S., RESTA, T. C. & WALKER, B. R. (2004) Disruption of smooth muscle gap junctions attenuates myogenic vasoconstriction of mesenteric resistance arteries. *Am J Physiol Heart Circ Physiol,* 287**,** H2677-H2686.

EISERT, W. G. & SCHLACHETZKI, F. (2008) Chapter 10 Vascular endothelium and the blood-brain barrier. *Handb Clin Neurol,* 92**,** 197-214.

EPELBAUM, S., BENISTY, S., REYES, S., O'SULLIVAN, M., JOUVENT, E., DÜRING, M., HERVÉ, D., OPHERK, C., HERNANDEZ, K., KURTZ, A., VISWANATHAN, A., BOUSSER, M. G., DICHGANS, M. & CHABRIAT, H. (2010) Verbal memory impairment in subcortical ischemic vascular disease. A descriptive analysis in CADASIL. *Neurobiol Aging,* In Press.

ERKINJUNTTI, T. (1994) Clinical criteria for vascular dementia: The NINDS-AIREN criteria. *Dementia,* 5**,** 189-192.

ERKINJUNTTI, T., KURZ, A., GAUTHIER, S., BULLOCK, R., LILIENFELD, S. & VENKATA DAMARAJU, C. R. (2002) Efficacy of galantamine in probable vascular dementia and Alzheimer's disease combined with cerebrovascular disease: A randomised trial. *Lancet,* 359**,** 1283-1290.

ESIRI, M. M., NAGY, Z., SMITH, M. Z., BARNETSON, L., SMITH, A. D. & JOACHIM, C. (1999) Cerebrovascular disease and threshold for dementia in the early stages of Alzheimer's disease. *Lancet,* 354**,** 919-920.

ESIRI, M. M., WILCOCK, G. K. & MORRIS, J. H. (1997) Neuropathological assessment of the lesions of significance in vascular dementia. *J Neurol Neurosur Ps,* 63**,** 749-753.

FEDERICO, A., BIANCHI, S. & DOTTI, M. T. (2005) The spectrum of mutations for CADASIL diagnosis. *Neurol Sci,* 26**,** 117-124.

FELICIAN, O., BARBEAU, E., GAVARET, M., PELLISSIER, J. F., TOURNIER-LASSERVE, E., PONCET, M. & CECCALDI, M. (2003) A case of late-onset CADASIL with interhemispheric disconnection features. *J Neurol,* 250**,** 1242-1244.

FERREIRA, S., COSTA, C. & OLIVEIRA, J. P. (2007) Novel human pathological mutations. Gene symbol: NOTCH3. Disease: cerebral autosomal dominant arteriopathy with subcortical infarcts and leucoencephalopathy (CADASIL). *Hum Genet,* 121**,** 649.

FISCHER, P., GATTERER, G., MARTERER, A., SIMANYI, M. & DANIELCZYK, W. (1990) Course characteristics in the differentiation of dementia of the Alzheimer type and multi-infarct dementia. *Acta Psychiatr Scand,* 81**,** 551-553.

FOGASSI, L. & LUPPINO, G. (2005) Motor functions of the parietal lobe. *Curr Opin Neurobiol,* 15**,** 626-631.

FOLSTEIN, M. F., FOLSTEIN, S. E. & MCHUGH, P. R. (1975) 'Mini mental state'. A practical method for grading the cognitive state of patients for the clinician. *J Psychiat Res,* 12**,** 189-198.

FORTINI, M. E. (2009) Notch Signaling: The Core Pathway and Its Posttranslational Regulation. *Dev Cell,* 16**,** 633-647.

FORTINI, M. E. & BILDER, D. (2009) Endocytic regulation of Notch signaling. *Curr Opin Genet Dev,* 19**,** 323-328.

FOUILLADE, C., CHABRIAT, H., RIANT, F., MINE, M., ARNOUD, M., MAGY, L., BOUSSER, M. G., TOURNIER-LASSERVE, E. & JOUTEL, A. (2008) Activating NOTCH3 mutation in a patient with small-vessel-disease of the brain. *Hum Mutat,* 29**,** 452.

FRYE, R. E., HASAN, K., MALMBERG, B., DESOUZA, L., SWANK, P., SMITH, K. & LANDRY, S. (2010) Superior longitudinal fasciculus and cognitive

dysfunction in adolescents born preterm and at term. *Dev Med Child Neurol,* 52**,** 760-766.

FUKUTAKE, T. (1999) Young-adult-onset hereditary subcortical vascular dementia: Cerebral autosomal recessive arteriosclerosis with subcortical infarcts and leukoencephalopathy (CARASIL). *Rinsho Shinkeigaku,* 39**,** 50-52.

GAGNON, M., LETENNEUR, L., DARTIGUES, J. F., COMMENGES, D., ORGOGOZO, J. M., BARBERGER-GATEAU, P., ALPÉROVITCH, A., DÉCAMPS, A. & SALAMON, R. (1990) Validity of the Mini-Mental State examination as a screening instrument for cognitive impairment and dementia in French elderly community residents. *Neuroepidemiology,* 9**,** 143-150.

GOBRON, C., VAHEDI, K., VICAUT, E., STUCKER, O., LAEMMEL, E., BAUDRY, N., BOUSSER, M. G. & CHABRIAT, H. (2007) Characteristic features of in vivo skin microvascular reactivity in CADASIL. *J Cerebr Blood F Met,* 27**,** 250-257.

GÓMEZ-ISLA, T., PRICE, J. L., MCKEEL JR., D. W., MORRIS, J. C., GROWDON, J. H. & HYMAN, B. T. (1996) Profound loss of layer II entorhinal cortex neurons occurs in very mild Alzheimer's disease. *J Neurosci,* 16**,** 4491-4500.

GÓMEZ-TORTOSA, E., IRIZARRY, M. C., GÓMEZ-ISLA, T. & HYMAN, B. T. (2000) Clinical and neuropathological correlates of dementia with Lewy bodies. *Ann NY Acad Sci,* 920**,** 9-15.

GRADY, C. L., FUREY, M. L., PIETRINI, P., HORWITZ, B. & RAPOPORT, S. I. (2001) Altered brain functional connectivity and impaired short-term memory in Alzheimer's disease. *Brain,* 124**,** 739-756.

GUNDERSEN, H. J. (1988) The nucleator. *J Microsc,* 151**,** 3-21.

GUNDERSEN, H. J. & JENSEN, E. B. (1987) The efficiency of systematic sampling in stereology and its prediction. *J Microsc,* 147**,** 229-263.

HACHINSKI, V., IADECOLA, C., PETERSEN, R. C., BRETELER, M. M., NYENHUIS, D. L., BLACK, S. E., POWERS, W. J., DECARLI, C., MERINO, J. G., KALARIA, R. N., VINTERS, H. V., HOLTZMAN, D. M., ROSENBERG, G. A., DICHGANS, M., MARLER, J. R. & LEBLANC, G. G. (2006) National Institute of Neurological Disorders and Stroke-Canadian Stroke Network vascular cognitive impairment harmonization standards. *Stroke,* 37**,** 2220-2241.

HAMBLETON, S., VALEYEV, N. V., MURANYI, A., KNOTT, V., WERNER, J. M., MCMICHAEL, A. J., HANDFORD, P. A. & DOWNING, A. K. (2004) Structural and Functional Properties of the Human Notch-1 Ligand Binding Region. *Structure,* 12**,** 2173-2183.

HAMEL, E. (2006) Perivascular nerves and the regulation of cerebrovascular tone. *J Appl Physiol,* 100**,** 1059-1064.

HANNESDOTTIR, K., NITKUNAN, A., CHARLTON, R. A., BARRICK, T. R., MACGREGOR, G. A. & MARKUS, H. S. (2009) Cognitive impairment and white matter damage in hypertension: A pilot study. *Acta Neurol Scand,* 119**,** 261-268.

HARA, K., SHIGA, A., FUKUTAKE, T., NOZAKI, H., MIYASHITA, A., YOKOSEKI, A., KAWATA, H., KOYAMA, A., ARIMA, K., TAKAHASHI, T., IKEDA, M., SHIOTA, H., TAMURA, M., SHIMOE, Y., HIRAYAMA, M., ARISATO, T., YANAGAWA, S., TANAKA, A., NAKANO, I., IKEDA, S.-I., YOSHIDA, Y., YAMAMOTO, T., IKEUCHI, T., KUWANO, R., NISHIZAWA, M., TSUJI, S. & ONODERA, O. (2009) Association of HTRA1 mutations and familial ischemic cerebral small-vessel disease. *New Engl J Med,* 360**,** 1729-1739.

HARDING, A. J., LAKAY, B. & HALLIDAY, G. M. (2002) Selective hippocampal neuron loss in dementia with lewy bodies. *Ann Neurol,* 51**,** 125-128.

HARITUNIANS, T., BOULTER, J., HICKS, C., BUHRMAN, J., DISIBIO, G., SHAWBER, C., WEINMASTER, G., NOFZIGER, D. & SCHANEN, C. (2002)

CADASIL Notch3 mutant proteins localize to the cell surface and bind ligand. *Circ Res,* 90**,** 506-508.

HARITUNIANS, T., CHOW, T., DE LANGE, R. P. J., NICHOLS, J. T., GHAVIMI, D., DORRANI, N., ST. CLAIR, D. M., WEINMASTER, G. & SCHANEN, C. (2005) Functional analysis of a recurrent missense mutation in Notch3 in CADASIL. *J Neurol Neurosur Ps* 76**,** 1242-1248.

HAWKINS, B. T. & DAVIS, T. P. (2005) The blood-brain barrier/neurovascular unit in health and disease. *Pharmacol Rev,* 57**,** 173-185.

HEIER, L. A., BAUER, C. J., SCHWARTZ, L., ZIMMERMAN, R. D., MORGELLO, S. & DECK, M. D. (1989) Large Virchow-Robin spaces: MR-clinical correlation. *Am J Neuroradiol,* 10**,** 929-936.

HEIMER, L. (1983) *The Human Brain and Spinal Cord: Functional Neuroanatomy and Dissection Guide* Springer-Verlag New York Inc.

HEYMAN, A., FILLENBAUM, G. G., WELSH-BOHMER, K. A., PETERSON, B. L., PIEPER, C. F., GEARING, M., MIRRA, S. S. & MOHS, R. C. (1998) Cerebral infarcts in patients with autopsy-proven Alzheimer's disease CERAD, part XVIII. *Neurology,* 51**,** 159-162.

HICKS, C., JOHNSTON, S. H., DISIBIO, G., COLLAZO, A., VOGT, T. F. & WEINMASTER, G. (2000) Fringe differentially modulates Jagged1 and Delta1 signalling through Notch1 and Notch2. *Nat Cell Biol,* 2**,** 515-520.

HOF, P. R., COX, K. & MORRISON, J. H. (1990) Quantitative analysis of a vulnerable subset of pyramidal neurons in Alzheimer's disease: I. Superior frontal and inferior temporal cortex. *J Comp Neurol,* 301**,** 44-54.

HOF, P. R., NIMCHINSKY, E. A. & MORRISON, J. H. (1995) Neurochemical phenotype of corticocortical connections in the macaque monkey: quantitative analysis of a subset of neurofilament protein-immunoreactive projection neurons in frontal, parietal, temporal, and cingulate cortices. *J Comp Neurol,* 362**,** 109-133.

HOFMANN, J. J. & IRUELA-ARISPE, M. L. (2007) Notch signaling in blood vessels: Who is talking to whom about what? *Circ Res,* 100**,** 1556-1568.

HOLNESS, C. L. & SIMMONS, D. L. (1993) Molecular cloning of CD68, a human macrophage marker related to lysosomal glycoproteins. *Blood,* 81**,** 1607-1613.

HUANG, L., YANG, Q., ZHANG, L., CHEN, X., HUANG, Q. & WANG, H. (2010) Acetazolamide improves cerebral hemodynamics in CADASIL. *J Neurol Sci,* 292**,** 77-80.

HUSSAIN, M. B., SINGHAL, S., MARKUS, H. S. & SINGER, D. R. J. (2004) Abnormal Vasoconstrictor Responses to Angiotensin II and Noradrenaline in Isolated Small Arteries from Patients with Cerebral Autosomal Dominant Arteriopathy with Subcortical Infarcts and Leukoencephalopathy (CADASIL). *Stroke,* 35**,** 853-858.

IADECOLA, C. (2004) Neurovascular regulation in the normal brain and in Alzheimer's disease. *Nature Rev Neurosci,* 5**,** 347-360.

IANNUCCI, G., DICHGANS, M., ROVARIS, M., BRUNING, R., GASSER, T., GIACOMOTTI, L., YOUSRY, T. A. & FILIPPI, M. (2001) Correlations between clinical findings and magnetization transfer imaging metrics of tissue damage in individuals with cerebral autosomal dominant arteriopathy with subcortical infarcts and leukoencephalopathy. *Stroke,* 32**,** 643-648.

IHALAINEN, S., SOLIYMANI, R., IIVANAINEN, E., MYKKÄNEN, K., SAINIO, A., PÖYHÖNEN, M., ELENIUS, K., JÄRVELÄINEN, H., VIITANEN, M., KALIMO, H. & BAUMANN, M. (2007) Proteome analysis of cultivated vascular smooth muscle cells from a CADASIL patient. *Mol Med,* 13**,** 305-314.

IHARA, M., POLVIKOSKI, T. M., HALL, R., SLADE, J. Y., PERRY, R. H., OAKLEY, A. E., ENGLUND, E., O'BRIEN, J. T., INCE, P. G. & KALARIA, R. N. (2010) Quantification of myelin loss in frontal lobe white matter in vascular

dementia, Alzheimer's disease, and dementia with Lewy bodies. *Acta Neuropathol* 119**,** 579-589.

INGLESE, M., BOMSZTYK, E., GONEN, O., MANNON, L. J., GROSSMAN, R. I. & RUSINEK, H. (2005) Dilated perivascular spaces: hallmarks of mild traumatic brain injury. *AJNR Am J Neuroradiol,* 26**,** 719-724.

INSAUSTI, R., JUOTTONEN, K., SOININEN, H., INSAUSTI, A. M., PARTANEN, K., VAINIO, P., LAAKSO, M. P. & PITKANEN, A. (1998) MR volumetric analysis of the human entorhinal, perirhinal, and temporopolar cortices. *Am J Neuroradiol,* 19**,** 659-671.

IRVIN, D. K., ZURCHER, S. D., NGUYEN, T., WEINMASTER, G. & KORNBLUM, H. I. (2001) Expression patterns of Notch1, Notch2, and Notch3 suggest multiple functional roles for the Notch-DSL signaling system during brain development. *J Comp Neurol,* 436**,** 167-181.

ISHIKO, A., SHIMIZU, A., NAGATA, E., TAKAHASHI, K., TABIRA, T. & SUZUKI, N. (2006) Notch3 ectodomain is a major component of granular osmiophilic material (GOM) in CADASIL. *Acta Neuropathol,* 112**,** 333-339.

ISO, T., HAMAMORI, Y. & KEDES, L. (2003) Notch signaling in vascular development. *Arterioscler Thromb Vasc Biol,* 23**,** 543-553.

ISO, T., SARTORELLI, V., CHUNG, G., SHICHINOHE, T., KEDES, L. & HAMAMORI, Y. (2001) HERP, a new primary target of Notch regulated by ligand binding. *Mol Cell Biol,* 21**,** 6071-6079.

JALECO, A. C., NEVES, H., HOOIJBERG, E., GAMEIRO, P., CLODE, N., HAURY, M., HENRIQUE, D. & PARREIRA, L. (2001) Differential effects of Notch ligands Delta-1 and Jagged-1 in human lymphoid differentiation. *J Exp Med,* 194**,** 991-1001.

JARRIAULT, S., BROU, C., LOGEAT, F., SCHROETER, E. H., KOPAN, R. & ISRAEL, A. (1995) Signalling downstream of activated mammalian notch. *Nature,* 377**,** 355-358.

JIA, L., YU, G., ZHANG, Y. & WANG, M. M. (2009) Lysosome-dependent degradation of Notch3. *Int J Biochem Cell B,* 41**,** 2594-2598.

JIN, S., HANSSON, E. M., TIKKA, S., LANNER, F., SAHLGREN, C., FARNEBO, F., BAUMANN, M., KALIMO, H. & LENDAHL, U. (2008) Notch signaling regulates platelet-derived growth factor receptor-β expression in vascular smooth muscle cells. *Circ Res,* 102**,** 1483-1491.

JOSEPH, R. (1996) 6. The Hippocampus, Amygdala, Memory, and Amnesia: Synaptic Potentiation and Cognitive and Emotional Neural Networks. *Neuropsychiatry, Neuropsychology, and Clinical Neuroscience.* 2nd ed. Baltimore, Williams & Wilkins.

JOUTEL, A., ANDREUX, F., GAULIS, S., DOMENGA, V., CECILLON, M., BATTAIL, N., PIGA, N., CHAPON, F., GODFRAIN, C. & TOURNIER-LASSERVE, E. (2000) The ectodomain of the Notch3 receptor accumulates within the cerebrovasculature of CADASIL patients. *J Clin Invest,* 105**,** 597-605.

JOUTEL, A., CORPECHOT, C., DUCROS, A., VAHEDI, K., CHABRIAT, H., MOUTON, P., ALAMOWITCH, S., DOMENGA, V., CECILLION, M., MARECHAL, E., MACIAZEK, J., VAYSSIERE, C., CRUAUD, C., CABANIS, E.-A., RUCHOUX, M. M., WEISSANBACH, J., BACH, J. F., BOUSSER, M. G. & TOURNIER-LASSERVE, E. (1996) Notch3 mutations in CADASIL, a hereditary adult-onset condition causing stroke and dementia. *Nature,* 383**,** 707-710.

JOUTEL, A., FAVOROLE, P., LABAUGE, P., CHABRIAT, H., C., L., ANDREUX, F., DOMENGA, V., CECILLON, M., VAHEDI, K., DUCROS, A., CAVE-RIANT, F., BOUSSER, M.-G. & TOURNIER-LASSERVE, E. (2001) Skin biopsy immunostaining with a Notch3 monoclonal antibody for CADASIL diagnosis. *Lancet,* 358**,** 2049-2051.

JOUTEL, A., MONET-LEPRETRE, M., GOSELE, C., BARON-MENGUY, C., HAMMES, A., SCHMIDT, S., LEMAIRE-CARRETTE, B., DOMENGA, V., SCHEDL, A., LACOMBE, P. & HUBNER, N. (2010) Cerebrovascular dysfunction and microcirculation rarefaction precede white matter lesions in a mouse genetic model of cerebral ischemic small vessel disease. *J Clin Invest,* 120**,** 433-445.

JOUTEL, A., MONET, M., DOMENGA, V., TOURNIER-LASSERVE, E. & RIANT, F. (2004) Pathogenic Mutations Associated with Cerebral Autosomal Dominant Arteriopathy with Subcortical Infarcts and Leukoencephalopathy Differently Affect Jagged1 Binding and Notch3 Activity via the RBP/JK Signaling Pathway. *Am J Hum Genet,* 74**,** 338-347.

KALARIA, R. N. & ERKINJUNTTI, T. (2006) Small vessel disease and subcortical vascular dementia. *J Clin Neurol,* 2**,** 1-11.

KALARIA, R. N., VIITANEN, M., KALIMO, H., DICHGANS, M. & TABIRA, T. (2004) The pathogenesis of CADASIL: an update. *J Neurol Sci,* 226**,** 35-39.

KALIMO, H., RUCHOUX, M.-M., VIITANEN, M. & KALARIA, R. N. (2002) CADASIL: a common form of hereditary arteriopathy causing brain infarcts. *Brain Pathol,* 12**,** 350-359.

KARLSGODT, K. H., VAN ERP, T. G. M., POLDRACK, R. A., BEARDEN, C. E., NUECHTERLEIN, K. H. & CANNON, T. D. (2008) Diffusion Tensor Imaging of the Superior Longitudinal Fasciculus and Working Memory in Recent-Onset Schizophrenia. *Biol Psychiatry,* 63**,** 512-518.

KARLSTRÖM, H., BEATUS, P., DANNAEUS, K., CHAPMAN, G., LENDAHL, U. & LUNDKVIST, J. (2002) A CADASIL-mutated Notch 3 receptor exhibits impaired intracellular trafficking and maturation but normal ligand-induced signaling. *P Natl Acad Sci USA,* 99**,** 17119-17124.

KATO, T., NAKAYAMA, N., YASOKAWA, Y., OKUMURA, A., SHINODA, J. & IWAMA, T. (2007) Statistical image analysis of cerebral glucose metabolism in patients with cognitive impairment following diffuse traumatic brain injury. *J Neurotrauma,* 24**,** 919-926.

KAVIRAJAN, H. & SCHNEIDER, L. S. (2007) Efficacy and adverse effects of cholinesterase inhibitors and memantine in vascular dementia: a meta-analysis of randomised controlled trials. *Lancet Neurol,* 6**,** 782-792.

KERTESZ, A. & CLYDESDALE, S. (1994) Neuropsychological deficits in vascular dementia vs Alzheimer's disease. Frontal lobe deficits prominent in vascular dementia. *Arch Neurol,* 51**,** 1226-1231.

KIM, Y., CHOI, E. J., CHOI, C. G., KIM, G., CHOI, J. H., YOO, H. W. & KIM, J. S. (2006) Characteristics of CADASIL in Korea: A novel cysteine-sparing Notch3 mutation. *Neurology,* 66**,** 1511-1516.

KIRKITADZE, M. D., BITAN, G. & TEPLOW, D. B. (2002) Paradigm shifts in Alzheimer's disease and other neurodegenerative disorders: The emerging role of oligomeric assemblies. *J Neurosci Res,* 69**,** 567-577.

KITAMOTO, T., TAKAHASHI, K., TAKIMOTO, H., TOMIZUKA, K., HAYASAKA, M., TABIRA, T. & HANAOKA, K. (2005) Functional redundancy of the Notch gene family during mouse embryogenesis: Analysis of Notch gene expression in Notch3-deficient mice *Biochem Bioph Res Co,* 331**,** 1154-1162.

KOPAN, R. & ILAGAN, M. X. G. (2009) The Canonical Notch Signaling Pathway: Unfolding the Activation Mechanism. *Cell* 137**,** 216-233.

KORDOWER, J. H., CHU, Y., STEBBINS, G. T., DEKOSKY, S. T., COCHRAN, E. J., BENNETT, D. & MUFSON, E. J. (2001) Loss and Atrophy of Layer II Entorhinal Cortex Neurons in Elderly People with Mild Cognitive Impairment. *Ann Neurol,* 49**,** 202-213.

KRAIN, A. L. & CASTELLANOS, F. X. (2006) Brain development and ADHD. *Clin Psychol Rev,* 26**,** 433-444.

KREBS, L. T., XUE, Y., NORTON, C. R., SHUTTER, J. R., MAGUIRE, M., SUNDBERG, J. P., GALLAHAN, D., CLOSSON, V., KITAJEWSKI, J., CALLAHAN, R., SMITH, G. H., STARK, K. L. & GRIDLEY, T. (2000) Notch signaling is essential for vascular morphogenesis in mice. *Gene Dev,* 14**,** 1343-1352.

KREBS, L. T., XUE, Y., NORTON, C. R., SUNDBERG, J. P., GRIDLEY, T., BEATUS, P., LENDAHL, U. & JOUTEL, A. (2003) Characterization of Notch3-Deficient Mice: Normal Embryonic Development and Absence of Genetic Interactions with a Notch1 Mutation. *Genesis,* 37**,** 139-143.

KRIL, J. J., PATEL, S., HARDING, A. J. & HALLIDAY, G. M. (2002a) Neuron loss from the hippocampus of Alzheimer's disease exceeds extracellular neurofibrillary tangle formation. *Acta Neuropathol,* 103**,** 370-376.

KRIL, J. J., PATEL, S., HARDING, A. J. & HALLIDAY, G. M. (2002b) Patients with vascular dementia due to microvascular pathology have significant hippocampal neuronal loss. *J Neurol Neurosur Ps,* 72**,** 747-751.

KUMAR, V., ANAND, R., MESSINA, J., HARTMAN, R. & VEACH, J. (2000) An efficacy and safety analysis of Exelon® in Alzheimer's disease patients with concurrent vascular risk factors. *Eur J Neurol,* 7**,** 159-169.

LACOMBE, P., OLIGO, C., DOMENGA, V., TOURNIER-LASSERVE, E. & JOUTEL, A. (2005) Impaired cerebral vasoreactivity in a transgenic mouse model of cerebral autosomal dominant arteriopathy with subcortical infarcts and leukoencephalopathy arteriopathy. *Stroke,* 36**,** 1053-1058.

LAGAUD, G., KARICHETI, V., KNOT, H. J., CHRIST, G. J. & LAHER, I. (2002) Inhibitors of gap junctions attenuate myogenic tone in cerebral arteries. *Am J Physiol Heart Circ Physiol,* 283**,** H2177-H2186.

LAMMIE, G. A., BRANNAN, F., SLATTERY, J. & WARLOW, C. (1997) Nonhypertensive cerebral small-vessel disease: An autopsy study. *Stroke,* 28**,** 2222-2229.

LARDELLI, M., DAHLSTRAND, J. & LENDAHL, U. (1994) The novel Notch homologue mouse Notch 3 lacks specific epidermal growth factor-repeats and is expressed in proliferating neuroepithelium. *Mech Develop,* 46**,** 123-136.

LE BORGNE, R., BARDIN, A. & SCHWEISGUTH, F. (2005) The roles of receptor and ligand endocytosis in regulating Notch signaling. *Development,* 132**,** 1751-1762.

LEIFER, D. & KOWALL, N. W. (1993) Immunohistochemical patterns of selective cellular vulnerability in human cerebral ischemia. *J Neurol Sci,* 119**,** 217-228.

LESNIK OBERSTEIN, S. A., VAN DUINEN, S. G., VAN DEN BOOM, R., MAAT-SCHIEMAN, M. L., VAN BUCHEM, M. A., VAN HOUWELINGEN, H. C., HEGEMAN-KLEINN, I. M., FERRARI, M. D., BREUNING, M. H. & HAAN, J. (2003) Evaluation of diagnostic NOTCH3 immunostaining in CADASIL. *Acta Neuropathol,* 106**,** 107-111.

LESNIK OBERSTEIN, S. A. J., VAN DEN BOOM, R., VAN BUCHEM, M. A., VAN HOUWELINGEN, H. C., BAKKER, E., VOLLEBREGT, E., FERRARI, M. D., BREUNING, M. H. & HAAN, J. (2001) Cerebral microbleeds in CADASIL. *Neurology,* 57**,** 1066-1070.

LEWANDOWSKA, E., SZPAK, G. M., WIERZBA-BOBROWICZ, T., MODZELEWSKA, J., STEPIEN, T., PASENNIK, E., SCHMIDT-SIDOR, B. & RAFAŁOWSKA, J. (2010) Capillary vessel wall in CADASIL angiopathy. *Folia Neuropathol,* 48**,** 104-115.

LI, Y., TAKESHITA, K., LIU, P.-Y., SATOH, M., OYAMA, N., MUKAI, Y., CHIN, M. T., KREBS, L., KOTLIKOFF, M. I., RADTKE, F., GRIDLEY, T. & LIAO, J. K. (2009) Smooth muscle notch1 mediates neointimal formation after vascular injury. *Circulation* 119**,** 2686-2692.

LIEM, M. K., VAN DER GROND, J., HAAN, J., VAN DEN BOOM, R., FERRARI, M. D., KNAAP, Y. M., BREUNING, M. H., VAN BUCHEM, M. A., MIDDELKOOP, H. A. M. & OBERSTEIN, S. A. J. L. (2007) Lacunar infarcts are the main correlate with cognitive dysfunction in CADASIL. *Stroke,* 38**,** 923-928.

LIN, L., MERNAUGH, R., YI, F., BLUM, D., CARBONE, D. P. & DANG, T. P. (2010) Targeting specific regions of the Notch3 ligand-binding domain induces apoptosis and inhibits tumor growth in lung cancer. *Cancer Res,* 70**,** 632-638.

LINDEBOOM, J., TER HORST, R., HOOYER, C., DINKGREVE, M. & JONKER, C. (1993) Some psychometric properties of the CAMCOG. *Psychol Med,* 23**,** 213-219.

LINDNER, M., FOKUHL, J., LINSMEIER, F., TREBST, C. & STANGEL, M. (2009) Chronic toxic demyelination in the central nervous system leads to axonal damage despite remyelination. *Neurosci Lett,* 453**,** 120-125.

LIU, W.-H., HSIAO, H.-W., TSOU, W.-I. & LAI, M.-Z. (2007) Notch inhibits apoptosis by direct interference with XIAP ubiquitination and degradation. *EMBO Journal,* 26**,** 1660-1669.

LOW, W. C., JUNNA, M., BÖRJESSON-HANSON, A., MORRIS, C. M., MOSS, T. H., STEVENS, D. L., ST. CLAIR, D., MIZUNO, T., ZHANG, W. W., MYKKÄNEN, K., WAHLSTROM, J., ANDERSEN, O., KALIMO, H., VIITANEN, M. & KALARIA, R. N. (2007) Hereditary multi-infarct dementia of the Swedish type is a novel disorder different from NOTCH3 causing CADASIL. *Brain,* 130**,** 357-367.

LOW, W. C., SANTA, Y., TAKAHASHI, K., TABIRA, T. & KALARIA, R. N. (2006) CADASIL-causing mutations do not alter Notch3 receptor processing and activation. *Neuroreport,* 17**,** 945-949.

LUNDKVIST, J., ZHU, S., HANSSON, E. M., SCHWEINHARDT, O., MIAO, Q., KALIMO, H. & LENDAHL, U. (2005) Mice carrying a R142C Notch 3 knock-in mutation do not develop a CADASIL-like phenotype. *Genesis,* 41**,** 13-22.

LUO, Y. & HALTIWANGER, R. S. (2005) O-fucosylation of notch occurs in the endoplasmic reticulum. *J Biol Chem,* 280**,** 11289-11294.

LYON, C. A., KOUTSOUKI, E., AGUILERA, C. M., BLASCHUK, O. W. & GEORGE, S. J. (2010) Inhibition of N-cadherin retards smooth muscle cell migration and intimal thickening via induction of apoptosis. *J Vasc Surg,* 52**,** 1301-1309.

MACCLELLAN, L. R., GILES, W., COLE, J., WOZNIAK, M., STERN, B., MITCHELL, B. D. & KITTNER, S. J. (2007) Probable migraine with visual aura and risk of ischemic stroke: the stroke prevention in young women study. *Stroke,* 38**,** 2438-2445.

MACLULLICH, A. M. J., WARDLAW, J. M., FERGUSON, K. J., STARR, J. M., SECKL, J. R. & DEARY, I. J. (2004) Enlarged perivascular spaces are associated with cognitive function in healthy elderly men. *J Neurol Neurosur Ps,* 75**,** 1519-1523.

MAKRIS, N., KENNEDY, D. N., MCINERNEY, S., SORENSEN, A. G., WANG, R., CAVINESS JR., V. S. & PANDYA, D. N. (2005) Segmentation of subcomponents within the superior longitudinal fascicle in humans: A quantitative, in vivo, DT-MRI study. *Cereb Cortex,* 15**,** 854-869.

MANGANELLI, F., RAGNO, M., CACCHIÒ, G., IODICE, V., TROJANO, L., SILVAGGIO, F., SCARCELLA, M., GRAZIOLI, M., SANTORO, L. & PERRETTI, A. (2008) Motor cortex cholinergic dysfunction in CADASIL: a transcranial magnetic demonstration. *Clin Neurophysiol,* 119**,** 351-355.

MARKUS, H. S. (2007) Genes, endothelial function and cerebral small vessel disease in man. *Exp Physiol,* 93**,** 121-127.

MATHIVANAN, S. & SIMPSON, R. J. (2009) ExoCarta: A compendium of exosomal proteins and RNA. *Proteomics,* 9**,** 4997-5000.

MAZZEI, R., CONFORTI, F. L., LANZA, P. L., SPROVIERI, T., LUPO, M. R., GALLO, O., PATITUCCI, A., MAGARIELLO, A., CARACCIOLO, M., GABRIELE, A. L., FERA, F., VALENTINO, P., BONO, F., CENACCHI, G., SANTORO, G., MUGLIA, M. & QUATTRONE, A. (2004) A novel Notch3 gene mutation not involving a cysteine residue in an Italian family with CADASIL. *Neurology,* 63**,** 561-564.

MAZZEI, R., GUIDETTI, D., UNGARO, C., CONFORTI, F. L., MUGLIA, M., CENACCHI, G., LANZA, P. L., PATITUCCI, A., SPROVIERI, T., RIGUZZI, P., MAGARIELLO, A., GABRIELE, A. L., CITRIGNO, L., PREDA, P. & QUATTRONE, A. (2008) First evidence of a pathogenic insertion in the NOTCH3 gene causing CADASIL. *J Neurol Neurosur Ps,* 79**,** 108-110.

MCFARLAND, R., SWALWELL, H., BLAKELY, E. L., HE, L., GROEN, E. J., TURNBULL, D. M., BUSHBY, K. M. & TAYLOR, R. W. (2008) The m.5650G > A mitochondrial tRNAAla mutation is pathogenic and causes a phenotype of pure myopathy. *Neuromuscul Disord,* 18**,** 63-67.

MELLIES, J. K., BAŬMER, T., MŬLLER, J. A., TOURNIER-LASSERVE, E., CHABRIAT, H., KNOBLOCH, O., HACKELOŒR, H. J., GOEBEL, H. H., WETZIG, L. & HALLER, P. (1998) SPECT study of a German CADASIL family: A phenotype with migraine and progressive dementia only. *Neurology,* 50**,** 1715-1721.

MESULAM, M., SIDDIQUE, T. & COHEN, B. (2003) Cholinergic denervation in a pure multi-infarct state: Observations on CADASIL. *Neurology,* 60**,** 1183-1185.

MIAO, J., XU, F., DAVIS, J., VAN NOSTRAND, W. E., OTTE-HÖLLER, I. & VERBEEK, M. M. (2005) Cerebral microvascular amyloid ß protein deposition induces vascular degeneration and neuroinflammation in transgenic mice expressing human vasculotropic mutant amyloid ß precursor protein. *Am J Pathol,* 167**,** 505-515.

MIAO, Q., PALONEVA, T., TUOMINEN, S., POYHONEN, M., TUISKU, S., VIITANEN, M. & KALIMO, H. (2004) Fibrosis and stenosis of the long penetrating cerebral arteries: The cause of the white matter pathology in cerebral autosomal dominant arteriopathy with subcortical infarcts and leukoencephalopathy. *Brain Pathol,* 14**,** 358-364.

MIGLIORE, L. & COPPEDÈ, F. (2009) Environmental-induced oxidative stress in neurodegenerative disorders and aging. *Mutat Res,* 674**,** 73-84.

MILLER, E. K. & COHEN, J. D. (2001) An integrative theory of prefrontal cortex function. *Annu Rev Neurosci,* 24**,** 167-202.

MIRRA, S. S., HEYMAN, A., MCKEEL, D., SUMI, S. M., CRAIN, B. J., BROWNLEE, L. M., VOGEL, F. S., HUGHES, J. P., VAN BELLE, G. & BERG, L. (1991) The Consortium to Establish a Registry for Alzheimer's Disease (CERAD). Part II. Standardization of the neuropathologic assessment of Alzheimer's disease. *Neurology,* 41**,** 479-486.

MIZUNO, T., KONDO, M., ISHIGAMI, N., TAMURA, A., ITSUKAGE, M., KOIZUMI, H., ISAYAMA, R., HOSOMI, A., NAGAKANE, Y., TOKUDA, T., SUGIMOTO, E., USHIJIMA, Y. & NAKAGAWA, M. (2009) Cognitive impairment and cerebral hypoperfusion in a CADASIL patient improved during administration of lomerizine. *Clin Neuropharmacol,* 32**,** 113-116.

MIZUNO, T., MAKINO, M., FUJIWARA, Y. & NAKAJIMA, K. (2002) Lack of association between NOTCH3 gene polymorphism and cerebrovascular disease in Japanese patients. *Ann NY Acad Sci,* 977**,** 252-257.

MIZUNO, T., MURANISHI, M., TORUGUN, T., TANGO, H., NAGAKANE, Y., KUDEKEN, T., KAWASE, Y., KAWABE, K., OSHIMA, F., YAOI, T., ITOH, K., FUSHIKI, S. & NAKAGAWA, M. (2008) Two Japanese CADASIL

families exhibiting Notch3 mutation R75P not involving cysteine residue. *Intern Med,* 47**,** 2067-2072.

MONET-LEPRÊTRE, M., BARDOT, B., LEMAIRE, B., DOMENGA, V., GODIN, O., DICHGANS, M., TOURNIER-LASSERVE, E., COHEN-TANNOUDJI, M., CHABRIAT, H. & JOUTEL, A. (2009) Distinct phenotypic and functional features of CADASIL mutations in the Notch3 ligand binding domain. *Brain,* 132**,** 1601-1612.

MONET, M., DOMENGA, V., LEMAIRE, B., SOUILHOL, C., LANGA, F., BABINET, C., GRIDLEY, T., TOURNIER-LASSERVE, E., COHEN-TANNOUDJI, M. & JOUTEL, A. (2007) The archetypal R90C CADASIL - Notch3 mutation retains Notch3 function in vivo. *Hum Mol Genet,* 16**,** 982-992.

MOUTON, P. R., GOKHALE, A. M., WARD, N. L. & WEST, M. J. (2002) Stereological length estimation using spherical probes. *J Microsc,* 206**,** 54-64.

MRABET, N. T., VAN DEN BROECK, A., VAN BRANDE, I. D., STANSSENS, P., LAROCHE, Y., LAMBEIR, A.-M., MATTHIJSSENS, G., JENKINS, J., CHIADMI, M., VAN TILBEURGH, H., REY, F., JANIN, J., QUAX, W. J., LASTERS, I., DE MAEYER, M. & WODAK, S. J. (1992) Arginine residues as stabilizing elements in proteins. *Biochemistry,* 31**,** 2239-2253.

MULDER, E. J., LINSSEN, W. H., PASSCHIER, J., ORLEBEKE, J. F. & DE GEUS, E. (1999) Interictal and postictal cognitive changes in migraine. *Cephalagia,* 19**,** 557-565.

MUNGAS, D. (1991) In-office mental status testing: a practical guide. *Geriatrics,* 46**,** 54-56.

MYKKÄNEN, K., JUNNA, M., AMBERLA, K., BRONGE, L., KÄÄRIÄINEN, H., PÖYHÖNEN, M., KALIMO, H. & VIITANEN, M. (2009) Different clinical phenotypes in monozygotic cadasil twins with a novel notch3 mutation. *Stroke,* 40**,** 2215-2218.

NAKAMURA, M., NESTOR, P. G., LEVITT, J. J., COHEN, A. S., KAWASHIMA, T., SHENTON, M. E. & MCCARLE, Y. R. W. (2008) Orbitofrontal volume deficit in schizophrenia and thought disorder. *Brain,* 131**,** 180-195.

NAKAMURA, T., WATANABE, H., HIRAYAMA, M., INUKAI, A., KABASAWA, H., MATSUBRARA, M., MITAKE, S., NAKAMURA, M., ANDO, Y., UCHINO, M. & SOBUE, G. (2005) CADASIL with NOTCH3 S180C presenting anticipation of onset age and hallucinations. *J Neurol Sci,* 238**,** 87-91.

NEVES, H., WEERKAMP, F., GOMES, A. C., NABER, B. A. E., GAMEIRO, P., BECKER, J. D., LÚCIO, P., CLODE, N., VAN DONGEN, J. J. M., STAAL, F. J. T. & PARREIRA, L. (2006) Effects of Delta1 and Jagged1 on early human hematopoiesis: Correlation with expression of Notch signaling-related genes in CD34+ cells; ligand difference. *Stem Cells,* 24**,** 1327-1337.

NICHOLS, J. T., MIYAMOTO, A., OLSEN, S. L., D'SOUZA, B., YAO, C. & WEINMASTER, G. (2007) DSL ligand endocytosis physically dissociates Notch1 heterodimers before activating proteolysis can occur. *J Cell Biol,* 176**,** 445-458.

NIEVEL, J. G. & CUMINGS, J. N. (1967) Nissl substance and ribosomal aggregates. *Nature,* 214**,** 1123-1124.

O'KEEFE, J. & NADEL, L. (1978) Chapter 3 - Anatomy. *The hippocampus as a cognitive map.* Walton Street, Oxford, Oxford University Press.

O'SULLIVAN, M., BARRICK, T. R., MORRIS, R. G., CLARK, C. A. & MARKUS, H. S. (2005) Damage within a network of white matter regions underlies executive dysfunction in CADASIL. *Neurology,* 65**,** 1584-1590.

O'SULLIVAN, M., SUMMERS, P. E., JONES, D. K., JAROSZ, J. M., WILLIAMS, S. C. & MARKUS, H. S. (2001) Normal-appearing white matter in ischemic leukoaraiosis: a diffusion tensor MRI study. *Neurology,* 57**,** 2307-2310.

OBERSTEIN, S. A. J. L., MAAT-SCHIEMAN, M. L. C., BOON, E. M. J., HAAN, J., BREUNING, M. H. & DUINEN, S. G. (2008) No vessel wall abnormalities in a human foetus with a NOTCH3 mutation. *Acta Neuropathol,* 115**,** 369-370.

OIDE, T., NAKAYAMA, H., YANAGAWA, S., ITO, N., IKEDA, S.-I. & ARIMA, K. (2008) Extensive loss of arterial medial smooth muscle cells and mural extracellular matrix in cerebral autosomal recessive arteriopathy with subcortical infarcts and leukoencephalopathy (CARASIL). *Neuropathology,* 28**,** 132-142.

OKEDA, R., ARIMA, K. & KAWAI, M. (2002) Arterial Changes in Cerebral Autosomal Dominant Arteriopathy with subcortical infarcts and leukoencephalopathy (CADASIL) in relation to pathogenesis of diffuse myelin loss of cerebral white matter: examination of cerebral medullary arteries by reconstruction of serial sections of and autopsy case. *Stroke,* 33**,** 2565-2569.

OKOCHI, M., FUKUMORI, A., JIANG, J., ITOH, N., KIMURA, R., STEINER, H., HAASS, C., TAGAMI, S. & TAKEDA, M. (2006) Secretion of the Notch-1 Aβ-like peptide during Notch signaling. *J Biol Chem,* 281**,** 7890-7898.

OLSON, I. R., PLOTZKER, A. & EZZYAT, Y. (2007) The Enigmatic temporal pole: a review of findings on social and emotional processing. *Brain,* 130**,** 1718-1731.

OPHERK, C., DUERING, M., PETERS, N., KARPINSKA, A., ROSNER, S., SCHNEIDER, E., BADER, B., GIESE, A. & DICHGANS, M. (2009) CADASIL mutations enhance spontaneous multimerization of NOTCH3. *Hum Mol Genet,* 18**,** 2761-2767.

OPHERK, C., PETERS, N., HERZOG, J., DICHGANS, M. & LUEDTKE, R. (2004) Long-term prognosis and causes of death in CADASIL: A retrospective study in 411 patients. *Brain,* 127**,** 2533-2539.

OPHERK, C., PETERS, N., HOLTMANNSPÖTTER, M., GSCHWENDTNER, A., MÜLLER-MYHSOK, B. & DICHGANS, M. (2006) Heritability of MRI lesion volume in CADASIL: Evidence for genetic modifiers. *Stroke,* 37**,** 2684-2689.

OSAWA, A., MAESHIMA, S., SHIMAMOTO, Y., MAESHIMA, E., SEKIGUCHI, E., KAKISHITA, K., OZAKI, F. & MORIWAKI, H. (2004) Relationship between cognitive function and regional cerebral blood flow in different types of dementia. *Disabil Rehabil,* 26**,** 739-745.

PANTONI, L. (2010) Cerebral small vessel disease: from pathogenesis and clinical characteristics to therapeutic challenges. *Lancet Neurol,* 9**,** 689-701.

PANTONI, L., PESCINI, F., NANNUCCI, S., SARTI, C., BIANCHI, S., DOTTI, M. T., FEDERICO, A. & INZITARI, D. (2010) Comparison of clinical, familial, and MRI features of CADASIL and NOTCH3-negative patients. *Neurology,* 74**,** 57-63.

PARISI, V., PIERELLI, F., COPPOLA, G., RESTUCCIA, R., FERRAZZOLI, D., SCASSA, C., BIANCO, F., PARISI, L. & FATTAPPOSTA, F. (2007) Reduction of optic nerve fiber layer thickness in CADASIL. *Eur J Neurol,* 14**,** 627-631.

PARISI, V., PIERELLI, F., FATTAPPOSTA, F., BIANCO, F., PARISI, L., RESTUCCIA, R., MALANDRINI, A., FERRARI, M. & CARRERA, P. (2003) Early visual function impairment in CADASIL. *Neurology,* 60**,** 2008-2010.

PARKS, A. L., KLUEG, K. M., STOUT, J. R. & MUSKAVITCH, M. A. T. (2000) Ligand endocytosis drives receptor dissociation an activation in the Notch pathway. *Development,* 127**,** 1373-1385.

PARKS, A. L., STOUT, J. R., SHEPARD, S. B., KLUEG, K. M., DOS SANTOS, A. A., PARODY, T. R., VASKOVA, M. & MUSKAVITCH, M. A. (2006) Structure-function analysis of delta trafficking, receptor binding and signaling in Drosophila. *Genetics,* 174**,** 1947-1961.

PATANKAR, T. F., MITRA, D., VARMA, A., SNOWDEN, J., NEARY, D. & JACKSON, A. (2005) Dilatation of the Virchow-Robin space is a sensitive

indicator of cerebral microvascular disease: study in elderly patients with dementia. *AJNR Am J Neuroradiol,* 26**,** 1512-1520.

PEI, Z. & BAKER, N. E. (2008) Competition between Delta and the Abruptex domain of Notch. *BMC Dev Biol,* 8**,** 4.

PENDLEBURY, S. T., BLAMIRE, A. M., LEE, M. A., STYLES, P. & MATTHEWS, P. M. (1999) Axonal injury in the internal capsule correlates with motor impairment after stroke. *Stroke,* 30**,** 956-962.

PENNANEN, C., KIVIPELTO, M., TUOMAINEN, S., HARTILAINEN, P., HANNINEN, T., LAAKSO, M. P., HALLIKAINEN, M., VANHANEN, M., NISSINEN, A., HELKALA, E.-L., VAINIO, P., VANNINEN, R., PARTANEN, K. & SOININEN, H. (2004) Hippocampus and entorhinal cortex in mild cognitive impairment and early AD. *Neurobiol Aging,* 25**,** 303-310.

PERSIDSKY, Y., RAMIREZ, S. H., HAORAH, J. & KANMOGNE, G. D. (2006) Blood-brain barrier: Structural components and function under physiologic and pathologic conditions. *J NeuroImmune Pharmacol,* 1**,** 223-236.

PETERS, N., FREILINGER, T., OPHERK, C., GSCHWENDTER, A., PFEFFERKORN, T. & DICHGANS, M. (2005a) Enhanced L-arginine-induced vasoreactivity suggests endothelial dysfunction in CADASIL. *J Neurol,* 255**,** 1203-1208.

PETERS, N., OPHERK, C., BERGMANN, T., CASTRO, M., HERZOG, J. & DICHGANS, M. (2005b) Spectrum of mutations in biopsy-proven CADASIL: Implications for diagnostic strategies. *Arch Neurol,* 62**,** 1091-1094.

PETERS, N., OPHERK, C., DANEK, A., BALLARD, C., HERZOG, J. & DICHGANS, M. (2005c) The pattern of cognitive performance in CADASIL: A monogenic condition leading to subcortical ischemic vascular dementia. *Am J Psychiat,* 162**,** 2078-2085.

PETERS, N., OPHERK, C., ZACHERLE, S., GEMPEL, P., DICHGANS, M. & CAPELL, A. (2004) CADASIL-associated Notch3 mutations have differential effects both on ligand binding and ligand-induced Notch3 receptor signaling through RBP-Jk. *Exp Cell Res,* 299**,** 454-464.

PHILLIPS, J. S., KING, J. A., CHANDRAN, S., PRINSLEY, P. R. & DICK, D. (2005) Cerebral autosomal dominant arteriopathy with subcortical infarcts and leukoencephalopathy (CADASIL) presenting with sudden sensorineural hearing loss. *J Laryngol Otol,* 119**,** 148-151.

POBRIC, G., JEFFERIES, E. & RALPH, M. A. (2007) Anterior temporal lobes mediate semantic representation: Mimicking semantic dementia by using rTMS in normal participants. *Proc Natl Acad Sci U S A,* 104**,** 20137-20141.

POLLOCK, J. M., DEIBLER, A. R., BURDETTE, J. H., KRAFT, R. A., TAN, H., EVANS, A. B. & MALDJIAN, J. A. (2008) Migraine Associated Cerebral Hyperperfusion with Arterial Spin-Labeled MR Imaging. *AJNR Am J Neuroradiol,* 29**,** 1494-1497.

RAMPAL, R., LI, A. S. Y., MOLONEY, D. J., GEORGIOU, S. A., LUTHER, K. B., NITA-LAZAR, A. & HALTIWANGER, R. S. (2005) Lunatic fringe, manic fringe, and radical fringe recognize similar specificity determinants in O-fucosylated epidermal growth factor-like repeats. *J Biol Chem,* 280**,** 42454-42463.

RANJEVA, J. P., AUDOIN, B., AU DUONG, M. V., IBARROLA, D., CONFORT-GOUNY, S., MALIKOVA, I., SOULIER, E., VIOUT, P., ALI-CHÉRIF, A., PELLETIER, J. & COZZONE, P. (2005) Local tissue damage assessed with statistical mapping analysis of brain magnetization transfer ratio: relationship with functional status of patients in the earliest stage of multiple sclerosis. *AJNR Am J Neuroradiol,* 26**,** 119-127.

RAUEN, T., RAFFETSEDER, U., FRYE, B. C., DJUDJAJ, S., MÜHLENBERG, P. J. T., EITNER, F., LENDAHL, U., BERNHAGEN, J., DOOLEY, S. &

MERTENS, P. R. (2009) YB-1 acts as a ligand for notch-3 receptors and modulates receptor activation. *J Biol Chem,* 284**,** 26928-26940.

RAZVI, S. S. M., DAVIDSON, R., BONE, I. & MUIR, K. (2005) The prevalence of cerebral autosomal dominant arteriopathy with subcortical infarcts and leucoencephalopathy (CADASIL) in the west of Scotland. *J Neurol Neurosur Ps,* 76**,** 739-741.

REYES, S., VISWANATHAN, A., GODIN, O., DUFOUIL, C., BENISTY, S., HERNANDEZ, Z., KURTZ, A., JOUVENT, E., O'SULLIVAN, M., CZERNECKI, V., BOUSSER, M. G., DICHGANS, M. & CHABRIAT, H. (2009) Apathy: A major symptom in Cadasil. *Neurology,* 72**,** 905-910.

RICHARDS, A., VAN DEN MAAGDENBERG, A. M. J. M., JEN, J. C., KAVANAGH, D., BERTRAM, P., SPITZER, D., LISZEWSKI, M. K., BARILLA-LABARCA, M.-L., TERWINDT, G. M., KASAI, Y., MCLELLAN, M., GRAND, M. G., VANMOLKOT, K. R. J., DE VRIES, B., WAN, J., KANE, M. J., MAMSA, H., SCHAËFER, R., STAM, A. H., HAAN, J., DE JONG, P. T. V. M., STORIMANS, C. W., VAN SCHOONEVELD, M. J., OOSTERHUIS, J. A., GSCHWENDTER, A., DICHGANS, M., KOTSCHET, K. E., HODGKINSON, S., HARDY, T. A., DELATYCKI, M. B., HAJJ-ALI, R. A., KOTHARI, P. H., NELSON, S. F., FRANTS, R. R., BALOH, R. W., FERRARI, M. D. & ATKINSON, J. P. (2007) C-terminal truncations in human 3′-5′ DNA exonuclease TREX1 cause autosomal dominant retinal vasculopathy with cerebral leukodystrophy. *Nature Genet,* 39**,** 1068-1070.

ROHER, A. E., KUO, Y. M., ESH, C., KNEBEL, C., WEISS, N., KALBACK, W., LUEHRS, D. C., CHILDRESS, J. L., BEACH, T. G., WELLER, R. O. & KOKJOHN, T. A. (2003) Cortical and leptomeningeal cerebrovascular amyloid and white matter pathology in Alzheimer's disease. *Mol Med,* 9**,** 112-122.

ROINE, S., HARJU, M., KIVELÄ, T. T., PÖYHÖNEN, M., NIKOSKELAINEN, E., TUISKU, S., KALIMO, H., VIITANEN, M. & SUMMANEN, P. A. (2006) Ophthalmologic Findings in Cerebral Autosomal Dominant Arteriopathy with Subcortical Infarcts and Leukoencephalopathy. A Cross-sectional Study. *Ophthalmology,* 113**,** 1417.e1-1417.e2.

ROMÁN, G. C. (2003) Vascular dementia: Distinguishing characteristics, treatment, and prevention. *J Am Geriatr Soc,* 51.

ROMÁN, G. C. (2004) Vascular dementia. Advances in nosology, diagnosis, treatment and prevention. *Panminerva Med,* 46**,** 207-215.

ROMÁN, G. C., SALLOWAY, S., BLACK, S. E., ROYALL, D. R., DECARLI, C., WEINER, M. W., MOLINE, M., KUMAR, D., SCHINDLER, R. & POSNER, H. H. (2010) Randomized, placebo-controlled, clinical trial of donepezil in vascular dementia: Differential effects by hippocampal size. *Stroke,* 41**,** 1213-1221.

ROMÁN, G. C., TATEMICHI, T. K., ERKINJUNTTI, T., CUMMINGS, J. L., MASDEU, J. C., GARCIA, J. H., AMADUCCI, L., ORGOGOZO, J.-M., BRUN, A., HOFMAN, A., MOODY, D. M., O'BRIEN, M. D., YAMAGUCHI, T., GRAFMAN, J., DRAYER, B. P., BENNETT, D. A., FISHER, M., OGATA, J. & KOKMEN, E. (1993) Vascular dementia: Diagnostic criteria for research studies: Report of the NINDS-AIREN International Workshop. *Neurology,* 43**,** 250-260.

ROTH, M., TYM, E., MOUNTJOY, C. Q., HUPPERT, F. A., HENDRIE, H., VERMA, S. & GODDARD, R. (1986) CAMDEX. A standardised instrument for the diagnosis of mental disorder in the elderly with special reference to the early detection of dementia. *Br J Psychiatry,* 149**,** 698-709.

ROUHL, R. P., VAN OOSTENBRUGGE, R. J., KNOTTNERUS, I. L., STAALS, J. E. & LODDER, J. (2008) Virchow-Robin spaces relate to cerebral small vessel disease severity. *J Neurol,* 255**,** 692-696.

RUCHOUX, M.-M., GUEROUAOU, D., VANDENHAUTE, B., PRUVO, J.-P., VERMERSCH, P. & LEYS, D. (1995) Systemic vascular smooth muscle cell impairment in cerebral autosomal dominant arteriopathy with subcortical infarcts and leukoencephalopathy. *Acta Neuropathol,* 89**,** 500-512.

RUCHOUX, M.-M. & MAURAGE, C.-A. (1998) Endothelial changes in muscle and skin biopsies in patients with CADASIL. *Neuropathol Appl Neurobiol,* 24**,** 60-65.

RUCHOUX, M. M., BRULIN, P., LIMOL, S., DOMENGA, V., MACIAZEK, J., TOURNIER-LASSERVE, E. & JOUTEL, A. (2003) Transgenic mice expressing mutant Notch3 develop vascular alterations characteristic of cerebral autosomal dominant arteriopathy with subcortical infarcts and leukoencephalopathy. *Am J Pathol,* 162**,** 329-342.

RUFA, A., MALANDRINI, A., DOTTI, M. T., BERTI, G., SALVADORI, C. & FEDERICO, A. (2005) Typical pathological changes of CADASIL in the optic nerve. *Neurol Sci,* 26**,** 271-274.

SALMINEN, A., OJALA, J., KAUPPINEN, A., KAARNIRANTA, K. & SUURONEN, T. (2009) Inflammation in Alzheimer's disease: Amyloid-β oligomers trigger innate immunity defence via pattern recognition receptors. *Prog Neurobiol,* 87**,** 181-194.

SANDOVAL, K. E. & WITT, K. A. (2008) Blood-brain barrier tight junction permeability and ischemic stroke. *Neurobiol Dis,* 32**,** 200-219.

SANTA, Y., CHUI, D. H., TAKAHASHI, K., TABIRA, T., UYAMA, E., ARIMA, M. & KOTORII, S. (2003) Genetic, clinical and pathological studies of CADASIL in Japan: A partial contribution of Notch3 mutations and implications of smooth muscle cell degeneration for the pathogenesis. *J Neurol Sci,* 212**,** 79-84.

SCHEIBEL, M. E., TOMIYASU, U. & SCHEIBEL, A. B. (1977) The aging human Betz cell. *Exp Neurol,* 56**,** 598-609.

SCHEID, R., PREUL, C., LINCKE, T., MATTHES, G., SCHROETER, M. L., GUTHKE, T., YVES VON CRAMON, D. & SABRI, O. (2006) Correlation of cognitive status, MRI- and SPECT-imaging in CADASIL patients. *Eur J Neurol,* 13**,** 363-370.

SCHLEY, D., CARARE-NNADI, R., PLEASE, C. P., PERRY, V. H. & WELLER, R. O. (2006) Mechanisms to explain the reverse perivascular transport of solutes out of the brain. *J Theor Biol,* 238**,** 962-974.

SCHMAHMANN, J. D., SMITH, E. E., EICHLER, F. S. & FILLEY, C. M. (2008) Cerebral white matter: Neuroanatomy, clincal neurology, and neurobehavioral correlates. *Ann NY Acad Sci,* 1142**,** 266-309.

SCHMIDT-KASTNER, R. & HOSSMANN, K.-A. (1988) Distribution of ischemic neuronal damage in the dorsal hippocampus of rat. *Acta Neuropath,* 76**,** 411-421.

SCHMIDTKE, K. & HÜLL, M. (2005) Cerebral small vessel disease: how does it progress? *J Neurol Sci,* 229-230**,** 13-20.

SCHMITZ, N., ARKINK, E. B., MULDER, M., RUBIA, K., ADMIRAAL-BEHLOUL, F., SCHOONMANN, G. G., KRUIT, M. C., FERRARI, M. D. & VAN BUCHEM, M. A. (2008) Frontal lobe structure and executive function in migraine patients. *Neurosci Lett,* 440**,** 92-96.

SCHRÖDER, J. M., ZÜCHNER, S., DICHGANS, M., NAGY, Z. & MOLNAR, M. J. (2005) Peripheral nerve and skeletal muscle involvement in CADASIL. *Acta Neuropathol,* 110**,** 587-599.

SCHWAAG, S., EVERS, S., SCHIRMACHER, A., STÖGBAUER, F., RINGELSTEIN, E. B. & KUHLENBÄUMER, G. (2005) Genetic variants of the NOTCH3 gene in migraine—a mutation analysis and association study. *Cephalalgia,* 26**,** 158-161.

SCOTT, J. E. & WILLETT, I. H. (1966) Binding of cationic dyes to nucleic acids and other biological polyanions. *Nature,* 209**,** 985-987.

SHAO, L., MOLONEY, D. J. & HALTIWANGER, R. (2003) Fringe modifies O-fucose on mouse Notch1 at epidermal growth factor-like repeats within the ligand-binding site and the Abruptex region. *J Biol Chem,* 278**,** 7775-7782.

SHAWBER, C. J. & KITAJEWSKI, J. (2004) Notch function in the vasculature: insights from zebrafish, mouse and man. *BioEssays,* 26**,** 225-234.

SHINOURA, N., SUZUKI, Y., TSUKADA, M., KATSUKI, S., YAMADA, R., TABEI, Y., SAITO, K. & YAGI, K. (2007) Impairment of inferior longitudinal fasciculus plays a role in visual memory disturbance. *Neurocase,* 13**,** 127-130.

SINGHAL, S., BEVAN, S., BARRICK, T., RICH, P. & MARKUS, H. S. (2004) The influence of genetic and cardiovascular risk factors on the CADASIL phenotype. *Brain,* 127**,** 2031-2038.

SINGHAL, S., RICH, P. & MARKUS, H. S. (2005) The spatial distribution of MR imaging abnormalities in cerebral autosomal leukoencephalopathy and their relationships to age and clinical features. *AJNR Am J Neuroradiol,* 26**,** 2481-2487.

SMITH, C. S. & GUTTMAN, L. (1953) Measurement of internal boundaries in three dimensional structures by random sectioning. *Trans. AIME,* 197**,** 81-92.

SNOWDON, D. A., GREINER, L. H., MORTIMER, J. A., RILEY, K. P., GREINER, P. A. & MARKESBERY, W. R. (1997) Brain infarction and the clinical expression of Alzheimer disease: The Nun Study. *JAMA-J Am Med Assoc,* 277**,** 813-817.

SORKIN, A. & VON ZASTROW, M. (2009) Endocytosis and signaling: Interwining molecular networks. *Nat Rev Mol Cell Bio,* 10**,** 609-622.

SOURANDER, P. & WALINDER, J. (1977) Hereditary multi infarct dementia. Morphological and clinical studies of a new disease. *Acta Neuropathol,* 39**,** 247-254.

SPILT, A., WEVERLING-RIJNSBURGER, A. W., MIDDELKOOP, H. A., VAN DER FLIER, W. M., GUSSEKLOO, J., DE CRAEN, A. J., BOLLEN, E. L., BLAUW, G. J., VAN BUCHEM, M. A. & WESTENDORP, R. G. (2005) Late-onset dementia: structural brain damage and total cerebral blood flow. *Radiology,* 236**,** 990-995.

STAEKENBORG, S. S., VAN STRAATEN, E. C., VAN DER FLIER, W. M., LANE, R., BARKHOF, F. & SCHELTENS, P. (2008) Small vessel versus large vessel vascular dementia: risk factors and MRI findings. *J Neurol,* 255**,** 1644-1651.

STENBORG, A., KALIMO, H., VIITANEN, M., TERENT, A. & LIND, L. (2007) Impaired endothelial function of forearm resistance arteries in CADASIL patients. *Stroke,* 38**,** 2692-2697.

STEVENS, D. L., HEWLETT, R. H. & BROWNELL, B. (1977) Chronic familial vascular encephalopathy. *Lancet,* 1**,** 1364-1365.

STOET, G. & SNYDER, L. H. (2009) Neural correlates of executive control functions in the monkey. *Trends Cogn Sci,* 13**,** 228-234.

STOUB, T. R., DETOLEDO-MORRELL, L., STEBBINS, G. T., LEURGANS, S., BENNETT, D. A. & SHAH, R. C. (2006) Hippocampal disconnection contributes to memory dysfunction in individuals at risk for Alzheimer's disease. *Proc Natl Acad Sci U S A,* 103**,** 10041-10045.

STROMILLO, M. L., DOTTI, M. T., BATTAGLINI, M., MORTILLA, M., BIANCHI, S., PLEWNIA, K., PANTONI, L., INZITARI, D., FEDERICO, A. & DE STEFANO, N. (2009) Structural and metabolic brain abnormalities in preclinical cerebral autosomal dominant arteriopathy with subcortical infarcts and leucoencephalopathy. *J Neurol Neurosur Ps,* 80**,** 41-47.

SWEATT, J. D. (2004) Hippocampal function in cognition. *Psychopharmacology,* 174**,** 99-110.

SWEENEY, C., MORROW, D., BIRNEY, Y. A., COYLE, S., HENNESSY, C., SCHELLER, A., CUMMINS, P. M., WALLS, D., REDMOND, E. M. &

CAHILL, P. A. (2004) Notch1 and 3 receptors signaling modulates vascular smooth muscle cell growth, apoptosis, and migration via a CBF-1/RBP^Jk dependent pathway. *FASEB J,* 18**,** 1421-1423.

TAKAHASHI, K., ADACHI, K., YOSHIZAKI, K., KUNIMOTO, S., KALARIA, R. N. & WATANABE, A. (2010) Mutations in NOTCH3 cause the formation and retention of aggregates in the endoplasmic reticulum, leading to impaired cell proliferation. *Hum Mol Genet,* 19**,** 79-89.

TATSCH, K., KOCH, W., LINKE, R., POEPPERL, G., PETERS, N., HOLTMANNSPOETTER, M. & DICHGANS, M. (2003) Cortical hypometabolism and crossed cerebellar diaschisis suggest subcortically induced disconnection in CADASIL: An 18F-FDG PET study. *J Nucl Med,* 44**,** 862-869.

TATU, L., VUILLIER, F. & MOULIN, T. (2008) Chapter 13 Anatomy of the circulation of the brain and spinal cord. *Handb Clin Neurol,* 92**,** 247-281.

THANGAVEL, R., VAN HOESEN, G. W. & ZAHEER, A. (2008) Posterior parahippocampal gyrus pathology in Alzheimer's disease. *Neuroscience,* 154**,** 667-676.

THOMAS, W. E. (1999) Brain macrophages: on the role of pericytes and perivascular cells. *Brain Res Brain Res Rev,* 31**,** 42-57.

TIKKA, S., MYKKNEN, K., RUCHOUX, M.-M., BERGHOLM, R., JUNNA, M., PYHNEN, M., YKI-JRVINEN, H., JOUTEL, A., VIITANEN, M., BAUMANN, M. & KALIMO, H. (2009) Congruence between NOTCH3 mutations and GOM in 131 CADASIL patients. *Brain,* 132**,** 933-939.

TONG, X.-K. & HAMEL, E. (2007) Transforming growth factor-β1 impairs endothelin-1-mediated contraction of brain vessels by inducing mitogen-activated protein (MAP) kinase phosphatase-1 and inhibiting p38 MAP kinase. *Mol Pharmacol,* 72**,** 1476-1483.

TOPAKIAN, R., BARRICK, T. R., HOWE, F. A. & MARKUS, H. S. (2010) Blood–brain barrier permeability is increased in normal-appearing white matter in patients with lacunar stroke and leucoaraiosis. *J Neurol Neurosur Ps,* 81**,** 192-197.

TRAPP, B. D., PETERSON, J., RANSOHOFF, R. M., RUDICK, R., MÖRK, S. & BÖ, L. (1988) Axonal transection in the lesions of multiple sclerosis. *N Engl J Med,* 338**,** 278-285.

TRAYKOV, L., BAUDIC, S., THIBAUDET, M. C., RIGAUD, A. S., SMAGGHE, A. & BOLLER, F. (2002) Neuropsychological deficit in early subcortical vascular dementia: comparison to Alzheimer's disease. *Dement Geriatr Cogn Disord,* 14**,** 26-32.

TUOMINEN, S., JUVONEN, V., AMBERLA, K., JOLMA, T., RINNE, J. O., TUISKU, S., KURKI, T., MARTTILA, R., PÖYHÖNEN, M., SAVONTAUS, M.-L., VIITANEN, M. & KALIMO, H. (2001) Phenotype of a homozygous CADASIL patient in comparison to 9 age-matched heterozygous patients with the same R133C Notch3 mutation. *Stroke,* 32**,** 1767-1774.

TUOMINEN, S., MIAO, Q., KURKI, T., TUISKU, S., PÖYHÖNEN, M., KALIMO, H., VIITANEN, M., SIPILÄ, H. T., BERGMAN, J. & RINNE, J. O. (2004) Positron emission tomography examination of cerebral blood flow and glucose metabolism in young CADASIL patients. *Stroke,* 35**,** 1063-1067.

UENO, M., TOMIMOTO, H., AKIGUCHI, I., WAKITA, H. & SAKAMOTO, H. (2002) Blood–Brain Barrier Disruption in White Matter Lesions in a Rat Model of Chronic Cerebral Hypoperfusion. *J Cerebr Blood F Met,* 22**,** 97-104.

UGGETTI, C., EGITTO, M. G., PICHIECCHIO, A., SINFORIANI, E., BEVILACQUA, M. S., CAVALLINI, A. & MICIELI, G. (2001) Subcortical dementia associated with striking enlargement of the Virchow-Robin spaces and transneural degeneration of the left mammillo-thalamic tract. *Cerebrobasc Dis,* 12**,** 287-290.

UNGARO, C., MAZZEI, R., CONFORTI, F. L., SPROVIERI, T., SERVILLO, P., LIGUORI, M., CITRIGNO, L., GABRIELE, A. L., MAGARIELLO, A., PATITUCCI, A., MUGLIA, M. & QUATTRONE, A. (2009) Cadasil: Extended polymorphisms and mutational analysis of the NOTCH3 gene. *J Neurosci Res,* 87**,** 1162-1167.

USPENSKAIA, O., LIEBETRAU, M., HERMS, J., DANEK, A. & HAMANN, G. F. (2004) Aging is associated with increased collagen type IV accumulation in the basal lamina of human cerebral microvessels. *BMC Neurosci,* 5**,** 6.

UTATSU, Y., TAKASHIMA, H., MICHIZONO, K., KANDA, N., UMEHARA, F., HIGUCHI, I., ARIMURA, K., NAKAGAWA, M., OSAME, M., ENDOU, K., MITSUYAMA, Y., FUJIMOTO, T. & NAGAI, M. (1997) Autosomal dominant early onset dementia and leukoencephalopathy in a Japanese family: Clinical, neuroimaging and genetic studies. *J Neurol Sci,* 147**,** 55-62.

UYGUNER, Z. O., SIVA, A., KAYSERILI, H., SAIP, S., ALTÝNTATH, A., APAK, M. Y., ALBAYRAM, S., ITHÝK, N., AKMAN-DEMIR, G., TAOYÜREKLI, M., ÖZ, B. & WOLLNIK, B. (2006) The R110C mutation in Notch3 causes variable clinical features in two Turkish families with CADASIL syndrome. *J Neurol Sci,* 246**,** 123-130.

VAHEDI, K., CHABRIAT, H., LEVY, C., JOUTEL, A., TOURNIER-LASSERVE, E. & BOUSSER, M.-G. (2004) Migraine with aura and brain magnetic resonance imaging abnormalities in patients with CADASIL. *Arch Neurol* 61**,** 1237-1240.

VAHEDI, K., MASSIN, P., GUICHARD, J.-P., MIOCQUE, S., POLIVKA, M., GOUTIÈRES, F., DRESS, D., CHAPON, F., RUCHOUX, M.-M., RIANT, F., JOUTEL, A., GAUDRIC, A., BOUSSER, M.-G. & TOURNIER-LASSERVE, E. (2003) Hereditary infantile hemiparesis, retinal arteriolar tortuosity, and leukoencephalopathy. *Neurology,* 60**,** 57-63.

VALENTI, R., POGGESI, A., PESCINI, F., INZITARI, D. & PANTONI, L. (2008) Psychiatric disturbances in CADASIL: a brief review. *Acta Neurol Scand,* 118**,** 291-295.

VAN AGTMAEL, T., BAILEY, M. A., SCHLÖTZER-SCHREHARDT, U., CRAIGIE, E., JACKSON, I. J., BROWNSTEIN, D. G., MEGSON, I. L. & MULLINS, J. J. (2010) Col4a1 mutation in mice causes defects in vascular function and low blood pressure associated with reduced red blood cell volume. *Hum Mol Gene,* 19**,** 1119-1128.

VAN DEN BOOM, R., LESNICK OBERSTEIN, S. A. J., VAN DEN BERG-HUYSMANS, A. A., FERRARI, M. D., VAN BUCHEM, M. A. & HAAN, J. (2006) Cerebral autosomal dominant arteriopathy with subcortical infarcts and leukoencephalopathy: Structural MR imaging changes and apolipoprotein E genotype. *AJNR Am J Neuroradiol,* 27**,** 359-362.

VAN GORP, W. G., MARCOTTE, T. D., SULTZER, D., HINKIN, C., MAHLER, M. & CUMMINGS, J. L. (1999) Screening for dementia: comparison of three commonly used instruments. *J Clin Exp Neuropsychol,* 21**,** 29-38.

VERNOOIJ, M. W., IKRAM, M. A., VROOMAN, H. A., WIELOPOLSK, I. P. A., KRESTIN, G. P., HOFMAN, A., NIESSEN, W. J., VAN DER LUGT, A. & BRETELER, M. M. (2009) White matter microstructural integrity and cognitive function in a general elderly population. *Arch Gen Psychiatry,* 66**,** 545-553.

VERREAULT, S., JOUTEL, A., RIANT, F., NEVES, G., SILVA, M. R., MACIAZEK, J., TOURNIER-LASSERVE, E., BOUSSER, M.-G. & CHABRIAT, H. (2006) A novel hereditary small vessel disease of the brain. *Ann Neurol,* 59**,** 353-357.

VESTERGAARD, M., MADSEN, K. S., BAARÉ, W. F., SKIMMINGE, A., EJERSBO, L. R., RAMSØY, T. Z., GERLACH, C., AKESON, P., PAULSON, O. B. & JERNIGAN, T. L. (2010) White matter microstructure in a superior longitudinal fasciculus associated with spatial working memory performance in children. *J Cogn Neurosci,* In Press.

VISWANATHAN, A., GRAY, F., BOUSSER, M. G., BAUDRIMONT, M. & CHABRIAT, H. (2006) Cortical neuronal apoptosis in CADASIL. *Stroke,* 37**,** 2690-2695.

VISWANATHAN, A., GSCHWENDTNER, A., GUICHARD, J. P., BUFFON, F., CUMURCIUC, R., O'SULLIVAN, M., HOLTMANNSPÖTTER, M., PACHAI, C., BOUSSER, M. G., DICHGANS, M. & CHABRIAT, H. (2007) Lacunar lesions are independently associated with disability and cognitive impairment in CADASIL. *Neurology,* 69**,** 172-179.

VOELKER, C. C., GARIN, N., TAYLOR, J. S., GAHWILER, B. H., HORNUNG, J. P. & MOLNAR, Z. (2004) Selective neurofilament (SMI-32, FNP-7 and N200) expression in subpopulations of layer V pyramidal neurons in vivo and in vitro. *Cerebral Cortex,* 14**,** 1276-1286.

VOSKUHL, R. R., PETERSON, R. S., SONG, B., AO, Y., MORALES, L. B., TIWARI-WOODRUFF, S. & SOFRONIEW, M. V. (2009) Reactive Astrocytes Form Scar-Like Perivascular Barriers to Leukocytes during Adaptive Immune Inflammation of the CNS. *J Neurosci,* 29**,** 11511-11522.

WAGNER, A. D., SHANNON, B. J., KAHN, I. & BUCKNER, R. L. (2005) Parietal lobe contributions to episodic memory retrieval. *Trends Cogn Sci,* 9**,** 445-453.

WANG, G. (2009) Perivascular space and neurological disorders. *Neurosci Bull,* 25**,** 33-37.

WANG, T., HOLT, C. M., XU, C., RIDLEY, C., P O JONES, R., BARON, M. & TRUMP, D. (2007) Notch3 activation modulates cell growth behavior and cross-talk to Wnt/TCF signaling pathway. *Cell Signal,* 19**,** 2458-2467.

WANG, W., PRINCE, C. Z., HU, X. & POLLMAN, M. J. (2003) HRT1 modulates vascular smooth muscle cell proliferation and apoptosis. *Biochem Bioph Res Co,* 308**,** 596-601.

WANG, W., PRINCE, C. Z., MOU, Y. & POLLMAN, M. J. (2002) Notch3 signaling in vascular smooth muscle cells induces c-FLIP expression via ERK/MAPK activation. Resistance to Fas ligand-induced apoptosis. *J Biol Chem,* 277**,** 21723-21729.

WARBURTON, E. C. & BROWNA, M. W. (2010) Findings from animals concerning when interactions between perirhinal cortex, hippocampus and medial prefrontal cortex are necessary for recognition memory *Neuropsychologia,* 48**,** 2262-2272.

WARDLAW, J. M. (2010) Blood-brain barrier and cerebral small vessel disease. *J Neurol Sci,* 299**,** 66-71.

WELLER, R. O., DJUANDA, E., YOW, H.-Y. & CARARE, R. O. (2009) Lymphatic drainage of the brain and the pathophysiology of neurological disease. *Acta Neuropathol,* 117**,** 1-14.

WELLER, R. O., GALEA, I., CARARE, R. O. & MINAGAR, A. (2010) Pathophysiology of the lymphatic drainage of the central nervous system: Implications for pathogenesis and therapy of multiple sclerosis. *Pathophysiology,* 17**,** 295-306.

WELLER, R. O., SUBASH, M., PRESTON, S. D., MAZANTI, I. & CARARE, R. O. (2008) Perivascular drainage of amyloid-beta peptides from the brain and its failure in cerebral amyloid angiopathy and Alzheimer's disease. *Brain Pathol* 18**,** 253-266.

WETTERLING, T., KANITZ, R. D. & BORGIS, K. J. (1996) Comparison of different diagnostic criteria for vascular dementia (ADDTC, DSM-IV, ICD-10, NINDS-AIREN). *Stroke,* 27**,** 30-36.

WOLFE, M. S. (2002) APP, Notch and Presenilin: molecular pieces in the puzzle of Alzheimer's disease. *Int Immunopharmacol,* 2**,** 1919-1929.

WOODS, A. S. (2004) The mighty arginine, the stable quaternary amines, the powerful aromatics, and the aggressive phosphate: Their role in the noncovalent minuet. *J Proteome Res,* 3**,** 478-484.

WUERFEL, J., HAERTLE, M., WAICZIES, H., TYSIAK, E., BECHMANN, I., WERNECKE, K. D., ZIPP, F. & PAUL, F. (2008) Perivascular spaces—MRI marker of inflammatory activity in the brain? *Brain,* 131**,** 2332-2340.

YANG, L. T., NICHOLS, J. T., YAO, C., MANILAY, J. O., ROBEY, E. A. & WEINMASTER, G. (2005) Fringe glycosyltransferases differentially modulate Notch1 proteolysis induced by Delta1 and Jagged1. *Mol Biol Cell,* 16**,** 927-942.

YETKIN, E., OZISIK, H., OZCAN, C., AKSOY, Y. & TURHAN, H. (2007) Increased dilator response to nitrate and decreased flow-mediated dilatation in migraineurs. *Headache,* 47**,** 104-110.

YOUSRY, T. A., SEELOS, K., MAYER, M., BRÜNING, R., UTTNER, I., DICHGANS, M., MAMMI, S., STRAUBE, A., MAI, N. & FILIPPI, M. (1999) Characteristic MR lesion pattern and correlation of T1 and T2 lesion volume with neurologic and neuropsychological findings in cerebral autosomal dominant arteriopathy with subcortical infarcts and leukoencephalopathy (CADASIL). *Am J Neuroradiol,* 20**,** 91-100.

YUAN, P., SALVADORE, G., LI, X., ZHANG, L., DU, J., CHEN, G. & MANJI, H. K. (2009) Valproate activates the Notch3/c-FLIP signaling cascade: a strategy to attenuate white matter hyperintensities in bipolar disorder in late life? *Bipolar Disord* 11**,** 256-269.

ZAROW, C., VINTERS, H. V., ELLIS, W. G., WEINER, M. W., MUNGAS, D., WHITE, L. & CHUI, H. C. (2005) Correlates of hippocampal neuron number in Alzheimer's disease and ischemic vascular dementia. *Ann Neurol,* 57**,** 896-903.